



**D**octorate program  
**M**ilan  
**EXPERIMENTAL**  
**MEDICINE**



**Università degli Studi di Milano**

**PhD Course in  
Experimental Medicine**

**CYCLE XXXV**

**PhD thesis**

**CHARACTERIZATION OF EpCAM IN THYROID CANCER  
BIOLOGY BY THREE-DIMENSIONAL SPHEROIDS  
*IN VITRO* MODEL.**

**Candidate: Dr. Viola Ghiandai**

Matr. R12639

**Tutor: Prof. Luca Persani**

**Supervisor: Dr. Elisa Stellaria Grassi**

**Director: Prof. Nicoletta Landsberger**

**Academic Year 2021-2022**

# **Table of contents**

|   |    |
|---|----|
| <b>Abstract</b> .....   | 1  |
| <b>Disclosure for research integrity</b> .....  | 4  |
| <b>Abbreviations</b> .....  | 4  |
| <b>Introduction</b> .....   | 6  |
| <b>1) THYROID CANCER</b> .....  | 7  |
| <b>1.1 Thyroid cancer epidemiology and risk factors</b> .....                           | 7  |
| <b>1.2 Thyroid cancer classification and diagnosis</b> .....                            | 9  |
| <b>1.3 Thyroid cancer pathogenesis and genetic alterations</b> .....                    | 11 |
| <b>1.4 Thyroid cancer conventional and new therapeutic approaches</b> .....             | 14 |
| <b>2) HETEROGENEITY OF SOLID TUMORS AND THE ROLE OF CANCER STEM-LIKE CELLS</b> .....    | 15 |
| <b>2.1 Thyroid cancer carcinogenesis models</b> .....                                   | 15 |
| <b>2.2 Thyroid cancer heterogeneity and the role of tumor microenvironment</b> .....    | 17 |
| <b>2.3 Normal Stem Cells and Cancer Stem-like Cells</b> .....                           | 19 |
| <b>2.4 Identification of putative thyroid CSCs</b> .....                                | 20 |
| <b>3) EPITHELIAL CELL ADHESION MOLECULE (EpCAM)</b> .....                               | 23 |
| <b>3.1 EpCAM: general features and protein structure</b> .....                          | 23 |
| <b>3.2 EpCAM-mediated signaling: role in cell-cell adhesion and proliferation</b> ..... | 24 |
| <b>3.3 EpCAM-mediated signaling by regulated intramembrane proteolysis (RIP)</b> .....  | 25 |
| <b>3.4 EpCAM role in health and disease</b> .....                                       | 27 |
| <b>Aim of the thesis</b> .....  | 30 |
| <b>Materials and Methods</b> .....  | 32 |
| <b>REAGENTS</b> .....   | 33 |
| <b>1) PATIENTS AND SAMPLE COLLECTION</b> .....  | 35 |
| <b>2) CELL CULTURES</b> .....   | 35 |

|   |           |
|---|-----------|
| <b>3) TC CELL LINES-DERIVED 3D SPHEROIDS GENERATION.....</b>  | <b>37</b> |
| <b>3.1 Hanging-drop technique.....</b>  | <b>37</b> |
| <b>3.2 Non-adhesive substrate technique.....</b>  | <b>38</b> |
| <b>3.3 Light microscopy for 3D spheres dimensions and morphology .....</b>                          | <b>38</b> |
| <b>4) CLONALITY ASSAY BY EXTREME LIMITING DILUTION ANALYSIS (ELDA).....</b>                         | <b>39</b> |
| <b>5) PROTEIN EXTRACTION AND WESTERN BLOTTING.....</b>  | <b>39</b> |
| <b>5.1 Solubilization with RIPA lysis buffer for 2D adherent cells .....</b>                        | <b>39</b> |
| <b>5.2 Solubilization with RIPA lysis buffer for 3D spheres.....</b>                                | <b>40</b> |
| <b>5.3 Solubilization with Laemmli lysis buffer for patient-derived tissue samples .....</b>        | <b>40</b> |
| <b>5.4 Protein quantification and sample preparation .....</b>                                      | <b>40</b> |
| <b>5.5 Western Blotting .....</b>   | <b>41</b> |
| <b>6) IMMUNOFLUORESCENCE AND CONFOCAL MICROSCOPY.....</b>   | <b>42</b> |
| <b>6.1 Immunofluorescence on patient-derived tissue samples .....</b>                               | <b>42</b> |
| <b>6.2 Immunofluorescence on 2D adherent cells .....</b>  | <b>43</b> |
| <b>6.3 Immunofluorescence on 3D spheres.....</b>  | <b>44</b> |
| <b>6.4 Fluorescent and confocal microscopy.....</b>   | <b>45</b> |
| <b>7) TRANSIENT TRANSFECTION.....</b>   | <b>46</b> |
| <b>8) EpCAM CLEAVAGE INDUCTION AND INHIBITION .....</b>   | <b>47</b> |
| <b>8.1 Epidermal Growth Factor (EGF) and 2,2'-Bipyridyl (DIP) treatments</b>                        | <b>47</b> |
| <b>8.2 EpCAM cleavages' inhibitors treatments on transfected cells .....</b>                        | <b>47</b> |
| <b>8.3 EpCAM cleavages' inhibitors and DIP treatments effects on sphere-forming abilities .....</b> | <b>48</b> |
| <b>9) ANTI-CANCER DRUG TREATMENTS AND PROLIFERATION ASSAYS</b>                                      | <b>49</b> |
| <b>9.1 2D adherent cells .....</b>  | <b>49</b> |
| <b>9.2 3D spheres .....</b>   | <b>49</b> |
| <b>10) STATISTICAL ANALYSIS.....</b>  | <b>50</b> |

|  |     |
|--|-----|
| <b>Results</b> .....   | 51  |
| <b>1) STUDIES ON THE CHARACTERIZATION OF EPITHELIAL CELL ADHESION MOLECULE (EpCAM) EXPRESSION AND CLEAVAGES</b> .....                  | 52  |
| <b>1.1 EpCAM and its cleaved domains are expressed differently in healthy and pathological patient-derived TC tissue samples</b> ..... | 52  |
| <b>1.2 TC cell lines have different EpCAM expression levels</b> .....  | 55  |
| <b>1.3 Thyroid cancer cell lines have different 3D sphere-forming ability..</b>  | 57  |
| <b>1.4 FRO-derived 3D spheres are a valid <i>in vitro</i> model to study EpCAM cleavage pattern</b> .....                              | 60  |
| <b>1.5 Characterization of EpCAM cleavages in FRO cells</b> .....  | 62  |
| <b>1.6 EpCAM cleavage manipulation influences sphere-forming abilities of FRO cells</b> .....  | 67  |
| <b>1.7 Vemurafenib (PLX-4032) treatments on FRO and HTCC3</b> .....  | 69  |
| <b>Discussion and Conclusions</b> .....  | 75  |
| <b>Acknowledgements</b> .....  | 88  |
| <b>Bibliography</b> .....  | 89  |
| <b>List of figures and tables</b> .....  | 107 |
| <b>List of figures</b> .....   | 107 |
| <b>List of tables</b> .....  | 108 |
| <b>Dissemination of results</b> .....  | 109 |
| <b>Appendix</b> .....  | 111 |

# **Abstract**

Thyroid cancer (TC) is the most common Endocrine malignancy. Currently, the mechanisms responsible for insensitivity to therapeutic treatments, tumor aggressiveness and tumor relapse described in undifferentiated thyroid cancers (UTCs) haven't been fully elucidated yet. The insurgence of therapy resistance and disease relapse is believed to be due to a subpopulation of cancer cells within the tumor bulk that shows stem-like phenotype and specific tumor-initiating abilities. These cells are called tumor-initiating cells (TICs), and a comprehensive understanding of how to specifically isolate and target them is necessary. In thyroid cancer, TICs have been identified using specific *in vitro* and *in vivo* assays, variations of enzymatic activities, expression of well-known stemness markers and expression of membrane markers. Among the possible membrane markers described in literature to identify TICs, Epithelial Cell Adhesion Molecule (EpCAM) has already been defined as a marker for cancer cells with tumor-initiating properties in many solid tumors, where its possible role in tumor progression and aggressiveness has been described. However, this protein is poorly studied in TC and its role in TC pathology, especially in the undifferentiated forms, needs further comprehension.

Hence, the aim of my PhD project was to: 1) characterize EpCAM as a putative thyroid TICs marker on poorly differentiated and anaplastic thyroid cancer cell lines, applying both classical monolayer cultures and 3D spheres cultures; 2) establish if the 3D model is a valid *in vitro* approach to study the expression and role of EpCAM in the context of TC; 3) observe whether TC cell lines respond differently when treated as adherent cells or as 3D spheres.

Our data demonstrated that EpCAM is subjected to an intense cleavage process in FRO-derived 3D tumor spheres and that the 3D model is representative of the variability of EpCAM expression and cleavage that we observed in patient-derived tissue samples, with the different gradient of EpCAM cleavages corresponding to different areas of the tumor sections. We also observed that the expression of EpCAM can be modulated by the regulation of its cleavages and that the integrity of the protein seem to be a crucial factor for the initial phase of the generation of 3D spheres in FRO, while the cleavage of the protein may occur in a subsequent phase, induced by the ability of cells to adapt to variations in

growth conditions and/or to the microenvironment within the spheres. Moreover, we demonstrated that EpCAM<sup>+</sup> and EpCAM<sup>-</sup> subpopulations respond differently to treatment with a well-known drug commonly used in clinical practice, Vemurafenib (PLX-4032), both in FRO and HTCC3 adherent cells, and EpCAM<sup>+</sup> cells appeared to be more resistant. Finally, the 3D sphere model is also a valid *in vitro* approach to assess cell response to PLX-4032 and we observed that FRO-derived 3D spheres seemed to be more resistant than HTCC3-derived spheres upon PLX-4032 treatment.

In conclusion, we believe that EpCAM expression and its cleavage in 3D spheres could play a significant role in putative TC TICs biology and may partially explain the therapeutic failure observed in the more undifferentiated TCs, concomitantly to other mechanisms of resistance and/or escape that may occur.



## **Disclosure for research integrity**

I state that this study was conducted following the ethics of good research practice of the European Code of Conduct for research integrity, based on the principles of reliability, honesty, respect and accountability.

## **Abbreviations**

ABC: ATP-binding cassette

ABCG2: ABC subfamily G member 2

ALDH: aldehyde dehydrogenase

ALDH1A1: ALDH 1 Family Member A1

ATA: American thyroid association

ATC: anaplastic thyroid cancer

CAFs: cancer-associated fibroblasts

cAMP/PKA: cyclic AMP-protein kinase A

CSCs: cancer stem-like cells

CT: computed tomography

CTLA-4: cytotoxic T lymphocytes antigen-4

DTCs: differentiated thyroid cancers

ECM: extracellular matrix

EGF: epidermal growth factor

ELDA: extreme limiting dilution analysis

EMP: epithelial-mesenchymal plasticity

EMT: epithelial to mesenchymal transition

EpCAM: epithelial cell adhesion molecule

EpEx: extracellular domain of EpCAM

EpICD: intracellular domain of EpCAM

FGF: fibroblast growth factor

FHL2: four and a half LIM domains protein 2

FMTC: familial medullary thyroid cancer

FNA: fine needle aspirate

FNMTC: familial non-medullary thyroid cancer

FTCs: follicular thyroid cancers  
HCC: Hurthle cell carcinoma  
ITH: intratumoral heterogeneity  
LDA: limiting dilution analysis  
LEF-1: lymphoid enhancer binding factor-1  
MAPK: mitogen-activated protein kinase  
MDR1: multi drug resistance mutation 1  
MEN2: multiple endocrine neoplasia type 2  
MRI: multi-resonance imaging  
MRP: multi drug resistance-associated protein  
MTCs: medullary thyroid cancers  
NT: normal thyroid tissue  
OCT4: octamer-binding transcription factor 4  
PD-L1: programmed death-ligand 1  
PDTs: poorly differentiated thyroid cancers  
PET: positron emission tomography  
PI3K: phosphoinositide 3-kinase  
Poly-hema: poly(2-hydroxyethyl methacrylate)  
POU5F1: POU class 5 homeobox 1  
PTC: papillary thyroid cancer  
RAI: radioiodine  
RIP: regulated intramembrane proteolysis  
SOX2: sex-determining region Y-box 2  
TAMs: tumor-associated macrophages  
TC: thyroid cancer  
TICs: tumor-initiating cells  
TK: tyrosine kinase  
TKI: tyrosine kinase inhibitor  
TME: tumor microenvironment  
TSH: thyroid stimulating hormone  
UTCs: undifferentiated thyroid cancers  
VEGF: vascular endothelial growth factor

# **Introduction**

# 1) THYROID CANCER

## 1.1 Thyroid cancer epidemiology and risk factors

Thyroid cancer (TC) represents the most common endocrine malignancy and has the fastest increasing incidence in the United States (1). This is probably due to improved medical surveillance and advent of new radiological diagnostic techniques that have contributed to the increment of detection of clinically indetermined tumors (2). In addition, many incidental thyroid nodules are found on imaging studies performed for other reasons than thyroid pathology. Most of these nodules are in early stages and are usually well differentiated, and they occur more frequently in women than in man (3). Indeed, in the past years, TC gender disparity became more pronounced, especially considering women at age 40–49 with a 3:1 female-to-male ratio in most geographic regions and demographic groups (4) (Figure 1). According to Cancer.net epidemiological data (5), TC has an overall 5-year survival rate of 98.3%, but it lower to only 55.5% for disseminated disease. However, survival rates are based on many factors, including the specific histological type of TC and stage of disease. In particular, concerning the undifferentiated forms of TC, especially anaplastic thyroid cancers (ATCs), the survival rate tends to get worse due to the limited therapeutic approaches that can be applied for these patients and the poor outcomes with conventional therapies (6,7).

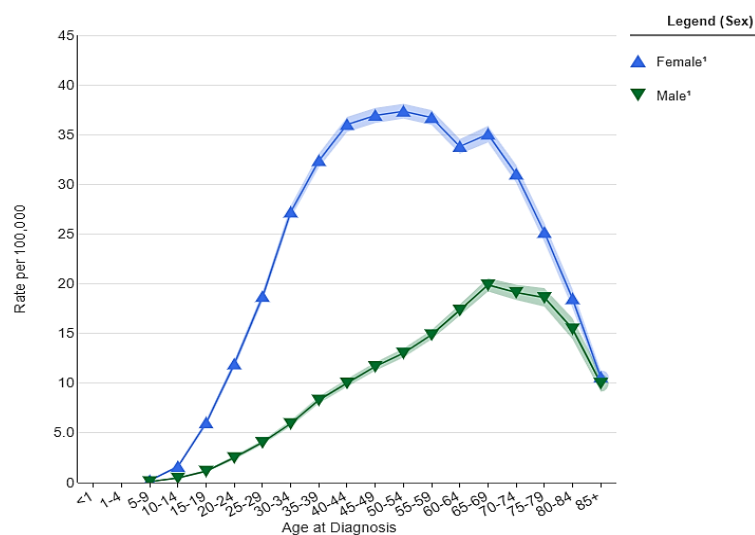


**Figure 1. SEER incidence rates by age at diagnosis, years 2015-2019.** Data grouped by sex, delay-adjusted SEER incidence rate, all races (1).

Apart from the improvement in diagnostic techniques, the increase in TC incidence could also be a consequence of exposure to external factors such as radiations or dangerous chemical substances, environmental factors, or it might be multifactorial. Many studies have explored potential risk factors involved in TC onset. The most-established risk factor for cancer in general but in particular for TC is the exposure to radiations. It is known that ionizing radiations directly affects the DNA, causing DNA strand breaks and consequently promoting carcinogenesis. The effect of these radiations is especially harmful in children, since the thyroid tissue is very radiosensitive at an early age (8), and is reported that those who have been exposed to radiations, e.g. after the Chernobyl accident, can frequently develop TC, especially papillary thyroid cancer (PTC) (9). Iodine deficiency is another factor that considerably affects thyroid functionality, since a reduction in the level of thyroid hormones induces an increment in thyroid-stimulating hormone (TSH) secretion, which is known to be a fundamental growth factor for follicular cells, and the differential iodine intake can also affect TC histotype distribution. Indeed, predominantly follicular tumors are observed in iodine-deficient areas, while papillary tumors in iodine-replete areas (10). Moreover, the increased papillary/follicular ratio may be due to long-term TSH stimulation and the frequency of BRAFV600E mutation, a typical molecular alteration of PTC (11).

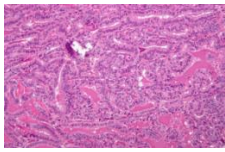
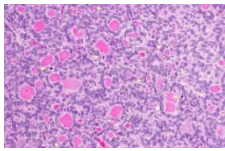
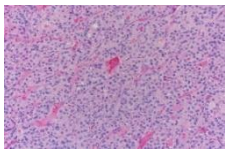
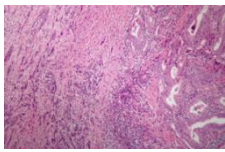
From a metabolic point of view, a strong correlation between obesity and cancer risk, as well as mortality, has been demonstrated for several malignancies, including thyroid cancer. The study conducted by Almquist and colleagues (12), strengthened the possibility that disruptions in insulin metabolism may be risk factors for TC. Indeed, insulin can modulate thyroid gene expression and can promote thyrocyte proliferation, differentiation, and transformation.

Genetic alterations and hereditary conditions are crucial factors to be considered for the onset of TC. It is well known that alterations in genes involved in mitogen-activated protein kinase (MAPK), phosphoinositide 3-kinase (PI3K) and cyclic AMP-protein kinase A (cAMP/PKA) signaling pathways play a fundamental role in the development of TC, thus they can be considered as major risk factors for TC. Moreover, several hereditary conditions (13) have been linked to different types of TC such as familial medullary thyroid cancer (FMTC), multiple endocrine

neoplasia type 2 (MEN2) which is a combination of FMTC and tumors of other endocrine glands, familial non-medullary thyroid cancer (FNMTC), and Hurthle cell carcinoma (HCC) (13).

## **1.2 Thyroid cancer classification and diagnosis**

The functional unit of the thyroid gland is represented by the thyroid follicles, spherical structures formed by an outer layer of thyrocytes and filled in colloid, which are the center of thyroid hormones production. Interspersed between the thyroid follicles there are also the parafollicular C cells, responsible for calcitonin secretion. According to the World Health Organization, it is possible to identify four main subtypes of TC based on the histopathological features and on the cell of origin (Table 1). Thyroid cancers that derive from the follicular cells can be classified in DTCs and in undifferentiated thyroid cancers (UTCs) The DTCs can be further classified in PTCs and in FTCs while the UTCs are classified in poorly differentiated thyroid cancers (PDTCs) and in ATCs. The thyroid cancer histotype that arises from thyroid parafollicular C cells is the MTCs, accounting for ~5% of all thyroid cancers (14). The vast majority of TCs is represented by PTCs and FTCs (80–85% and 10–15% respectively) (15) and usually show a good prognosis. On the contrary, PDTCs and ATCs are rare tumors (5% and 1% respectively) (15) but are characterized by poor prognosis and by an aggressive phenotype, with complete disruption of the biological features and functions of thyrocytes. Even if ATCs represent only 1% of all TC cases, they display rapid evolution, local invasion and metastatic spread, and account for higher mortality with a median survival time of 6 months. Moreover, they often acquire therapy resistance (16,17).

| Stage of differentiation                | Tumor type & prevalence                                | Morphology  | Main features   | 10-year mortality (%) |
|---|--|---|---|-----------------------|
| Differentiated Thyroid Cancers (DTCs)   | Papillary Thyroid Cancer (PTC)<br>-<br>80-84%          |    | Papillary architecture with variable size and organization, distinctive nuclear features that include enlargement, oval shape, elongation, overlapping and clearing, inclusions and grooves; lymph node metastases. | 5                     |
|   | Follicular Thyroid Cancer (FTC)<br>-<br>10-15%         |    | Small-medium size follicular structures filled with colloid, lacking nuclear features of PTC; hematological spreading; bone and lung metastases.  | 15                    |
| Undifferentiated Thyroid Cancers (UTCs) | Poorly Differentiated Thyroid Cancer (PDTC)<br>-<br>5% |   | Poorly differentiated, often overlapping with PTC and FTC; locoregional invasion; bone and lung metastases. Intermediate aggressiveness between differentiated and undifferentiated thyroid cancers.                | -50                   |
|   | Anaplastic Thyroid Cancer (ATC)<br>-<br>1%             |  | Undifferentiated; mixture of spindle, pleomorphic giant and epithelioid cells; extremely invasive and metastatic; highly lethal; may occur <i>de novo</i> or derive from PTC, FTC or PDTC.                          | 95                    |

**Table 1. Classification of thyroid tumors of epithelial origin with prevalence (%), morphological features, and 10-year mortality (%). Adapted from (18).**

The diagnosis of TC is based on several approaches spacing from imaging tests to biopsy to molecular analyses. Concerning imaging tests, the most used diagnostic approach is the ultrasound examination of the neck. Advance imaging techniques to monitor disease stage and localization are radioiodine (RAI) scans, computed tomography (CT) scan, multi-resonance imaging (MRI) scan and positron emission tomography (PET) scan. However, the most trustworthy

diagnostic approach for the evaluation of thyroid nodules is the cytological examination of cells collected after fine-needle aspirate (FNA) biopsy (19). To avoid unnecessary surgery or a second surgical procedure, additional diagnostic approaches are needed to manage patients with indeterminate thyroid nodules: gene expression markers (20), somatic mutations panels (21), liquid biopsy (22), circulating miRNAs (23).

### 1.3 Thyroid cancer pathogenesis and genetic alterations

The pathogenesis of the majority of TCs involves the dysregulation of the main signaling pathways involved in thyrocyte proliferation and differentiation, such as Raf/Ras/MEK/ERK, PI3K/AKT and cAMP/PKA, through acquisition of various alterations in genes coding for the effector molecules of these pathways (Figure 2). In TC, the hyperactivation of Raf/Ras/MEK/ERK pathway is mainly due to point mutations in genes like *BRAF* and *RAS* or *RET/PTC* rearrangements. It contributes to dysregulation of growth of tumor cells and promotes tumorigenesis mainly in PTCs (24).

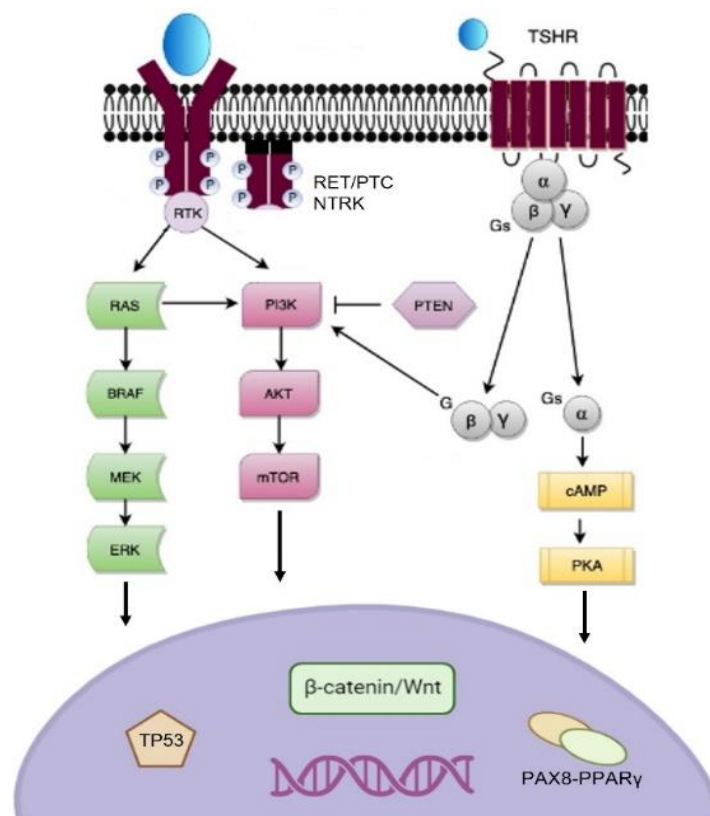


**Figure 2. Molecular pathogenesis of TC.** The molecular pathogenesis of TC involves dysregulation of the MAPK, PI3K/AKT and the cAMP signaling pathways. In TC, the



MAPK pathway is frequently activated due to point mutations of BRAF and RAS genes and RET/PTC and TRK rearrangements. The PI3K pathway is frequently activated due to point mutations of PI3KCA and mutation/deletion of PTEN. Modified from (20,25). BRAF or RAS gene mutations are found in mutually exclusive modality in nearly 70% of PTCs (26). In particular, BRAF is a serine/threonine protein kinase that is activated by RAS, and promotes the phosphorylation and activation of MAPK kinase and other downstream effectors of the MAPK signaling pathway. In TC, the most frequent point mutation of this protein is BRAF T1799A which results in a valine-to-glutamate replacement at residue 600 (Val600Glu) inducing a constitutional activation of the protein (27). RAS is a family of GTP-binding proteins that is located at the inner surface of the cell membrane and transmit signals arising from tyrosine kinase receptors (RTKs) along the MAPK and PI3K-AKT pathways. Four different but related proteins H-Ras, N-Ras, K-Ras4A, and K-Ras4B, encoded by HRAS, NRAS and KRAS respectively, are fundamental in controlling cell growth, differentiation and survival. Mutations occurring in codons 12, 13 and 61 of the RAS genes lead to a constitutive activation of RAS signaling. In TC, RAS mutations are found in 40–50% of FTC pathogenesis, with NRAS codon 61 and HRAS codon 61 mutations as most common (28).

Alterations in the effectors of the PI3K-AKT pathway are fundamental for the progression of FTCs: in this case, the hyperactivation of the pathway is mainly due to deletions of *PTEN*, a major human tumor suppressor, and genomic copy gain of *PIK3CA*. This last event associates with increased expression of the protein and activation of downstream effectors including AKT (29). Advanced TCs such as PDTCs and ATCs frequently have additional genetic alterations which may be responsible for TC progression toward a less differentiated and more aggressive phenotype (30). These events include mutations in genes coding for effectors molecules of the PI3K-AKT pathway, as well as mutations of *TP53* and *CTNNB1* genes. Point mutations of *TP53* gene lead mostly to loss of function of p53 cell cycle regulator, while mutations in *CTNNB1* gene affect the function of  $\beta$ -catenin, which is known to be involved in cell adhesion and Wnt signaling pathway. Both mutations are frequently reported in ATCs (31).

Other common mutational events in TC are chromosomal rearrangements such as *RET/PTC*, *NTRK* and *PAX8/PPAR $\gamma$* . *RET/PTC* rearrangement, usually found in PTCs, consists in the fusion of a portion of *RET* gene, that encodes for an intact tyrosine kinase domain of RET protein, to the active promoter of another gene that drives the expression of RET/PTC protein. The result of this rearrangement

is known to constantly stimulate and hyperactivate the MAPK signaling pathway, thus promoting tumorigenesis in thyroid cells (32). Another chromosomal rearrangement that occurs in PTCs involves the *NTRK1* gene. Recently, *NTRK* fusions have been reported in some series of advanced cancers and have been proposed as novel targets of cancer therapy (33). Finally, *PAX8/PPAR $\gamma$*  is characterized by the fusion of a portion of the *PAX8* gene, a member of the paired-box family of transcription factors, and the *PPAR $\gamma$*  gene, a member of the nuclear receptor family of transcription factors. This rearrangement results in the overexpression of the *PAX8/PPAR $\gamma$*  protein and is usually found in FTCs (31,34). Quite recently, *TERT* promoter mutations have been described in all the histological TC types. *TERT* encodes for the telomerase reverse transcriptase, and two hotspot genetic alterations have been reported in its promoter (C228T and C250T) (35,36). These mutations are known to stimulate telomerase activity and to promote the maintenance of telomere length in tumor cells, induce oxidative stress, sensitivity to TKI and were found in 12% of PTCs and in 14% of FTCs (37), where they are associated with increased tumor aggressiveness and worse prognostic expectations (38). Moreover, the presence of *TERT* mutations together with driver mutations like *BRAF* or *RAS* (39) is particularly frequent in advanced TCs: 33-40% of PDTCs and 43-73% of ATCs are found to carry a *TERT* promoter mutation, leading to an increased risk of distant metastasis (39). The distribution and frequency of known somatic mutations among the different TC histotypes is reported in Figure 3.

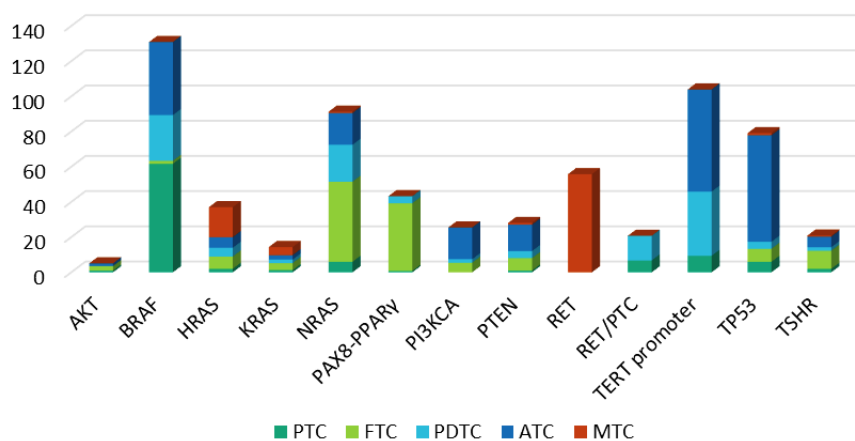


**Figure 3. Distribution and frequency of known somatic mutations in the different histotypes of thyroid cancer.** Data adapted from Prete et al (26).

#### 1.4 Thyroid cancer conventional and new therapeutic approaches

The treatment of DTCs patients relies first of all on prognostic classification, where two risk end points are used: one is the risk of cancer-related death assessed by TNM classification, and the second is the risk of recurrence estimated by the American Thyroid Association (ATA) risk stratification (40). According to the ATA risk stratification for DTCs (41), patients are classified as being at low (<5%), intermediate (5-20%) or high (>20%) risk of recurrence, and more than 80% of patients are classified as being at low risk. The general treatment of DTCs for low-risk and intermediate-risk patients is mainly based on surgery and radioactive iodine [(RAI), <sup>131</sup>I] treatment. Surgery can include lobectomy or total thyroidectomy, and therapeutic neck lymph node dissection in patients that present also lymph node metastases. Following surgery, <sup>131</sup>I administration (also called ablation) can be used to destroy residual thyroid tissue, non-identified remaining pathological tissues and/or known residual or recurrent disease (41–43). Since it is known that circulating TSH can stimulate cells proliferation in normal thyrocytes and in most of TC cells (44), the treatment with TSH suppressors, like Levothyroxine, after surgery can significantly reduce recurrence and tumor-related mortality in patients with DTCs (44). The therapeutic approaches for PDTCs and ATCs must be as tempestive as possible, since these tumors are very aggressive and the progression is extremely rapid. Conventional therapies for the treatment of these tumors include surgery and chemotherapy, often with concurrent radiotherapy. Cytotoxic therapy with doxorubicin, paclitaxel and docetaxel alone or in combination with cisplatin or carboplatin used for other neoplasms is not very effective for the treatment of UTCs, giving considerable side effects and minor clinical responses (45,46). In the last years, novel drugs targeting specific thyroid oncogenes like RET and c-Met and/or growth factors involved in TC pathogenesis like vascular endothelial growth factor (VEGF), epidermal growth factor (EGF), fibroblast growth factor (FGF), have been developed. These drugs belong to the category of tyrosine kinase inhibitors (TKIs), since their target are genes associated with the family of tyrosine kinase (TK) receptors (47). With regard to TC, the ideal inhibitors are those that are able to specifically prevent the oncogenic signaling pathways such as those activated by *BRAF*, *RAS* and *RET/PTC* mutations. Nevertheless, this

approach might not be sufficient for the treatment of many TCs, and combination therapy to block multiple pathways may be necessary to enhance their therapeutic efficacy (48). During the past decades, immunotherapy has become an important way of treatment for many tumors, including ATCs (49,50). It is well known that tumor progression is supported by the interactions of tumor cells within the different components of the tumor microenvironment (TME). In particular, the ability of tumor cells to escape the immune surveillance within the TME led the immune system to be considered a new promising therapeutic target. A negative correlation between thyroid differentiation and immunosuppressive markers such as programmed death-ligand 1 (PD-L1) and cytotoxic T lymphocytes antigen-4 (CTLA-4) has been described in TC (51). In particular, tumors cells that show PD-L1 expression inhibit T cells activation in the tumor microenvironment, thus protecting thyroid tumors cells from the immune response. These markers were also highly expressed in BRAFV600E mutated tumors compared to wild-type tumors (51). The combination of anti-PD-L1 antibody and PLX-4720, a BRAFV600E inhibitor, reduced tumor growth and increased the presence of NK cells, FoxP3+ Tregs (T regulatory cells) and CD8+ cytotoxic T cells, thus observing an induction of the immunosuppressive TME (52).

## **2) HETEROGENEITY OF SOLID TUMORS AND THE ROLE OF CANCER STEM-LIKE CELLS**

### **2.1 Thyroid cancer carcinogenesis models**

Throughout the years, different carcinogenesis models have been reported to describe TC origin. According to the classic multistep carcinogenesis model, TC cells arise from the gradual accumulation of genetic alterations within normal thyroid epithelial cells, leading to uncontrolled proliferation and invasive phenotype. Thus, PTC and FTC are the result of randomly occurring genetic alterations, such as *BRAF* and *RAS* or *RET/PTC* and *PAX8/PPARY* rearrangements. The sequential accumulation of further genetic alterations, particularly the inactivating mutations of TP53 and CTNNB1, can give rise to ATC.

These events are associated to a dedifferentiation process that occurs as the tumor cells acquire the neoplastic phenotype, with a marked epithelial to mesenchymal transition (EMT), a process that finally results in cancer stem-like cells (CSCs) phenotype acquisition (53,54). However, this model (Figure 5 A) has some intrinsic limitations: the introduction of large scale genome sequencing techniques revealed that PTC and FTC already have much more complex genetic alterations than what the classical multistep model can explain (55). In 2005, Takano et al. (56) proposed that TC cells are derived from normal stem cells or precursor cells of fetal origin that survive in the mature gland rather than from differentiated thyroid follicular cells. According to this model (Figure 5 B), normal fetal thyroid stem cells, which express oncofetal fibronectin but none of the markers typical of differentiated thyroid cells, give rise to ATC. Thyroblasts, which express both oncofetal fibronectin and the differentiation marker thyroglobulin (Tg), give rise to PTC. Finally, prothyrocytes, the more differentiated cell type, should give origin to FTC and follicular adenoma (56,57). However, in this model there is no explanation on how quiescent thyroid stem cells acquire the different genetic alterations, and about the coexistence of cellular subpopulations with different degree of differentiation. The evidence that cancer cell population is heterogeneous and that molecular alterations are not present in the whole tumor bulk finally brought to the CSCs or Tumor Initiating Cells (TICs) hypothesis for TC tumorigenesis (Figure 5 C). This hypothesis was firstly established by the previous observation that leukemia may contain hierarchical multi-lineage cells (58). In this perspective, only a subset of tumor cells that possesses high tumorigenic activity and increased self-renew ability can produce progenitor cells able to reconstitute and sustain tumor growth (59). According to this view, CSCs may originate from either normal stem cells through a transformation process or from differentiated tumor cells as the result of a dedifferentiation process (58).

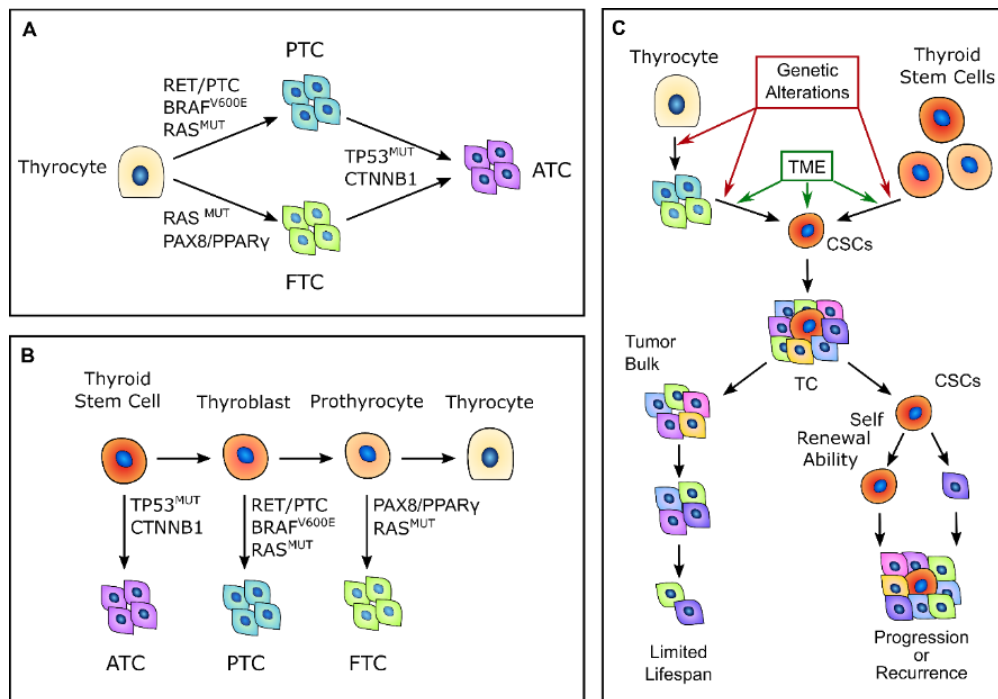


**Figure 4. TC carcinogenesis models.** (A) Multistep model: a progressive accumulation of somatic genetic alterations give rise to step-by-step dedifferentiation process from mature thyrocytes, to DTCs and finally to PDCs and ATCs. Mutations in driver genes such as BRAF and RAS or RET/PTC and PAX8/PPAR $\gamma$  rearrangements give rise to PTCs and FTCs, while the acquisition of TP53 and CTNNB1 mutations leads to the transformation in PDCs and ATCs. (B) Fetal model: TC cells derive from fetal thyroid cells such as thyroid stem cells, thyroblasts and prothyrocytes, that acquire transforming mutations which may give rise to ATC, PTC and FTC, respectively. (C) CSCs model: CSCs with high self-renewal and tumorigenic abilities originate from either normal thyroid stem cells through a transformation process or from dedifferentiation process of differentiated tumor cells, that acquire CSCs characteristics. Adapted from (60).

## 2.2 Thyroid cancer heterogeneity and the role of tumor microenvironment

In the last years TC heterogeneity has emerged as a critical aspect for further explain the tumorigenic potential and aggressiveness of the most undifferentiated forms of TC. Not surprisingly, the CSCs or TICs model is based on the presence of cellular subpopulations with different genetic profile, proliferative and/or differentiation ability, metastatic potential, and therapy resistance. These features that can be observed within the tumor bulk refer to a subclonal diversity that is defined in literature as intratumoral heterogeneity (ITH) (61). The bidirectional

and dynamic interactions between tumor cells and their microenvironment, consisting of stromal cells, that constitute the cellular part, and extracellular matrix (ECM) components (collagen, fibronectin, laminin), that constitute the non-cellular part, is essential to stimulate and maintain the ITH (62). In this complex landscape, TICs survive predominantly in specific microenvironmental niches, the so-called stem cell niches, where the exchange of factors within the TME allows for the maintenance of a stem-like phenotype (Figure 5). This phenotype is characterized by quiescence, slow-cycling rate, lack of tissue-specific differentiation, and theoretically unlimited self-renew abilities (63–65). TME actors are critical for the modulation of thyroid CSCs features. The principal regulators are the cancer associated fibroblasts (CAFs) and especially the matrix that is produced and secreted when they became reactive. CAFs can also release pro-stemness factors that may support tumor cells to acquire a stem-like phenotype, and already existing CSCs to maintain their survival and self-renew abilities (66). Moreover, a correlation between specific TC mutations and fibroblast activation in the TME have been reported in several studies. For instance, in this work by Xing M (67) the BRAFV600E mutation in PTC cells has been associated to a metastatic phenotype by regulating the TME and the ECM. In addition to the ECM, variations in the levels of oxygen and nutrients may also generate hypoxic and pseudo hypoxic niches, that further influence the adaptation to the changes of TME mainly through hypoxia-inducible factors (HIFs) activated pathways (68). Finally, also the immune cells components of the TME, grouped in the so-called immune niche, are crucial for the regulation of CSCs phenotypes, such as tumor-associated macrophages (TAMs), neutrophils and T lymphocytes. Indeed, immune cells inside the TME may promote pro-tumorigenic processes thanks to the secretion of several cytokines and chemokines that can contribute to the survival of tumor cells, particularly those with a stem-like phenotype (69).

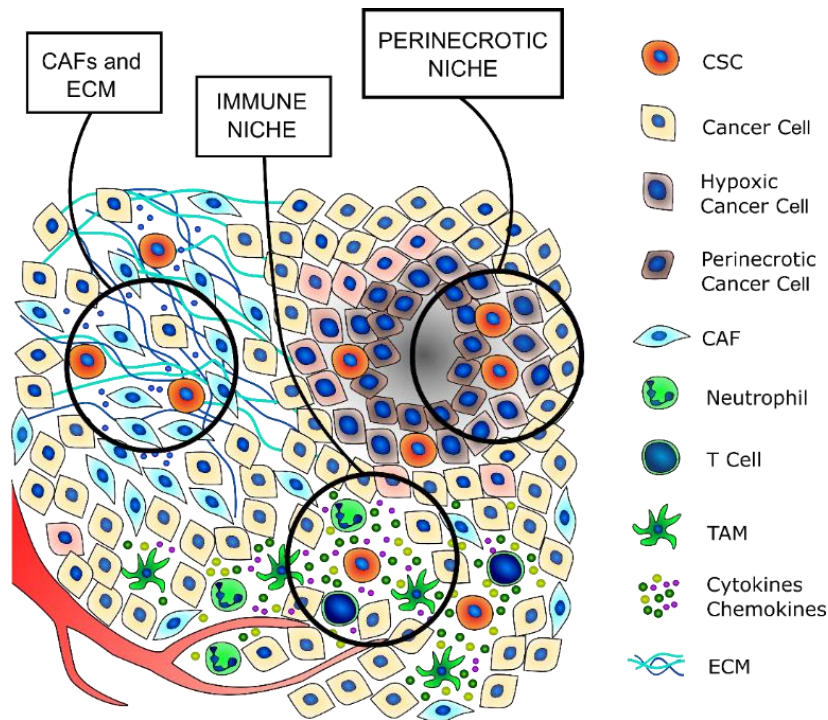


**Figure 5. Stem cell niche in TC.** CSCs are mainly present in the stem cell niches, tumor areas with specific microenvironmental conditions that are fundamental for promoting and supporting the survival and self-renewal abilities of already existing CSCs. To ensure that, a thick extracellular matrix (ECM) and pro-stemness soluble factors are secreted by cancer-associated fibroblasts (CAFs); a wide variety of cytokines and chemokines are secreted by different immune cells (T cells, neutrophils and tumor-associated macrophages, TAMs) in the immune niche, to support the maintenance of the stem-like phenotype; the induction of hypoxia-inducible factors (HIFs) in the hypoxic niche regulate the maintenance of CSCs subpopulation by enhancing the stem-like phenotype of undifferentiated tumor cells. Adapted from (60).

### 2.3 Normal Stem Cells and Cancer Stem-like Cells

The characterization of normal stem cells and CSCs in solid tumors in general, and in TC as well, is fundamental to understand the involvement of CSCs in development of tumor progression and eventually therapy resistance. CSCs display two main features, occurring also in normal stem cells: self-renewal, which consists in the capacity of a cell to generate daughter cells that presents stem-like properties and phenotypes, and pluripotency, which is the ability to differentiate into specialized cells, and, in case of tumor stem cells, to give rise to an heterogenous cell population (70). The self-renewal abilities of stem cells is a



crucial feature for the maintenance of a cell lineage with the same characteristics, and two different cell division processes may occur to guarantee this stem cells property: one is the symmetric division, that gives rise to two identical daughter cells with stem cell properties, and the other one is the asymmetric replication, that gives rise to one daughter cell identical to the mother and the other daughter cell undergoing a differentiation process (71,72). In this context, these properties of stem cells are influenced by the surrounding microenvironment that may affect the survival of these cells (71). It is well known that conventional anti-cancer treatments are usually able to kill tumor cells that are proliferating and well differentiated, but they fail in eradicating the slow-dividing subpopulation of CSCs, bringing to eventual tumor progression. Indeed, CSCs that develop resistance to anti-cancer drugs are considered the main responsible for metastatic spread and tumor relapse (73–75).

## **2.4 Identification of putative thyroid CSCs**

The presence of thyroid CSCs is confirmed in literature by several studies that were able to characterize these cells by precise *in vitro* and *in vivo* assays (e.g. clonality assays and tumor grafts), variations of enzymatic activities, expression of well-known stemness markers and expression of membrane markers. Nevertheless, there is still the lack of a standardized method to accurately identify them. Several *in vitro* assays can be applied to demonstrate the ability of putative CSCs to self-renew such as limiting-dilution assay, serial colony formation and differentiation assay, or the 3D sphere formation assays. Among them, the 3D sphere assay is probably the best approach to determine the clonality and multipotency of putative CSCs in the thyroid (59,76) since the ability to generate spheres in a specialized serum-free medium, even after several passages, may suggest the presence of cells with a strong self-renew ability. Differently from the classical monolayer cultures, the 3D sphere organization improves intercellular contacts and usually display low levels of oxygen and metabolites creating an hypoxic core that resembles the hypoxic niche occurring in solid tumors (77). Moreover, this model can be applied for better characterization of a EMT, that is strongly implicated in cancer progression (78–81). Indeed, the phenotypic and functional properties of tumor cells in transition between the epithelial and

mesenchymal status can be explored through 3D spheres, that provide an adequate environment for mimicking the solid tumor of origin. With respect to TC, Lan et al. (82) observed that the majority of ATC cells show an EMT phenotype and observed that the content of CSCs in the ATC cell population directly correlates with the presence of EMT. Nevertheless, the most complete way to evaluate the presence of possible CSCs is to inject these cells into immunocompromised mice to validate the ability of these cells to develop tumor over time (77). The identification of long-term tumorigenic potential and self-renew ability of these cells can be defined by serial transplantations of cells isolated from secondary and tertiary xenografts, and the combination of the serial transplantations with limiting-dilution assays can determine the number of CSCs required for the generation of the tumor (79).

A well-known approach for the identification of putative CSCs in TC is the evaluation of aldehyde dehydrogenase (ALDH) enzymatic activity, since is known that high levels of ALDH activity are observed in stem and progenitor cells and appear to be related to their resistance to anti-cancer drugs. Todaro et al. (83) isolated CSCs from primary TCs by evaluating ALDH activity, and observed that the PTC, FTC and PDTC expressed a small population of cells (1.2-3.5% of the whole tumor bulk) that was ALDH high and was able to generate 3D spheres when expanded *in vitro*. Moreover, these cells were able to create sequential tumor xenografts in immunocompromised mice (83).

A crucial aspect for the identification of putative thyroid CSCs is the ability of these cells to escape the killing mechanism of conventional chemotherapy and radiotherapy, causing the relapse of the disease, and many mechanisms can be applied by CSCs to induce therapy resistance. One of them is the ability of CSCs to induce drug export (65), and this ability can be demonstrated through the side population (SP) assay. This assay identifies a small subpopulation of cells that is able to exclude the DNA binding dye Hoechst 33342 through the ATP binding cassette (ABC) family of membrane transporters (65). Another mechanism is also represented by bypass pathways that respond to the therapeutic activity. In the context of TC, Gianì et al. (84) observed that the treatment of mutant BRAFV600E whole thyroid cancer cell population by Vemurafenib induced a decrease of ERK phosphorylation and inhibition of cell growth, but induced a re-activation of ERK and increased AKT activation in a subpopulation of potential CSCs. They also

noted that this resistance of thyroid CSCs was depending on the higher MAP3K8 expression as an alternative pathway to elude Vemurafenib activity (84). Another important feature of putative CSCs is that they display dysregulated signaling pathways and abnormal phenotypes. Among the dysregulated pathways there are Wnt/ $\beta$ -catenin, Hedgehog, JAK/STAT and Notch signaling, which are all involved in self-renew ability of normal stem cells (85–87). The alteration of these pathways consequently modulate the downstream effectors, including transcription factors, and is also related to an improved EMT and resistance to anti-cancer drugs (87). Several transcription factors have been reported to be expressed in cancer cells with stem-like properties. Of them, octamer-binding transcription factor 4 (OCT4), sex-determining region Y-box 2 (SOX2), Nanog and C-myc, comprise a well-known fundamental regulatory network for stemness maintenance and self-renewal (88,89).

Similar to these transcription factors, many surface markers that are highly expressed in stem cells are also expressed in several human cancers (breast, colorectal, pancreatic, lung cancer, ovarian and prostate cancer, hepatocellular carcinoma) such as ALDH 1 Family Member A1 (ALDH1A1), Epithelial Cell Adhesion Molecule (EpCAM), CD13, CD24, CD44, CD166, CD133, CD117/c-kit, CD138. These surface markers are less studied and characterized in TC, but some of them have been identified throughout the years. A possible CSCs marker is CD133, also called prominin-1, a transmembrane glycoprotein that acts as a stemness marker both in normal and cancer cell that has been evaluated by Tseng et al. (90) in the context of TC. The authors evaluated both ATC primary tumors and ATC cell lines and were able to isolate CD133+ cells, noticing that these cells also expressed typical stemness-associated genes such as POU class 5 homeobox 1 (*POU5F1*), *SOX2* and *NANOG1*, as well as drug resistance-associated genes such as ABC subfamily G member 2 (*ABCG2*), multi-drug resistance mutation 1 (*MDR1*), and multi-drug resistance-associated protein (MRP). They also observed that these cells were resistant to anti-cancer drugs and were able to generate 3D thyrospheres in *in vitro* system and tumors in *in vivo* system. The identification of cell surface markers such as CD44 and CD24 is a further confirm that cells expressing these markers, especially in the combination of CD44<sup>+</sup>/CD24<sup>-</sup>, are potential CSCs. Concerning TC, Ahn et al. (91) identified CD44 and CD24 expression in a small population of cells with

tumorigenic potential in PTC human primary samples and cell lines. In particular, they observed elevated levels of CD44 but no expression of CD24 (CD44+/CD24- phenotype) in a subset of cells, together with high expression of stem cell markers POU5F1 and OCT4 and low expression of thyroid differentiation markers (91). Quite recently, Shimamura et al. (92) performed a comprehensive study where they characterized the expression of a panel of markers (ALDH activity, CD13, CD15, CD24, CD44, CD90, CD117, CD133, CD166, EpCAM) among eight TC cell lines. In this study they identified ALDH activity and EpCAM expression (ALDH<sup>pos</sup>/EpCAM<sup>high</sup>) in a subpopulation of cells as reliable candidates to spot thyroid CSCs, indeed these cells showed higher sphere-forming efficiency and both self-renew and differentiation ability. EpCAM has already been defined as a CSCs marker in many solid tumors where its possible role in tumor progression and aggressiveness has been described (93–95). However, this protein is poorly studied in TC and its role in TC pathology, especially in the undifferentiated forms, needs further comprehension.

### **3) EPITHELIAL CELL ADHESION MOLECULE (EpCAM)**

#### **3.1 EpCAM: general features and protein structure**

Human epithelial cell adhesion molecule (EpCAM; CD326), also called TROP-1, is a type 1 transmembrane glycoprotein of approximately 40 kDa that was first discovered years ago during monoclonal antibody screening against antigens derived from colorectal cancer cells (96). EpCAM structure and role have been studied in a wide-variety of human tumors and normal epithelia and has been investigated as a potential marker for diagnosis, prognosis and therapeutic application in epithelial tumors due to its overexpression and its location at the cell surface (95). The EpCAM gene (*EPCAM*) is conserved in many species including mouse, rat and zebrafish, and the protein seems to be highly conserved among higher vertebrates (97). The protein aminoacidic sequence has been described in 1989 (98), a single transmembrane protein of 314 amino acids (aa), characterized by a large extracellular domain of 265-aa, a single-spanning hydrophobic transmembrane domain of 23-aa and a short hydrophilic intracellular

domain of 26-aa (C-terminal). The extracellular domain of the protein (EpEx) comprises the aminoacidic sequence from Gln24 to Lys265, since the very short stretch of signal peptide (Met1-Ala23), localized at the N-terminal of EpCAM, is cleaved during synthesis (95). The domain also contains an EGF-like small domain, called EpCAM motif-1 and formed by cysteine rich residues (12 cysteines), followed by a motif that resembles the thyroglobulin (TY) type 1A domain, suggested by the assignment of intramolecular disulphide bonds, and a cysteine-poor residue (99). Moreover, the protein contains three N-glycosylation sites and the differential glycosylation may cause differences in the function of EpCAM in healthy and malignant tissues (100). Following the transmembrane domain, which is involved in the association with the protein Claudin-7, member of tight junctions (101), there is the cytoplasmic domain of EpCAM, also called EpCAM cleaved intracellular domain (EpICD). This small domain presents a couple of  $\alpha$ -actinin binding sites which are apparently critical for EpCAM localization at cell-cell interaction sites and thus for the adhesion properties of the protein (102). Finally, the last three aa of the EpICD can interact with multi-PDZ domain proteins that are essential for complex formation with signaling or structural proteins (97).

### **3.2 EpCAM-mediated signaling: role in cell-cell adhesion and proliferation**

Early studies on EpCAM (103) suggested that this molecule can induce  $\text{Ca}^{2+}$ -independent cell-cell adhesion by interacting with other EpCAM molecules on near cells to promote an homophilic interaction in cells that normally lack cell-cell interactions, and that the expression of the protein in EpCAM negative cells can induce cells aggregation and the generation of cell-cell contacts. Balzar et al. (104) have demonstrated that both EpEx and EpICD may contribute to cell-cell adhesion: they observed that all the EpEx motifs are required for the creation of homophilic intermolecular binding and EpCAM accumulation at cell-cell adhesion sites, and that the EpICD fragment can mediate cell adhesion through the association with the actin cytoskeleton via  $\alpha$ -actinin (104,105). Nevertheless, EpCAM expressing cells are only lightly interconnected and EpCAM itself is a relatively weak cell-cell adhesion molecule when compared to E-Cadherin (103,106). When co-expressed with E-Cadherin, EpCAM is able to weaken E-

cadherin-mediated adhesion by disturbing E-Cadherin connection with the cytoskeleton (106). In addition, EpCAM is also involved in the regulation of epithelial integrity by influencing the composition and functionality of tight junctions, through interaction with claudins, especially with claudin-7 (107). The multiple cellular functions of EpCAM may depend on the tumor type and localization, and differently affect single cells within tumors (108). Numerous *in vitro* and *in vivo* studies showed that overexpression of EpCAM can induce cell proliferation (109,110) while downregulation of the protein decreases cell proliferation (111). The upregulation of the oncogenic transcription factor c-Myc and cell cycle-related proteins cyclin A and E, and a direct effect on cyclin D1 at transcriptional level has been observed after stimulation of EpCAM expression in some *in vitro* models (110).

### **3.3 EpCAM-mediated signaling by regulated intramembrane proteolysis (RIP)**

In literature is reported that the mechanism of human EpCAM-induced proliferation in tumor cells involve a process called regulated intramembrane proteolysis (RIP), firstly described in EpCAM by Maetzel and colleagues (112). This process is an evolutionarily conserved event that implies the shedding of the extracellular domain of a ligand, usually upon induction, and the consecutive release of the intracellular domain (ICD). Of note, both the extracellular and intracellular part are able to activate signaling events (112). EpCAM is subjected to an intense RIP process mainly due to the activity of the metalloprotease ADAM17 (also known as tumor necrosis factor-alpha-converting enzyme, TACE) and  $\gamma$ -secretase containing presenilin-2 (PS-2), at the level of the plasma membrane. The cleavage of ADAM17 occurs between Asp241/Gln246 residues and is mainly responsible for the shedding of EpEx into the extracellular space, which in turn may act as a ligand for non-cleaved EpCAM to promote homophilic interaction and induce RIP (112). In head and neck cancers, the EpEx domain seems also to act as a ligand for EGFR, stimulating ERK and AKT pathways (113). However, this connection promoted proliferation but antagonized the normal EGF-dependent activation of EMT-associated factors, and raised some questions regarding the involvement of full length EpCAM in the binding to EGFR

and whether this may establish an autocrine, paracrine or juxtacrine signal (113). After the first cleavage step by ADAM17, the EpICD is then cleaved by  $\gamma$ -secretase and released into the cytoplasm where it binds  $\beta$ -catenin and four and a half LIM domains protein 2 (FHL2). This complex can then translocate into the nucleus, where it associates with lymphoid enhancer binding factor-1 (LEF-1), and bind to promoter regions of regulators of cell division (110), genes involved in regulation of EMT-associated events (114), and pluripotency genes (115). The cleavages of  $\gamma$ -secretase/PS-2 complex may occur in different sites: between Val273/Val274, Val274/Val275 and Val275/Val276 residues, and between Val284/Val285 and Leu286/Val287 residues. Nevertheless, in recent years several additional cleavages have been identified, suggesting that EpCAM signaling may be regulated through different proteolytic pathways, not exclusively by RIP. Schnell et al. (116) described the presence of C-terminal fragments (CTFs) with distinctive molecular weight that could be generated by the activity of other membrane-associated proteases rather than by  $\gamma$ -secretase itself, without necessarily induce EpEx shedding. Another example is the cleavage made by another protease called  $\beta$ -secretase (also known as  $\beta$ -site amyloid precursor protein-cleaving enzyme, BACE), that is responsible for EpCAM cleavage at position Tyr250/Tyr251 of the extracellular domain of EpCAM. This protease has an optimal activity at pH 4 and is effective in the endosomal/lysosomal compartment (117). Moreover, since tumor microenvironment tends to be acidic, the extracellular shedding of EpCAM by BACE is feasible.

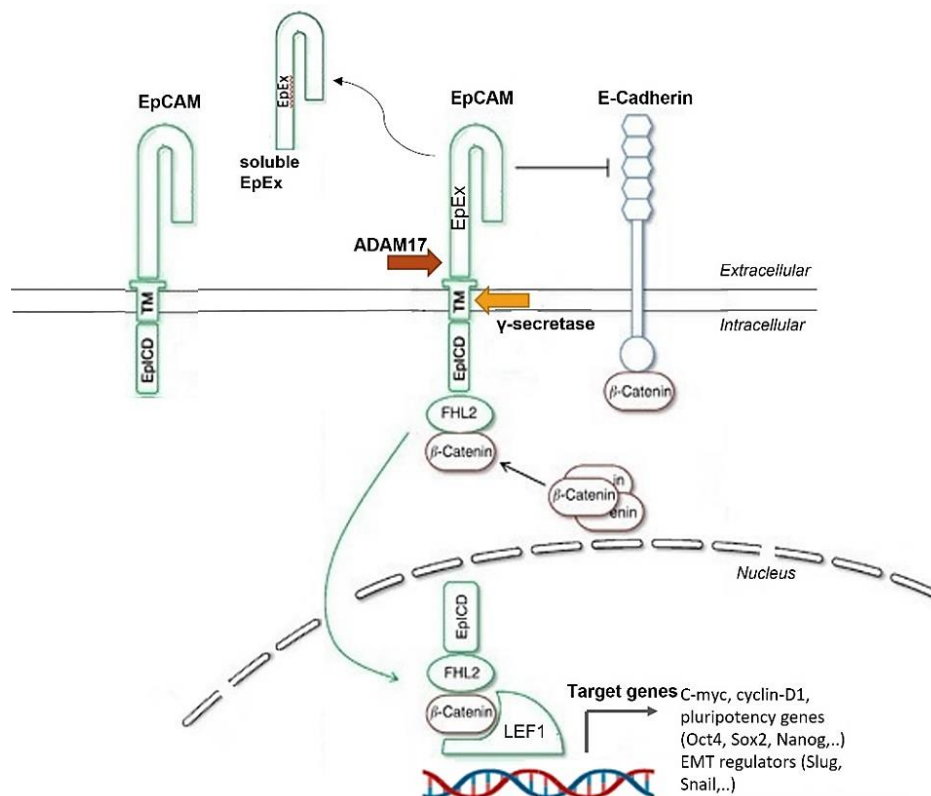


**Figure 6. EpCAM and regulated intramembrane proteolysis (RIP).** EpCAM full length is cleaved by ADAM17 inducing the release of EpEx in the extracellular domain. Soluble EpEx may in turn interact with other EpCAM molecules, inducing RIP. EpCAM intracellular domain (EpICD) is released in the cytoplasm after  $\gamma$ -secretase cleavage. EpICD associates with FHL2 and  $\beta$ -catenin and translocate into the nucleus, promoting the transcription of target genes through binding to LEF-1 consensus sites. EpCAM may also weaken E-Cadherin-mediated cell adhesion by interrupting the link between E-Cadherin and the actin cytoskeleton. This may in turn result in increased availability of non-bound  $\beta$ -catenin that may be stabilized by association with EpICD. Modified from (97,118).

### 3.4 EpCAM role in health and disease

In adult normal tissues, EpCAM is expressed in many organs and glands, with the highest expression occurring in colon, but the level of expression is quite variable among the different tissues. The protein is not detected in bone marrow-derived and lymphoid-derived cells, in mesenchymal, muscular and neuroendocrine tissues (119,120), and is more expressed in proliferating cells respect to differentiated cells in several tissues (119). EpCAM can regulate



adhesive properties between cells and cell-matrix, even if its overexpression can induce a negative effect on the strength of adhesion properties mediated by E-cadherin (106). EpCAM can be also found in stem/progenitor cells of different tissues such as the intestinal epithelium or the liver: hepatocytes, indeed, are EpCAM-positive during embryonic liver development, whereas in adults the protein is only expressed during liver regeneration in cells with a precursor/stem-like phenotype (121). Moreover, in undifferentiated human embryonic stem cells (hESCs), EpCAM is co-expressed with several pluripotency markers (122,123). The expression of EpCAM is strongly increased in many tumors of epithelial origin compared to normal epithelia of the same localization, supporting tumor growth and progression. EpCAM has been evaluated as a potential prognostic marker based on its strong expression, but its prognostic value and association with a specific clinical outcome may be different depending on the origin of the tumor and/or the stage of tumor progression. High expression of EpCAM usually correlates with poor prognosis, since it can promote proliferation and tumor/metastatic development, e.g. in pancreatic (124), colorectal (125), breast (126), ovarian (127) and prostate cancer (128). On the contrary, high levels of EpCAM expression are associated with an increased survival and better prognosis for renal (129), head and neck (130) and thyroid cancer (131). However, the cleavage rate of the protein was not evaluated in these studies, but only its expression. Indeed, Ralhan and colleagues (132) applied an antibody targeting the EpICD fragment for the evaluation of EpCAM cleavage at immunohistochemistry on healthy and pathological patient-derived tissue samples of different histotypes of TC. They observed that nuclear/cytoplasmic staining of the EpICD fragment correlates with the aggressiveness of TC and overall patient survival. Moreover, this nuclear/cytoplasmic staining was found in tumor tissues rather than normal tissues, where the expression of EpCAM was mainly membranous (132–134). Moreover, the role of EpCAM in promoting or counteracting processes like EMT is still not entirely clear and needs further investigation since opposite situations are widely described in literature in different epithelial tumors. As an example, Sankpal and colleagues (135) observed that the expression of EpCAM was diminished after the activation of ERK pathway in primary tumor samples and in cancer cell lines (breast cancer). In particular, they observed a double-negative feedback loop between EpCAM

and ERK2, where the latter was able to block EpCAM transcription by directly binding to its promoter region or indirectly by inducing the activation of EMT-associated factors. On the other hand, they also noticed that EpCAM itself was able to modulate ERK, by blocking its activation and thus inhibiting EMT (135). In other epithelial tumors, such as colon cancer, the expression of EpCAM improved the transcription of stemness and reprogramming factors genes such as c-Myc, Oct4, Sox2 and Nanog, and the EMT-associated factors Slug and Snail, via intracellular EpICD signaling (136). Tumor cells with stem-like properties and tumor cells with tumor-initiating abilities are also found to be enriched with EpCAM, thus classifying this protein as potential CSC marker in different tumors (136–138). These observations also deal with the fact that EpICD fragment may be necessary for the maintenance of the stem-like phenotype in these cells, being associated with the downstream effectors of the Wnt pathway, such as  $\beta$ -catenin and LEF-1, when it moves into the nucleus. Therefore, novel therapeutic strategies could be developed to further counteract tumor aggressiveness and progression by specifically targeting or removing EpCAM-expressing tumor cells, especially those with a stem-like phenotype.

## **Aim of the thesis**

The mechanisms responsible for insensitivity to therapeutic treatments, tumor aggressiveness and tumor relapse described in PDTC and ATC patients haven't been fully elucidated yet. Nevertheless, it is known that TC displays a certain degree of intra-tumoral heterogeneity within the tumor bulk, highlighting the coexistence of cellular subpopulations (normal cells, tumor cells, CSCs or TICs) with distinct proliferative capacities and differentiation abilities. In particular, CSCs or TICs give rise to progenitor cells that may drive tumor growth and their presence is fundamental for the maintenance of the malignant phenotype and eventual development of therapy resistance. As a consequence, a comprehensive understanding of how to specifically isolate and target this subset of tumor cells is necessary.

This project is focusing on investigating the biology of putative thyroid TICs and observe their sensitivity to anticancer drugs, applying both classical monolayer cultures and 3D spheres cultures on PDTC and ATC-derived TC cell lines, in order to get more understanding of the pathogenesis of undifferentiated TCs. In particular, *in vitro* studies include:

1. Characterization of TC cell lines-derived 3D spheres to establish if the 3D model is a valid *in vitro* approach to study the expression and role of EpCAM as a potential TICs marker for undifferentiated TCs. EpCAM was mainly studied through Western Blot and Immunofluorescence on patient-derived tissue samples, 2D adherent cell cultures and 3D spheres cultures.
2. Observation of TC cell lines response to treatment with a well-known anticancer drug, currently used in clinical setting, through MTT assay performed on both 2D adherent cell cultures and 3D spheres cultures, to evaluate whether cells respond differently when treated as adherent cells or as 3D sphere

# **Materials and Methods**

## REAGENTS

- Euroclone: Trypsin-EDTA Solution 1X, L-Glutamine 100X 200 mM, Penicillin-Streptomycin (P/S) Solution 100X, RPMI 1640 w/o L-Glutamine, Dulbecco's Phosphate Buffered Saline (PBS) w/o Ca<sup>2+</sup> and Mg<sup>2+</sup>.
- Gibco: Fetal Bovine Serum (FBS), Dulbecco's Modified Eagle Medium (DMEM) w/ 4.5 g/L D-Glucose and pyruvate, DMEM/F12 (1:1) Nutrient Mixture (Ham), Opti-MEM™ (w/o phenol red).
- MedChem Express: MTT (3-(4,5-Dimethyl-2-thiazolyl)-2,5-diphenyl-2H-tetrazolium).
- Roche: PhosSTOP EASYpack phosphatase inhibitor and cOmplete EASYpack protease inhibitor.
- SigmaAldrich (Merck Millipore): PBS tablets, Poly(2-hydroxyethyl methacrylate) (poly-hema), Amersham™ ECL™ Rainbow™ Marker - Full Range, Ponceau Staining (0,1% PonceauS (w/v) in 5% (v/v) acetic acid), Goat Anti-Rabbit IgG Antibody (H+L) HRP, Goat Anti-Mouse IgG Antibody (H+L) HRP, Triton™ X-100, poly-L-lysine solution (mol wt 150,000-300,000), ampicillin, TAPI-2, BACE and DAPT inhibitors.
- Thermo Fisher Scientific: B-27™ Supplement, BCA Pierce™ Protein Assay Kit, NuPage™<sup>®</sup> Antioxidant.
- Invitrogen (part of Thermo Fisher Scientific): NuPAGE™ MOPS SDS Running Buffer (20X), NuPAGE™ 10% Bis-Tris gels, iBlot Dry Blotting System, Donkey Anti-Goat IgG (H+L) Secondary Antibody HRP conjugate, Wheat Germ Agglutinin (WGA) Alexa-Fluor 594 Conjugate, Donkey anti-Rabbit IgG (H+L) Alexa Fluor™ Plus 488, Donkey anti-Rabbit IgG (H+L) Alexa Fluor™ Plus 555, Donkey anti-Mouse IgG (H+L) Alexa Fluor™ 555,

Donkey anti-Goat IgG (H+L) Highly Cross-Adsorbed Alexa Fluor Plus 488,  
PureLink™ HiPure Plasmid Filter DNA Purification Kit.

- Fisher scientific (part of Thermo Fisher Scientific): Corning™ membrane matrix Matrigel™
- Abcam: Anti-EpCAM Ab [E144] Rabbit Monoclonal, Anti-GFP Ab Rabbit Polyclonal, Anti-E Cadherin Ab [M168] Mouse Monoclonal, Recombinant Anti-Vimentin Ab [EPR3776] Rabbit Monoclonal.
- R&D: EpCAM/TROP-1 (AF960) goat polyclonal Ab.
- BD Biosciences: Purified Mouse Anti-Actin Ab-5.
- Selleckchem: Vemurafenib (PLX-4032).
- Venor®GeM Classic (Minerva Biolabs®).

## **1) PATIENTS AND SAMPLE COLLECTION**

The application of patient-derived tissue samples was performed after institutional review board approval (Ethical Committee of the Istituto Auxologico Italiano IRCCS #2018\_09\_25\_04) and informed consent for the use of thyroid tumor tissues was obtained from all participants. All methods were carried out in accordance with relevant guidelines and regulations (Declaration of Helsinki). Frozen thyroid tissues from 15 patients undergone total thyroidectomy were used for Western Blot and Immunofluorescence analysis. In particular, we studied 4 papillary (PTC), 3 follicular (FTC), 4 poorly differentiated (PDTC) thyroid cancers and 4 normal thyroid tissues. Patients are followed in a single tertiary care endocrine center and were diagnosed and treated according to the recent guidelines for the management of thyroid cancer during the period 2001–2020 (41,139). Tumors were classified and staged according to the thyroid malignancy World Health Organization classification and the 8th edition of TNM staging (140).

## **2) CELL CULTURES**

Poorly differentiated thyroid cancer cell lines (SW579, HTCC3, B-CPAP) and anaplastic thyroid cancer cell lines (FRO and SW1736) with different genetic drivers (141) used in the present study were kindly provided by Dr. I. Bongarzone (Istituto Nazionale dei Tumori, Milan, Italy). Human embryonic kidney 293T (HEK 293T) cell line was kindly gifted from Professor V. Silani (Istituto Auxologico Italiano, Milan, Italy) (Table 2). All cells were cultured as monolayers in 100 mm tissue-culture treated Petri dishes and kept in a humidified incubator at 37°C, 5% CO<sub>2</sub>, with medium change every 2-3 days. Cells were routinely split when reaching ~80% confluency. All cell lines were routinely screened for mycoplasma contamination with Venor<sup>®</sup>GeM Classic (Minerva Biolabs<sup>®</sup>).



| <b>Cell lines</b> | <b>Identification (Cellosaurus)</b> | <b>Culture medium</b>                     | <b>Histotype of origin</b> | <b>Key genetic drivers</b> | <b>Other</b>               |
|-------------------|-------------------------------------|---|----------------------------|----------------------------|----------------------------|
| <b>SW579</b>      | CVCL_3603                           | DMEM/F12 (1:1) with 10% FBS, 1% P/S       | PDTC                       | P53 I255S                  | -                          |
| <b>HTCC3</b>      | CVCL_1295                           | DMEM with 10% FBS, 1% P/S                 | PDTC                       | BRAFV600E                  | P53 P152L                  |
| <b>B-CPAP</b>     | CVCL_0153                           | DMEM with 10% FBS, 1% P/S                 | PDTC                       | BRAFV600E                  | P53 D259Y                  |
| <b>SW1736</b>     | CVCL_3883                           | DMEM with 10% FBS, 1% P/S                 | ATC                        | BRAFV600E                  | P53 silenced               |
| <b>FRO</b>        | CVCL_6287                           | RPMI with 10% FBS, 1% P/S, 1% L-Glutamine | ATC                        | BRAFV600E                  | P53 silenced, CDKN2A C238T |
| <b>HEK 293T</b>   | CVCL_0063                           | RPMI with 10% FBS, 1% P/S, 1% L-Glutamine | Human Embryonic Kidney     | -                          | -                          |

**Table 2. Cell lines.** Cell lines applied for the study, with histotype of origin and principal genetic alterations for each cell lines were adapted from Landa I et al (141).

### 3) TC CELL LINES-DERIVED 3D SPHEROIDS GENERATION

#### 3.1 Hanging-drop technique

This technique takes advantage of gravity to keep cells in suspension inside a drop, preventing them from adhering to a surface. To obtain the 3D spheres, cells were seeded at clonal density through serial dilutions (20 cells, 10 cells, 5 cells, 1 single cell per drop) in a volume of 33  $\mu$ l for each drop. The drops were directly spotted onto the inner surface of a 48-well plate lid, while all wells of the plate were filled with sterile H<sub>2</sub>O to ensure a humid environment to prevent the drying of drops. Cells were kept in a humidified incubator at 37°C, 5% CO<sub>2</sub> for 7-10 days, without medium changing, until 3D spherical structures appeared (Figure 7). 3D spheres were obtained after seeding cells in their appropriate culture medium or in Sphere Medium (DMEM/F12 (1:1) Nutrient Mixture (Ham) supplemented with human EGF (PeproTech EC) 20 ng/ml, human b-FGF (PeproTech EC) 20 ng/ml, and B-27™ Supplement 1:50 (Thermo Fisher Scientific) (142).

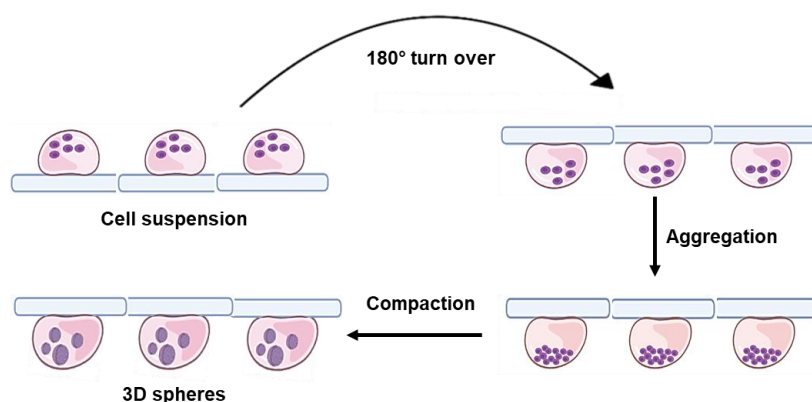


**Figure 7. Hanging-drop technique for the generation of 3D spheres when cells were seeded at clonal density.**

### **3.2 Non-adhesive substrate technique**

Poly(2-hydroxyethyl methacrylate) is an acrylic compound mainly used for inhibiting cell adhesion to growth surfaces first used in 1984 by Minnet and colleagues (143). In the present study, the protocol by McCaffrey et al (144) was applied: poly-hema was dissolved in 95% ethanol to a final concentration of 20 mg/ml by heating in a water bath at 65°C for 3/4 hours or until crystals were completely dissolved. Plates were then coated with different amount of poly-hema solution, depending on the well's diameter: for 6-well plates were used 700 µl per well, for 48-well plates were used 70 µl per well, while for 100 mm Petri dishes were used ~ 4 ml. Plates were dried under the sterile hood until the complete evaporation of ethanol, and subsequently exposed to UV for sterilization. Coated plates were stored at RT up to 1 year or indefinitely at 4°C. To obtain the 3D spheres, cells were seeded in their culture medium or in Sphere Medium at the desired concentration on top of the dried non-adhesive layer and left in a humidified incubator at 37°C, 5% CO<sub>2</sub> for 7-10 days until were obtained 3D spherical structures.

### **3.3 Light microscopy for 3D spheres dimensions and morphology**

Light microscopy images of TC cell line-derived 3D spheres were obtained by taking pictures with Leica MC 120 HD light microscope and Leica Microsystems camera at 5X magnification. Images were then used for further determination of 3D spheres morphology and for quantification of the area. An average of the measurements of the area of at least 7 spheres for each independent replicate was reported. The area of each sphere was calculated on Fiji Software applying the ellipses formula.

#### **4) CLONALITY ASSAY BY EXTREME LIMITING DILUTION ANALYSIS (ELDA)**

Limiting dilution analysis (LDA) assay is an experimental technique that quantifies the proportion of biologically active particles in a larger population and is a commonly applied in stem cell research. LDA presumes the Poisson single-hit model, which assumes that the number of biological active particles in each culture varies according to a Poisson distribution, and a single biologically active cell is sufficient for a positive response from a culture (145). Extreme limiting dilution analysis (ELDA) assay is a further evolution of LDA for extreme data situations, non-Poisson distribution and multiple populations (145).

For clonality evaluation, cells were seeded at different densities (1, 5, 10, 20 cells) and sphere formation was performed with hanging drop technique. After 7-10 days the number of wells containing spheres was counted and ELDA analysis performed with an on line tool (146). The parameters required by ELDA web tool for the analysis were:

- Dose: number of cells seeded (1, 5, 10, 20 cells).
- Tested: number of wells tested for each condition.
- Response: number of wells where the generation of 3D spheres occurred, for each condition.

#### **5) PROTEIN EXTRACTION AND WESTERN BLOTTING**

##### **5.1 Solubilization with RIPA lysis buffer for 2D adherent cells**

Cells were seeded at optimal density (200000/well) in 6-well plates and, the day of protein extraction, washed with PBS and then lysed with 80-100 µl of ice-cold RIPA buffer per well (10 mM Tris-HCl pH 7.5, 500 mM NaCl, 0,1% SDS, 1% NP40, 1% Na-deoxycholate, 2 mM EDTA), supplemented with freshly added protease inhibitors (cOmplete EASYpack, Roche) and phosphatase inhibitors (PhosSTOP EASYpack, Roche) by scraping. Samples were collected in pre-cooled 1.5 ml tubes and sonicated (10-20 hits). Samples were then centrifugated

at 12000g for 20 minutes at 4°C; the supernatant was collected to new tubes and the pellet discarded.

## **5.2 Solubilization with RIPA lysis buffer for 3D spheres**

Cells were seeded at the optimal density (24240 cells) in pre-coated poly-hema Petri dishes and cultured until the generation of 3D spheres. The day of protein extraction, spheres were collected by gentle centrifuging at 400g for 2 minutes, washed with PBS, pelleted again and directly resuspended in 80-100 µl of ice-cold RIPA buffer. Samples were then transferred in pre-cooled 1.5 ml tubes and the procedure continued as for 2D monolayer cells.

## **5.3 Solubilization with Laemmli lysis buffer for patient-derived tissue samples**

Protein extraction from patient-derived tissues was performed with Laemmli buffer (62.5 mM Trish-HCl pH 6.8, 1% SDS), supplemented with protease and phosphatases inhibitors cocktail. First of all, a small piece of frozen tissue was dissociated mechanically with a surgical scalpel and placed in 1.5 ml Eppendorf tube. 50-100 µl of Laemmli buffer pre-heated at 99°C was added to each sample. Samples were boiled for 5 minutes, placed on ice and vortexed 10 seconds for three times. Samples were sonicated (20 hits, two or three times if requested) and then centrifugated at 12000g for 20 minutes at 4°C; the supernatant was collected and the pellet discarded.

## **5.4 Protein quantification and sample preparation**

Proteins amount was quantified with bicinchoninic acid method (BCA, Pierce™ Protein Assay Kit, Thermo Fisher Scientific) following manufacturer's instructions. After 30 minutes at 37°C on a plate shaker, absorbance was read at 540 nm using ELx800 Absorbance Microplate Reader. For each experiment, a range of 20-60 µg of protein extracts were denatured in Laemmli Sample Buffer at final

concentration 1X, by heating at 99°C for 5 minutes (Eppendorf ® Thermomixer Compact) and analyzed by electrophoresis.

## 5.5 Western Blotting

Protein electrophoresis was performed on NuPAGE™ 10% Bis-Tris gels (Thermo Fisher Scientific) with MOPS Running Buffer 1X (Thermo Fisher Scientific) and 500 µl of NuPage™ Antioxidant (Thermo Fisher Scientific) following manufacturer's instructions. Amersham™ ECL™ Rainbow™ Marker - Full Range (Merck Millipore) was used for molecular weight determination. Proteins were run at 120 V until the leading edge reached the bottom of the gel. Proteins transfer was then performed with iBlot dry Blotting System (Thermo Fisher Scientific) on iBlot Gel Transfer Stacks, Nitrocellulose (Thermo Fisher Scientific) followed by Ponceau Staining (0,1% PonceauS (w/v) in 5% (v/v) acetic acid, Merck Millipore) to quickly assess the quality of protein loading, running and the total amount of transferred proteins.

Nitrocellulose membranes were incubated for 1 hour in blocking solution consisting of 5% milk in TBS-T (20 mM Tris-HCl pH 7.5, 150 mM NaCl, 0.1% Tween-20) in agitation, washed three times with TBS-T and incubated with primary antibody (Table 3), following manufacturer instruction, at 4°C over night. The following day, membranes were washed three times with TBS-T and incubated for 1 hour at room temperature in secondary antibody solution (anti-rabbit, anti-mouse or anti-goat HRP-conjugated Ab (Merck Millipore), 1:5000 in 5% milk in TBS-T.

After three times washing with TBS-T, a chemiluminescence-based immunodetection was performed with ECL Star Detection (Euroclone) or with Westar Supernova (Cyanagen). Chemiluminescence was detected with Azure C-400 (Azure Biosystems®) detection system. Images were then quantified with Fiji software.

| <b>Antibody</b>                        | <b>Concentration used</b> | <b>Solution</b> | <b>Productor</b> | <b>Expected molecular weight</b> |
|--|---------------------------|-----------------|------------------|----------------------------------|
| Anti-EpCAM Ab [E144]                   | 1:1000                    | 5% milk TBS-T   | Abcam (ab32392)  | ~ 40 kDa                         |
| Anti-EpCAM/TROP-1 Ab                   | 1:1000                    | 5% milk TBS-T   | R&D (AF960)      | ~ 40 kDa                         |
| Anti-GFP Ab                            | 1:2000<br>1:5000          | 5% milk TBS-T   | Abcam (ab290)    | ~ 20 kDa                         |
| Anti-E-Cadherin Ab [M168]              | 1:1000                    | 5% milk TBS-T   | Abcam (ab76055)  | 135 kDa                          |
| Recombinant Anti-Vimentin Ab [EPR3776] | 1:2000<br>1:4000          | 5% milk TBS-T   | Abcam (ab92547)  | 57 kDa                           |
| Purified Mouse Anti-Actin Ab 5         | 1:1000                    | 5% milk TBS-T   | BD Biosciences   | 42 kDa                           |

**Table 3. Primary antibodies applied for Western Blot experiments with respective dilutions and molecular weight.**

## **6) IMMUNOFLOURESCENCE AND CONFOCAL MICROSCOPY**

### **6.1 Immunofluorescence on patient-derived tissue samples**

Patient-derived tissue samples were included in O.C.T. solution (Bio Optica), a cryoprotectant that prevents the formation of crystals, and 10 µm thick cryosections on SuperFrost® slides were obtained. Cryosections were stored at -80°C. The day of staining, the slides were allowed to dry horizontally for 20 minutes at room temperature, and then moved to Hellendahl staining jars containing PBS. Fixation was carried out using 4% paraformaldehyde (PFA) for 30 minutes. The fixed tissue samples were washed with PBS for three times, permeabilized with 0.3% Triton™ X-100 (Merck Millipore) permeabilization solution in PBS for 10 minutes and washed again with PBS for three times. Slides were move back to horizontally holder and the outline of the tissue area on the slide was defined through a Pap Pen (ImmEdge™ Pen, VECTOR LABORATORIES) that created an hydrophobic contour around the tissue sample to prevent subsequent washings, blocking solution and incubation with antibodies from leaking from the slide. Slides were placed for 1 hour in 200 µl of blocking

solution consisting of 5% BSA in PBS and incubated with primary antibody following manufacturer instruction over night at 4°C in the dark in a humidified chamber. The following day, slides were washed three times with PBS, incubated in secondary antibody solution (anti-goat IgG Alexa-Fluor 488 or anti-rabbit IgG Alexa-Fluor 555, Thermo Fisher Scientific, 1:500) for 1 hour at room temperature in the dark and washed again. Mounting solution (VECTASHIELD® Hardset™) containing DAPI was added and, once the slides were dried, the edges were fixed with transparent polish sealer.

## **6.2 Immunofluorescence on 2D adherent cells**

Sterile coverslips were coated with 1 ml of poly-L-lysine solution (Merck Millipore) and leaved at 37°C for 1 hour; poly-lysine was then removed and coverslips washed with PBS for three times before seeding cells at the optimal density (100000 cells/well); if required, cells were treated with PLX-4032 24 hours later. For cell membrane visualization, living cells were incubated with 5 µg/ml Wheat Germ Agglutinin (WGA) Alexa-Fluor 594 Conjugate (Thermo Fisher Scientific) in PBS for 10 minutes at room temperature prior to samples fixation. From now on, coverslips were kept in the dark as much as possible. Cells were washed three times with PBS and fixated by incubation with 4% PFA for 10 minutes at room temperature. Fixed cells were washed with PBS for three times, permeabilized with 0.2% saponin in PBS for 10 minutes, washed again and incubated for 1 hour in 5% BSA in PBS blocking solution. Cells were then incubated with primary antibody (Table 4a) following manufacturer instruction over night at 4°C in the dark. The following day, cells were washed three times in PBS, incubated in secondary antibody solution (anti-goat IgG Alexa-Fluor 488, anti-rabbit IgG Alexa-Fluor 555 or anti-mouse IgG Alexa-Fluor 555, Thermo Fisher Scientific, 1:500) (Tab 4b) for 1 hour at room temperature in the dark, and washed again. Slides were mounted with VECTASHIELD® Hardset™ with DAPI. Once the slides were completely dry, the edges of the coverslip were fixed with transparent polish sealer.



### 6.3 Immunofluorescence on 3D spheres

Cells were seeded at the optimal density (24240 cells) in pre-coated poly-hema Petri dishes and left in the incubator at 37°C, 5% CO<sub>2</sub> for 7-10 days, until the generation of 3D spheres. Sterile coverslips were covered with 1 ml of cold Corning™ membrane matrix Matrigel™ (Thermo Fisher Scientific), previously thawed on ice; 10 µl of Matrigel were mixed with 1 ml of ice-cold culture medium without FBS and P/S. Coverslips were incubated at 37°C, 5% CO<sub>2</sub> for 30 minutes and washed with PBS for three times. The 3D spheres obtained in poly-hema Petri dishes were collected, gently centrifuged at 400g for 2 minutes, seeded on Matrigel-coated coverslips and let attach for 2/3 hours. When needed, for cell membrane visualization, the 3D spheres were incubated with 5 µg/ml WGA in PBS for 10 minutes at room temperature prior to fixation. From now on, coverslips were kept in the dark as much as possible. The procedure continued as for 2D monolayer cells even if with some time variations: the fixation with 4% PFA was 20 minutes instead of 10, the permeabilization with 0.2% saponin in PBS was 15 minutes instead of 10, the incubation with primary antibody was 2 hours at room temperature in the dark before overnight incubation at 4°C, and the incubation with secondary antibody solution was 3 hours at room temperature instead of 1 hour. Moreover, 2 µg/ml of DAPI solution (Thermo Fisher Scientific 1 mg/ml) were added to each coverslip and left at room temperature for 20 minutes, prior to the mounting on microscope slides.

(a)

| Primary antibody            | Concentration used | Solution   | Productor                |
|-----------------------------|--------------------|------------|--------------------------|
| Anti-EpCAM Ab [E144]        | 1:150              | 5% BSA PBS | Abcam (ab32392)          |
| Anti- EpCAM/TROP-1 Ab       | 1:150              | 5% BSA PBS | R&D (AF960)              |
| Anti-E-Cadherin Ab [M168]   | 1:150              | 5% BSA PBS | Abcam (ab76055)          |
| Wheat Germ Agglutinin (WGA) | 5 µg/ml            | 5% BSA PBS | Thermo Fisher Scientific |

(b)

| Secondary antibody                        | Concentration used | Solution   | Conjugated fluorophore | Productor                |
|---|--------------------|------------|------------------------|--------------------------|
| Donkey anti-Rabbit IgG (H+L) Secondary Ab | 1:500              | 5% BSA PBS | Alexa Fluor™ 488       | Thermo Fisher Scientific |
| Donkey anti-Rabbit IgG (H+L) Secondary Ab | 1:500              | 5% BSA PBS | Alexa Fluor™ 555       | Thermo Fisher Scientific |
| Donkey anti-Mouse IgG (H+L) Secondary Ab  | 1:500              | 5% BSA PBS | Alexa Fluor™ 555       | Thermo Fisher Scientific |
| Donkey anti-Goat IgG (H+L) Secondary Ab   | 1:500              | 5% BSA PBS | Alexa Fluor™ 488       | Thermo Fisher Scientific |

**Table 4. Primary (a) and secondary (b) antibodies applied for Immunofluorescence experiments with respective dilutions and conjugated fluorophores.**

## 6.4 Fluorescent and confocal microscopy

Images were acquired with Nikon EclipseTi-E inverted microscope with IMA10X Argon-ion laser System by Melles Griot. Fluorescent microscopy was applied for 2D adherent cells images acquisition with CFI Plan Apo VC 20X (Nikon) objective. For FRO, HTCC3 and SW1736 adherent cells images, at least 10 different fields were acquired for each cell line. For PLX-4032 treatment on FRO and HTCC3 adherent cells images, at least 10 different fields were acquired for each condition for each cell line. Confocal microscopy was applied for tissue sections and 3D sphere images acquisition:

- Z-series acquisition were acquired with CFI Plan Apo VC 20X objective for healthy tissue and 40X Oil (Nikon) objective for PTC. At least 10 different

fields were acquired for both healthy tissue and PTC sections. For each acquisition, 8 stack (2  $\mu\text{m}$  z-step) were acquired, comprising the whole thickness of the tissue section. Lasers parameters were the same for every acquisition: CH1 (DAPI) laser power: 2.8, HV: 152, offset: -11; CH2 (FITC) laser power: 3.1, HV: 76, offset: -7; CH3 (TexasRed) laser power: 3.8, HV: 86, offset: -4. Pinhole size ( $\mu\text{m}$ ): 20. The maximal intensity projection for each z-series acquisition is reported in the Results.

- 3D spheres images were acquired with CFI Plan Apo VC 40X Oil (Nikon) objective. Z-series acquisition was performed for 3D spheres images and 3D structure was reconstructed with Nikon NIS-Elements AR software. For each acquisition, 17 stack (2  $\mu\text{m}$  z-step) were acquired, comprising the whole thickness of the sphere. Lasers parameters were the same for every acquisition: CH1 (DAPI) laser power: 2.8, HV: 115 offset: -5; CH2 (FITC) laser power: 3.1, HV: 84, offset: -7; CH3 (TexasRed) laser power: 3.8, HV: 83, offset: 0. Pinhole size ( $\mu\text{m}$ ): 20. The maximal intensity projection of 6 central merged stack for each z-series is reported in the Results. We used the central stacks for better visualization of Epithelial Cell Adhesion Molecule (EpCAM) intracellular domain (EpICD) and extracellular domain (EpEx). For FRO-derived 3D spheres experiments a total number of 27 spheres were acquired with 40X magnification.

## 7) TRANSIENT TRANSFECTION

Human EpCAM and the C-terminal EGFP [enhanced GFP (green fluorescent protein)]-tagged version were previously described (106,116,147) and were a kind gift of professor B.G. Giepmans (University of Groningen, The Netherlands). EpCAM cDNA was originally subcloned into the pMep4 vector (Invitrogen BV, Leek, The Netherlands), using the *HindIII/Bgl* restriction sites (106,147). The construct contained the Epstein-Barr virus's origin of replication and the EBNA-1 gene, and was placed under the control of the methallothionin promotor (106). For transient transfection, FRO and HEK293T were seeded at the optimal density (300000 cells/well for FRO and 350000 cells/well for HEK293T) in 6-well plates. The day after, transfection of 1  $\mu\text{g}$  DNA per well was performed with FuGENE®

HD transfection reagent (Promega Corporation) in Opti-MEM™ (Gibco), following manufacturer's instructions. Four hours after transfection, medium was changed with the appropriate culture medium. Cells were then treated with EpCAM cleavages' inhibitors 48 hours post transfection and Western Blot was performed the following day.

## **8) EpCAM CLEAVAGE INDUCTION AND INHIBITION**

### **8.1 Epidermal Growth Factor (EGF) and 2,2'-Bipyridyl (DIP) treatments**

Epidermal growth factor (EGF) is one of the main growth factors used for 3D sphere maintenance (142) and treatments were performed in order to assess if the growing condition of the spheres may affect EpCAM expression. EGF is also known to up-regulate EpCAM expression by activating ERK1/2 signaling in some human epithelial cancers (148,149). 2,2'-Bipyridyl (DIP) is an iron chelating agent used as an hypoxia-mimetic compounds in several *in vitro* studies (68,150–152). It is known to mimic the pseudo-hypoxic state that is present in undifferentiated TC, and to increase the proteolytic activity of ADAM17 and  $\gamma$ -secretase (68,153–156). Treatments with EGF and DIP were performed 24 hours after seeding FRO as adherent cells at the optimal density (200000 cells/well) in 6-well plate; increasing concentrations of EGF (10 ng/ml, 20 ng/ml and 40 ng/ml) and DIP (50  $\mu$ M, 100  $\mu$ M, 200  $\mu$ M) were used. For EGF treatment, since the concentration of EGF used for Sphere Medium is 20 ng/ml, we decided to use the half and the double of that concentration. For DIP treatment, the range was determined by searching in literature (68,150–152). Proteins extraction was performed the following day.

### **8.2 EpCAM cleavages' inhibitors treatments on transfected cells**

Treatments with inhibitors of EpCAM cleavages were performed 48 hours after cells transfection. Each inhibitor selectively decreased the proteolytic activity of the enzymes involved in EpCAM cleavages (ADAM17,  $\beta$ -secretase and  $\gamma$ -secretase) as previously described. The inhibitors used are:

- TAPI-2 (Merck Millipore): ADAM17 inhibitor, final concentration 20  $\mu\text{M}$  (68,157,158);
- BACE (Merck Millipore):  $\beta$ -secretase inhibitor, final concentration 30 nM (159,160);
- DAPT (Merck Millipore):  $\gamma$ -secretase inhibitor, final concentration 10  $\mu\text{M}$  (68,112,116,161,162).

Transfected cells were treated with the selected concentration of inhibitor and placed in the incubator for 4 hours before treatment with DIP at final concentration of 100  $\mu\text{M}$ . Proteins extraction was performed the following day.

### **8.3 EpCAM cleavages' inhibitors and DIP treatments effects on sphere-forming abilities**

Treatments with EpCAM cleavages' inhibitors were performed 24 hours after seeding FRO as adherent cells at the optimal density (200000 cells/well) in 6-well plate. Cells were treated with selected concentrations of EpCAM cleavages' inhibitors TAPI-2 (20  $\mu\text{M}$ ), BACE (30 nM) and DAPT (10  $\mu\text{M}$ ) or with increasing concentrations of DIP (25  $\mu\text{M}$ , 50  $\mu\text{M}$ , 100  $\mu\text{M}$ ). After 48 h, cells were collected and seeded at clonal density as hanging-drops (10 cells per drop) 24 hours after treatments. The ability to generate 3D spheres was assessed after 7-10 days of culture.

## **9) ANTI-CANCER DRUG TREATMENTS AND PROLIFERATION ASSAYS**

### **9.1 2D adherent cells**

Cells were seeded at the optimal density (2000 cells/well for FRO and 3000 cells/well for HTCC3) in 96-well plates with the exception of the outer wells that were filled with sterile water; cells were treated with increasing concentrations of Vemurafenib (PLX-4032, Selleckchem). Vemurafenib is a potent inhibitor of wild type (wt) BRAF, BRAFV600E mut, and of several non-Raf kinases. It is known to be highly effective in the treatment of melanoma, for the inhibition of BRAFV600E mutated cells. The range of concentrations used for treatments was 0-100  $\mu$ M for both FRO and HTCC3. Effects on cell proliferation were assessed after 72 hours with MTT assay. MTT solution (5 mg/ml in PBS) was equilibrated at room temperature and 10  $\mu$ l were added to each well to a final concentration of 0.5 mg/ml, in the dark. Plates were then incubated at 37°C for different period of time, depending on the cell line: 40 minutes for FRO and 1 hour for HTCC3. Culture medium was gently removed and formazan crystals solubilized in 200  $\mu$ l of mixture of EtOH-DMSO 1:1 solution. After 5 minutes solubilization on a plate shaker, absorbance was read at 540 nm using ELx800 Absorbance Microplate Reader (BioTek).

### **9.2 3D spheres**

Cells were seeded at the optimal density (1212 cells/well) in pre-coated poly-hema 48-well plates with the exception of the outer wells that were filled with sterile water, and grown for 7-10 days. Based on the proliferation curve obtained after treating adherent cells with increasing doses of PLX-4032, three concentrations were selected to test on FRO-derived and HTCC3-derived 3D spheres: 1.56, 12.5 and 100  $\mu$ M. MTT assay was performed 72 hours after treatments. On the day of the assay, 10  $\mu$ l of MTT solution 5 mg/ml were added to each well and incubated at 37°C for 1 h for both FRO and HTCC3-derived 3D spheres. The spheres treated for each different PLX-4032 concentration were collected by centrifuged at 400g for 2 minutes and directly resuspended in 200  $\mu$ l

of EtOH:DMSO 1:1 solution. After resuspension, absorbance was read at 540 nm using ELx800 Absorbance Microplate Reader.

## **10) STATISTICAL ANALYSIS**

All Western Blot quantifications were made with Fiji Software. Confocal microscopy quantifications were made with Nikon NIS-Elements AR Software, followed by Fiji analysis when necessary. All statistical analysis were performed with GraphPad Prism Software version 9, on a minimum of three independent experiments. Values are expressed as mean standard error. Shapiro-Wilk normality test was first carried out to determine normal or non-normal distribution of data. One-way and 2way ANOVA followed by appropriate post-hoc test were used as indicated in figure legends. Levels of significance were reported as follows: \*\*\*\* $p < 0.0001$ , \*\*\* $p < 0.001$ , \*\* $p < 0.01$ , \* $p < 0.05$ .

# Results



## **1) STUDIES ON THE CHARACTERIZATION OF EPITHELIAL CELL ADHESION MOLECULE (EpCAM) EXPRESSION AND CLEAVAGES**

### **1.1 EpCAM and its cleaved domains are expressed differently in healthy and pathological patient-derived TC tissue samples**

To evaluate Epithelial Cell Adhesion Molecule (EpCAM) expression and its cleavage in thyroid cancer (TC), Western Blot and Immunofluorescence experiments were performed on samples from a small cohort of TC patients representative of the different histotypes (Table 5). We noticed that the expression of EpCAM in healthy tissues is quite similar between patients, with a strong signal of the full length form and very feeble bands with lower molecular weight, corresponding to EpCAM cleavage products (Figure 8a). In agreement with Western Blot, Immunofluorescence on tissue cryosections showed a constant EpCAM signal in thyrocytes (Figure 8b). Despite a great inter-patient variability, EpCAM full length signal was similar to healthy tissues in follicular thyroid cancers (FTCs) while a consistent decrease was observed in papillary thyroid cancers (PTCs) (Figure 8a). In poorly differentiated thyroid cancers (PDTCs) tissue samples, EpCAM full length signal was strongly reduced, even if not significantly, and this was accompanied by an increase of the cleavages' bands intensity. This was associated with a strong increase in Vimentin, a well-known mesenchymal marker, and absence of E-Cadherin, a typical epithelial marker (Figure 8a). Immunofluorescence and confocal microscopy experiments on tissues cryosections, confirmed high variability of EpCAM expression and subcellular localization in aggressive cancers. We noticed areas with a uniform expression of extracellular domain, EpEX, together with transmembrane domain, TMD (EpEx+TMD), at the plasma membrane together with almost total absence of intracellular domain (EpICD) signal, flanked by other regions with a variable expression of both EpEx+TMD and EpICD (Figure 8b). In particular, in some fields we detected cells with high EpICD cytoplasmic and/or nuclear signal together with variable membrane EpEx+TMD signal while in other areas we could observe an almost total loss of EpCAM signal with nuclear localization of EpICD alone. We hypothesize that these variations could be due to different degree of differentiation of tumor cells and/or microenvironment changes in

specific areas of the tumor and on these premises we moved forward to better characterize EpCAM role in TC biology.

| Patient | Gender | Genetic                 | Histotype      | Patient age at diagnosis (year old) |
|---------|--------|-------------------------|----------------|-------------------------------------|
| 1       | M      | BRAF V600E              | PTC            | 35                                  |
| 2       | F      | BRAF V600E              | PTC            | 39                                  |
| 3       | F      | BRAF V600E              | aggressive PTC | 69                                  |
| 4       | M      | BRAF V600E +<br>RET/PTC | PTC            | 64                                  |
| 5       | M      | RAS                     | FTC            | 47                                  |
| 6       | F      | NRAS Q61R +<br>TERT     | FTC            | 81                                  |
| 7       | M      | n.d.                    | aggressive FTC | n.d.                                |
| 8       | F      | TERT + p53              | PDTC           | n.d.                                |
| 9       | F      | BRAF V600E +<br>TERT    | PDTC           | 72                                  |
| 10      | M      | PTEN mut                | PDTC           | 34                                  |
| 11      | F      | P53                     | PDTC           | n.d.                                |

**Table 5. Cohort of TC patients representative of the different histotypes. PTC= papillary thyroid cancer; FTC= follicular thyroid cancer; PDTC= poorly differentiated thyroid cancer.**

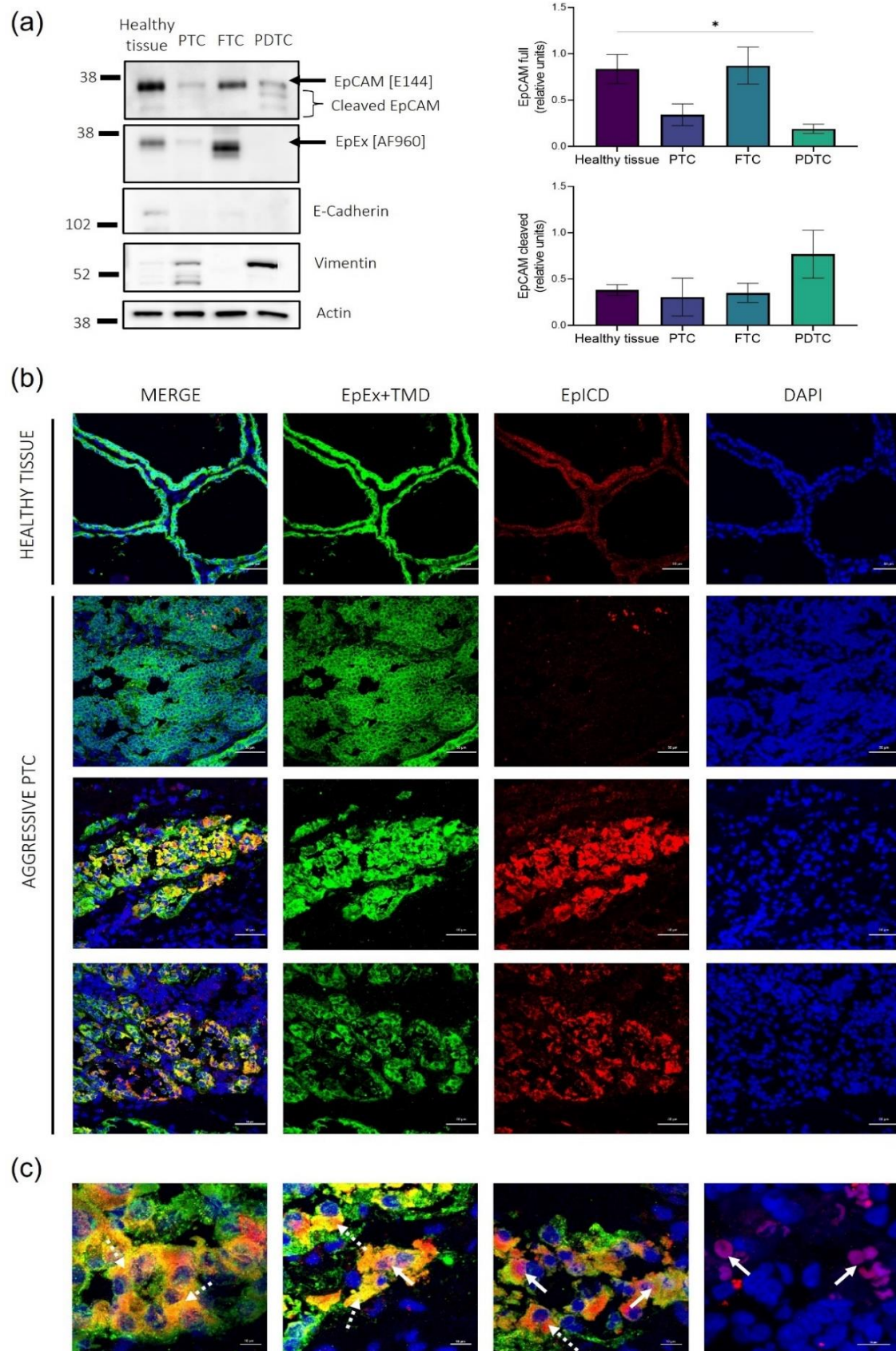


**Figure 8. EpCAM is subjected to differential expression and cleavage pattern in patient-derived tissue samples.** (a) Western Blot representative images and

corresponding quantifications of proteins extracted from 4 healthy thyroid, 4 PTC, 3 FTC and 4 PDTC tissue samples. EpCAM expression was evaluated with two different antibodies, Recombinant Anti-EpCAM antibody [E144] (EpICD) that is directed against an epitope localized in the ICD and is able to recognize both full length (arrow) and intracellular cleaved fragments (bracket) and EpCAM/TROP-1 Antibody [AF960] (EpEX) that recognizes the full length form but not the ICD. E-Cadherin was used as epithelial marker, Vimentin was used as mesenchymal marker, while actin was used as loading control. Statistical analysis: One way ANOVA followed by Dunnett's multiple comparisons test. \* $p < 0.05$ . (b) Confocal microscopy representative images of tissue cryosections of healthy thyroid and aggressive PTC, characterized by undifferentiated regions, showing expression of EpEx+TMD (EpCAM/TROP-1 Antibody [AF960]) in green, EpICD (Recombinant Anti-EpCAM antibody [E144]) in red and DAPI staining for nuclei in blue. Images were acquired with 20X magnification for healthy tissue and 40X magnification for PTC sections. Scalebars represent 50  $\mu\text{m}$ . (c) Higher magnification images representative of the different EpCAM signal observed in the tumor tissue. Nuclear and cytoplasmic staining for EpICD fragment is indicated by white arrows and dotted white arrows, respectively. Scalebars represent 10  $\mu\text{m}$ . PTC= papillary thyroid cancer; FTC= follicular thyroid cancer; PDTC= poorly differentiated thyroid cancer; ATC= anaplastic thyroid cancer; EpEx= extracellular domain of EpCAM; TMD= transmembrane domain of EpCAM; EpICD= intracellular domain of EpCAM.

## 1.2 TC cell lines have different EpCAM expression levels

As first step we evaluated EpCAM expression in TC cell lines, to select a suitable model for further *in vitro* studies. The screening of five TC cell lines (FRO, SW1736, HTCC3, SW579 and B-CPAP) by Western Blot revealed that FRO, and in small amount HTCC3, expressed full length EpCAM at basal conditions (Figure 9a). Immunofluorescence experiments performed on adherent cells confirmed this result and revealed that EpCAM expression was not uniformly distributed among cells, but instead two cellular subpopulations were observed, one EpCAM positive (EpCAM+) and one EpCAM negative (EpCAM-), both in FRO (61,9%  $\pm$  5,9 EpCAM+; 38,1%  $\pm$  5,9 EpCAM-) and HTCC3 (77,8%  $\pm$  10,44 EpCAM+; 22,2%  $\pm$  10,44 EpCAM-) (Figure 9b). On the basis of these results, FRO cell line was mainly used for further experiments on EpCAM characterization.

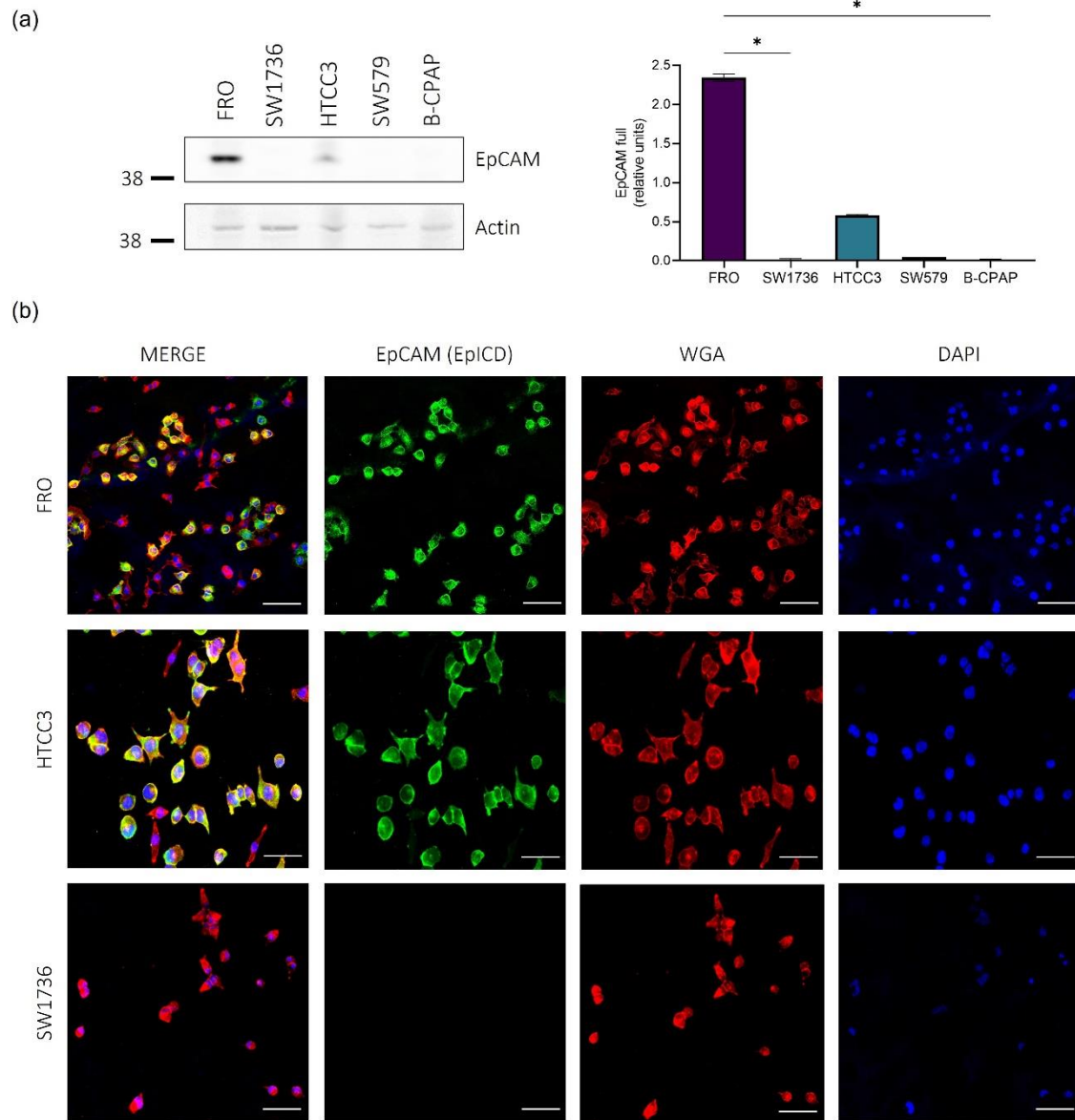


**Figure 9. EpCAM is mainly expressed by FRO and HTCC3 cell lines.** (a) Western Blot of protein extracts obtained from FRO, SW1736, HTCC3, SW579 and B-CPAP cultured as 2D adherent cells. Statistical analysis: ANOVA Kruskal-Wallis test followed by Dunn's multiple comparisons test. \* $p < 0.05$ . (b) Immunofluorescence experiment of FRO, HTCC3 and SW1736 adherent cells showing EpCAM+ and EpCAM-subpopulations. Scalebars represent 100  $\mu\text{M}$ . EpCAM (EpiCD), green; membrane marker Wheat Germ Agglutinin (WGA), red; DAPI staining for nuclei, blue.

### **1.3 Thyroid cancer cell lines have different 3D sphere-forming ability**

Prior to deepen EpCAM analysis using the 3D sphere model, we tested the ability of our TC cell lines to actually generate 3D spheres when seeded at clonal density as hanging drops both in their culture medium and in Sphere Medium. After 7-10 days in culture, we observed that all cell lines were able to create 3D spheres, but with a strong variability in number, morphology and dimensions (Figure 10a). In particular, we observed that very few 3D structures were obtained in Sphere Medium; they were also smaller and with more irregular shape than those obtained in the original culture medium. The dimensions of the spheres were determined only for spheres obtained after seeding cells in their culture medium, since we didn't obtain a sufficient number of spheres for any statistical evaluation in Sphere Medium. Our results showed that the two EpCAM positive cell lines, FRO and HTCC3, were forming bigger spheres than other cell lines in their culture medium (Figure 10a,b). Nevertheless, we observed that FRO cell line was the only one that displayed more rounded shape morphology and larger dimensions in both culture medium and Sphere Medium respect to the other cell lines. Moreover, when FRO were seeded as hanging-drops in Sphere Medium, independently from the cell density, they created 3D structures with complex architectures that weren't observed in the other cell lines. Irrespective of spheres dimension, when seeded at 10 cells dilution all the cell lines had similar sphere-forming abilities (Figure 10c).

Moreover, to assess the frequency of tumor cells with potential tumor-initiating ability able to generate 3D spheres within the different cell lines, we performed an Extreme Limiting Dilution Assay (ELDA) (145,146). Interestingly, we noticed that FRO cell line seem to have the greatest frequency of tumor cells with possible tumor-initiating ability respect to the other cell lines when cells were seeded in their culture medium (Figure 10d). Indeed, as reported in the estimate values computed by ELDA analysis, 1 out of 5.07 cells in FRO could potentially have tumor-initiating properties (Table 6a). Moreover, pairwise comparisons between FRO and HTCC3 and FRO and SW1736 were significant only in spheres obtained in their culture medium, but not in Sphere Medium (Table 6b). When cells were seeded in Sphere Medium (Figure 10e), we detected high

variability between the different cell lines, with lowest ratio represented by HTCC3 and SW579 characterized by an estimate value of 1 out of 160 and 1 out of 173 respectively (Table 6a), and pairwise comparisons were not significant in Sphere Medium between the different cell lines (Table 6b).

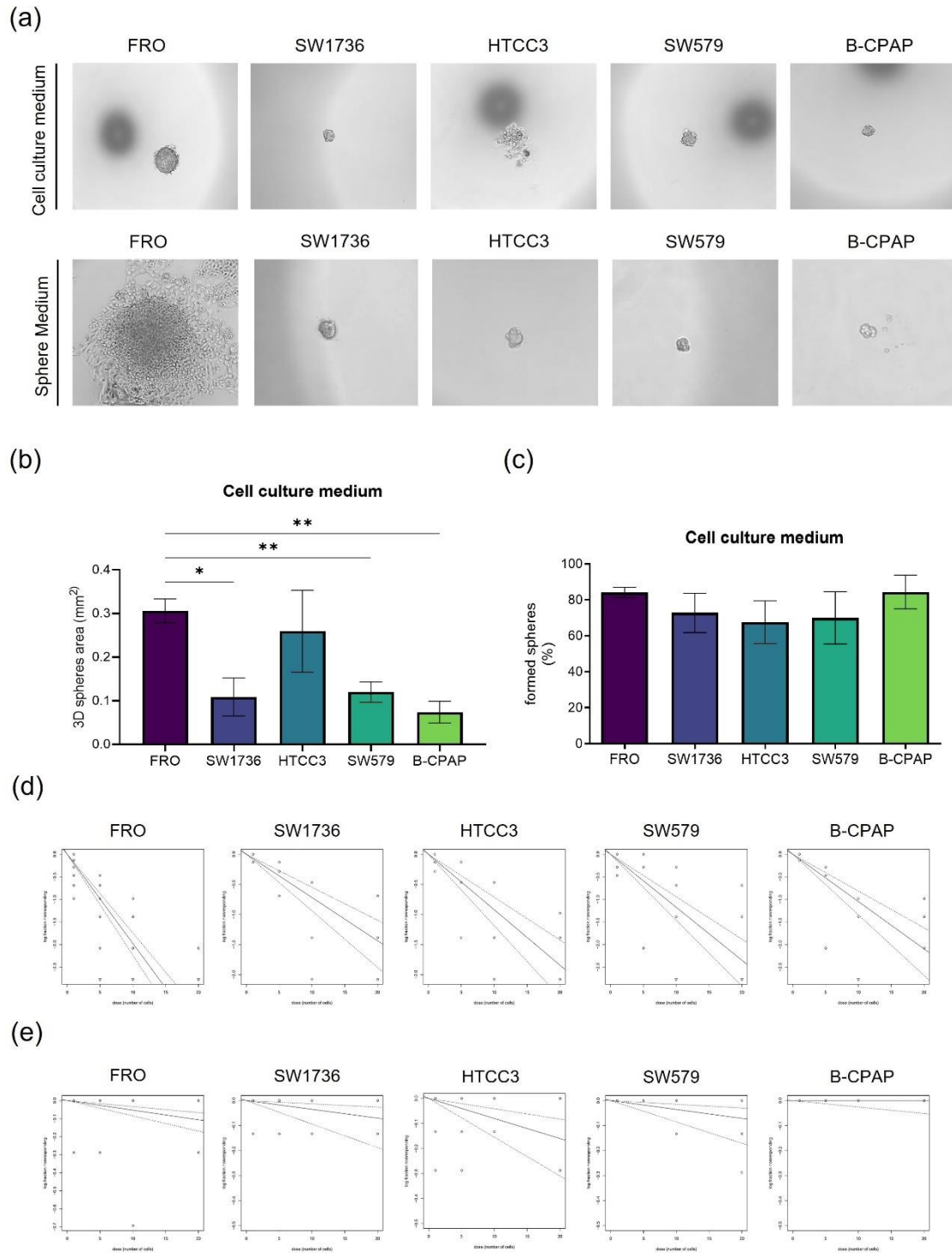


**Figure 10. 3D sphere-forming abilities in TC cell lines.** (a) Representative morphological panel of spheres obtained from different TC cell lines when 10 cells were



seeded as hanging drops in their culture medium (upper panel) or in Sphere Medium (lower panel). (b) Sphere's dimensions quantification: for each cell line, an average of the measurements of the area of at least 7 spheres for each independent replicate was reported. The area of each sphere was calculated on Fiji applying the ellipses formula. The number of replicates for each cell line was reported as follows: SW579 n= 5, HTCC3 n= 3, B-CPAP n= 3, HTH74 n= 6, SW1736 n= 3, FRO n= 13. Statistical analysis: One way ANOVA followed by Tukey's multiple comparisons test. \*\*p < 0.01, \*p < 0.05. (c) Sphere-forming abilities of the different cell lines when only 10 cells were seeded as hanging drops in their culture medium. (d), (e) Extreme Limiting Dilution Assay of cells seeded in their culture medium (d) and in Sphere Medium (e) displayed by ELDA web tool.

(a)

Confidence intervals for 1/tumor-initiating ability

| Cell line | Culture Medium |          |       | Sphere Medium |          |       |
|-----------|----------------|----------|-------|---------------|----------|-------|
|           | Lower          | Estimate | Upper | Lower         | Estimate | Upper |
| B-CPAP    | 15.79          | 9.53     | 5.84  | Inf           | Inf      | 96.6  |
| FRO       | 8.32           | 5.07     | 3.18  | 946           | 189      | 37.9  |
| HTCC3     | 18.16          | 10.84    | 6.56  | 712           | 160      | 36.4  |
| SW1736    | 23.94          | 13.89    | 8.15  | 1813          | 268      | 39.9  |
| SW579     | 14             | 8.51     | 5.26  | 812           | 173      | 37.1  |

(b)

Pairwise tests for differences in tumor-initiating abilities

| Cell line (group 1) | Cell line (group 2) | Culture medium Pr(<Chisq) | Sphere Medium Pr(<Chisq) |
|---------------------|---------------------|---------------------------|--------------------------|
| FRO                 | HTCC3               | 0.0285                    | 0.884                    |
| FRO                 | SW1736              | 0.00486                   | 0.781                    |
| FRO                 | SW579               | 0.128                     | 0.939                    |
| FRO                 | B-CPAP              | 0.0642                    | 0.147                    |
| B-CPAP              | HTC/C3              | 0.716                     | 0.115                    |
| B-CPAP              | SW1736              | 0.304                     | 0.223                    |
| B-CPAP              | SW579               | 0.742                     | 0.13                     |
| HTC/C3              | SW1736              | 0.509                     | 0.671                    |
| HTC/C3              | SW579               | 0.491                     | 0.945                    |
| SW1736              | SW579               | 0.179                     | 0.723                    |



**Table 6. Extreme Limiting Dilution Analysis.** ELDA web tool was applied to perform the analysis (146). Confidence intervals for frequency of tumor cells with potential tumor-initiating ability, for each cell line, are described in (a); pairwise comparison tests for differences in tumor-initiating abilities between the different cell lines are reported in (b). Pairwise comparisons between FRO and HTCC3 and FRO and SW1736 were significant ( $p= 0.0285$ ,  $p= 0.00486$  respectively) only in spheres obtained in their culture medium but not in Sphere Medium.

#### **1.4 FRO-derived 3D spheres are a valid *in vitro* model to study EpCAM cleavage pattern**

Given the previously described results on the ability of FRO to generate 3D spheres, we selected this cell line for the study of the role of EpCAM and its cleavage also in a three-dimensional organization. Comparing the expression of EpCAM in FRO when seeded as 2D adherent cells or as 3D spheres at Western Blot, we appreciated a decrease in the expression of the full length protein in 3D spheres, accompanied by a slight increased expression of E-Cadherin and a strong increase in Vimentin signal (Figure 11a). Immunofluorescence and confocal experiments performed on FRO-derived 3D spheres with antibodies directed against EpEx+TMD and EpICD fragments confirmed Western Blot data and gave more insight into EpCAM cleavage in a tridimensional environment (Figure 11b). We noticed a trend of EpCAM cleavage and subcellular localization that resembled what was observed in patient-derived tumor tissues. A progressive reduction of EpEx+TMD signal was detected, proceeding from the outer surface to the inner core of the spheres. This was paired to almost opposite variations in EpICD signal, that also showed increased cytoplasmic and even nuclear localization in the intermediate/inner part of the spheres (Figure 11b).

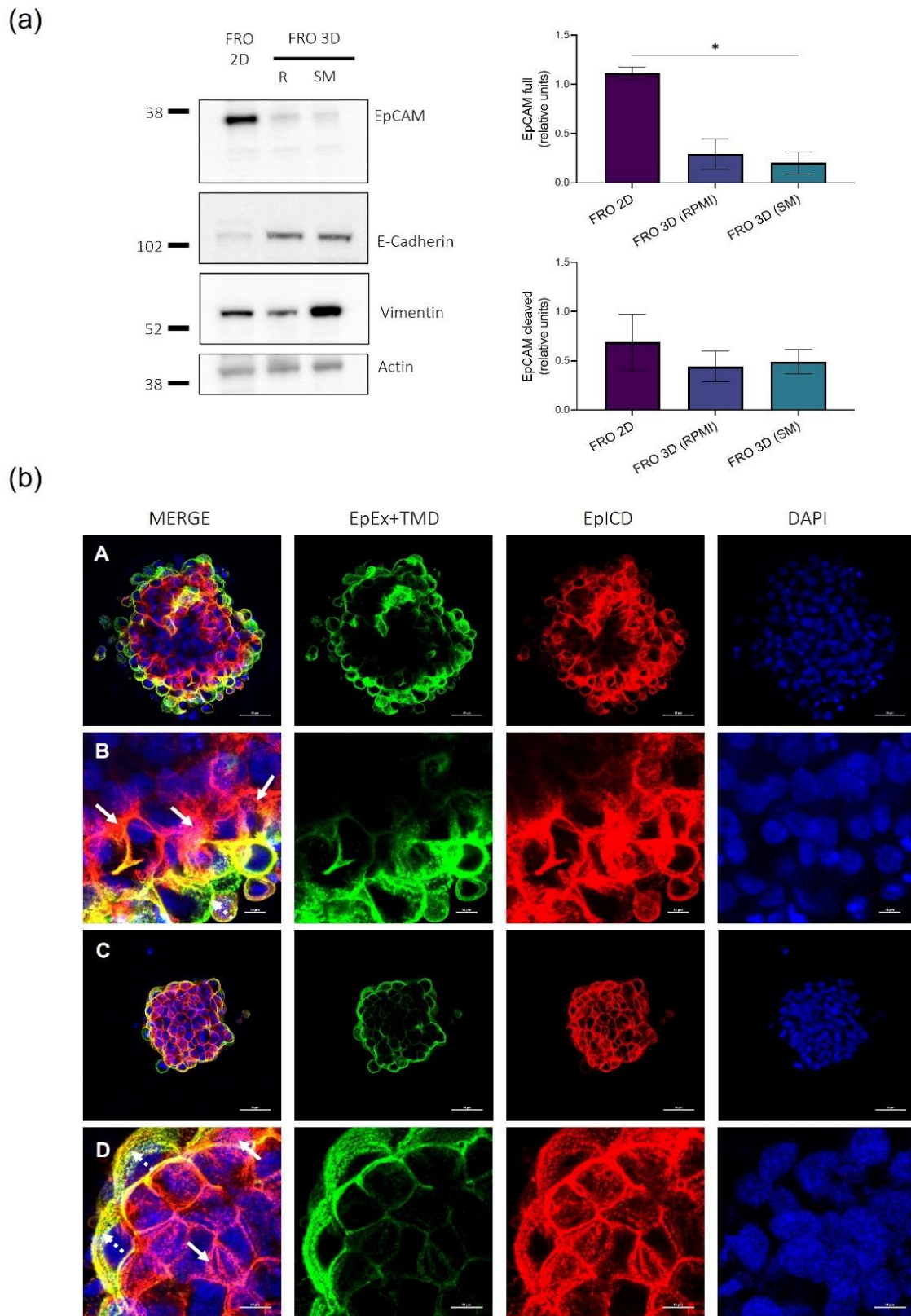


**Figure 11. FRO-derived 3D spheres are representative of the variability of EpCAM cleavage.** (a) Western Blot of protein extracts obtained from FRO adherent cells and from FRO-derived 3D spheres. R= RPMI, SM= Sphere Medium. (b) Confocal microscopy

representative images of 3D spheres obtained in Sphere Medium (A, C) and respective magnification of a selected area of the sphere (B, D). A strong cytoplasmic, and even nuclear, staining of EpICD fragment was appreciated inside the spheres compared to the EpEx+TMD fragment that was mainly located at the plasma membrane. White arrows indicate cytoplasmic/nuclear signal of EpICD; dotted white arrows indicate membranous EpEx+TMD signal. Expression of EpEx+TMD in green, EpICD in red and DAPI staining for nuclei in blue. Statistical analysis: ANOVA Kruskal-Wallis test followed by Dunn's multiple comparisons test. \* $p < 0.05$ . Scale bar (A, C)= 50  $\mu\text{m}$ ; (B, D)= 10  $\mu\text{m}$ .

### **1.5 Characterization of EpCAM cleavages in FRO cells**

To study if and how the growing conditions of the spheres or the 3D organization alone may affect EpCAM expression and cleavage, we performed Western Blots on FRO adherent cells treated with different concentrations of epidermal growth factor (EGF), since is one of the main growth factors used for 3D sphere maintenance (142), and increasing concentrations of 2,2'-Bipyridyl (DIP), used as an hypoxia-mimetic compound (Figure 12). We observed that EGF, at the concentration of 20 ng/ml, which is the exact concentration applied for Sphere Medium, seems to increase EpCAM full length expression respect to the untreated control, even if not significantly. On the other hand, increasing concentrations of DIP induced a significant reduction of EpCAM full length expression respect to the untreated control, probably due to the fact that DIP increases the proteolytic activity of ADAM17 and  $\gamma$ -secretase (68,152–156), and the full-length protein is rapidly cleaved. We also observed that treatments with either EGF and DIP did not affect in a significant manner the expression of E-Cadherin and Vimentin.

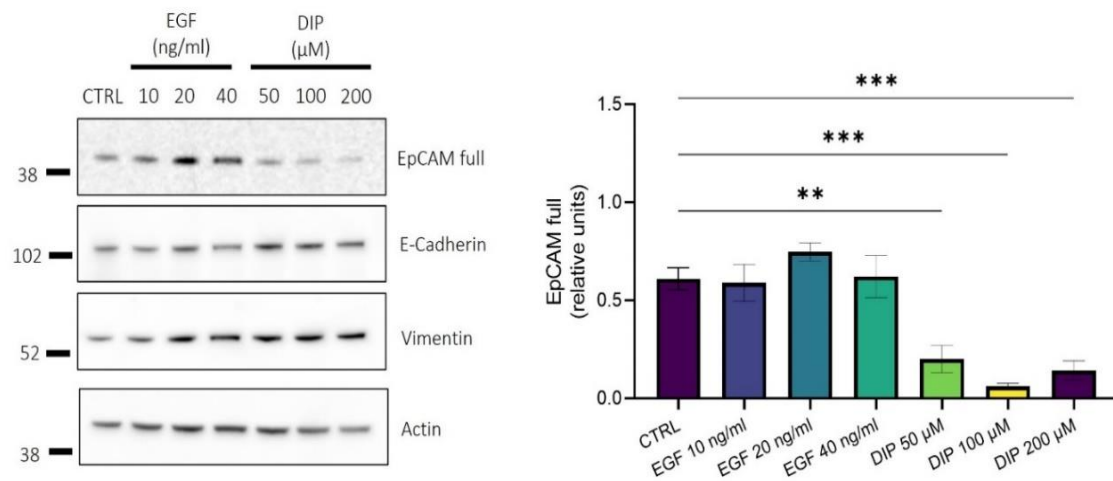


**Figure 12. Pseudo-hypoxic state induced by DIP significantly affects EpCAM full length expression in FRO adherent cells.** Adherent FRO were treated with increasing concentrations of EGF (10 ng/ml, 20 ng/ml and 40 ng/ml) and DIP (50 μM, 100 μM, 200 μM); Western Blot of protein extracts was performed 24 h after treatments and relative expression of EpCAM, E-Cadherin and Vimentin was quantified. CTRL= untreated control; EGF= epidermal growth factor; DIP= 2,2'-Bipyridyl. Statistical analysis: One way ANOVA followed by Dunnett's multiple comparisons test. \*\*\*p < 0.001, \*\*p < 0.01, n= 4.

Despite Immunofluorescence experiments on TC tissues and FRO spheres were indicative of a complex EpCAM cleavage pattern at Western Blot experiments on adherent FRO, we were able to detect mainly the full-length form and only some faint cleavage bands. Indeed, EpCAM intermediate cleavage products may have an extremely short half-life in adherent cells and it was impossible to visualize the EpICD fragment due to its low molecular weight (about 2-3 kDa). To better characterize EpCAM cleavages bands in FRO adherent cells at Western Blot, we transiently transfected cells with a C-terminal EGFP-tagged EpCAM plasmid (106,116,147). Transfected cells were then treated with selected concentrations of the inhibitors of the different proteases involved in EpCAM shedding: TAPI-2 (ADAM17 inhibitor) (68,157,158), BACE (β-secretase inhibitor) (159,160) and DAPT (γ-secretase inhibitor) (68,112,116,161,162). DIP treatment was used as previously to mimic hypoxia (68,150–152). Thanks to the inhibition of the different proteases, we were able to identify different EpCAM cleavage bands with an increase in molecular weight of around 20-25 kDa because of the EGFP tag (Figure 13a): the full length protein of 67/68 kDa, the TMD plus EpICD fragment

(TMD+EpICD) of 35/36 kDa and the EpICD fragment alone of 25/26 kDa. We also observed other cleavages bands with molecular weight comprised between 30 and 34 kDa, called C-terminal fragments (CTFs) (116), whose expression remained unchanged despite treatments with inhibitors, suggesting that probably other proteases may be involved.

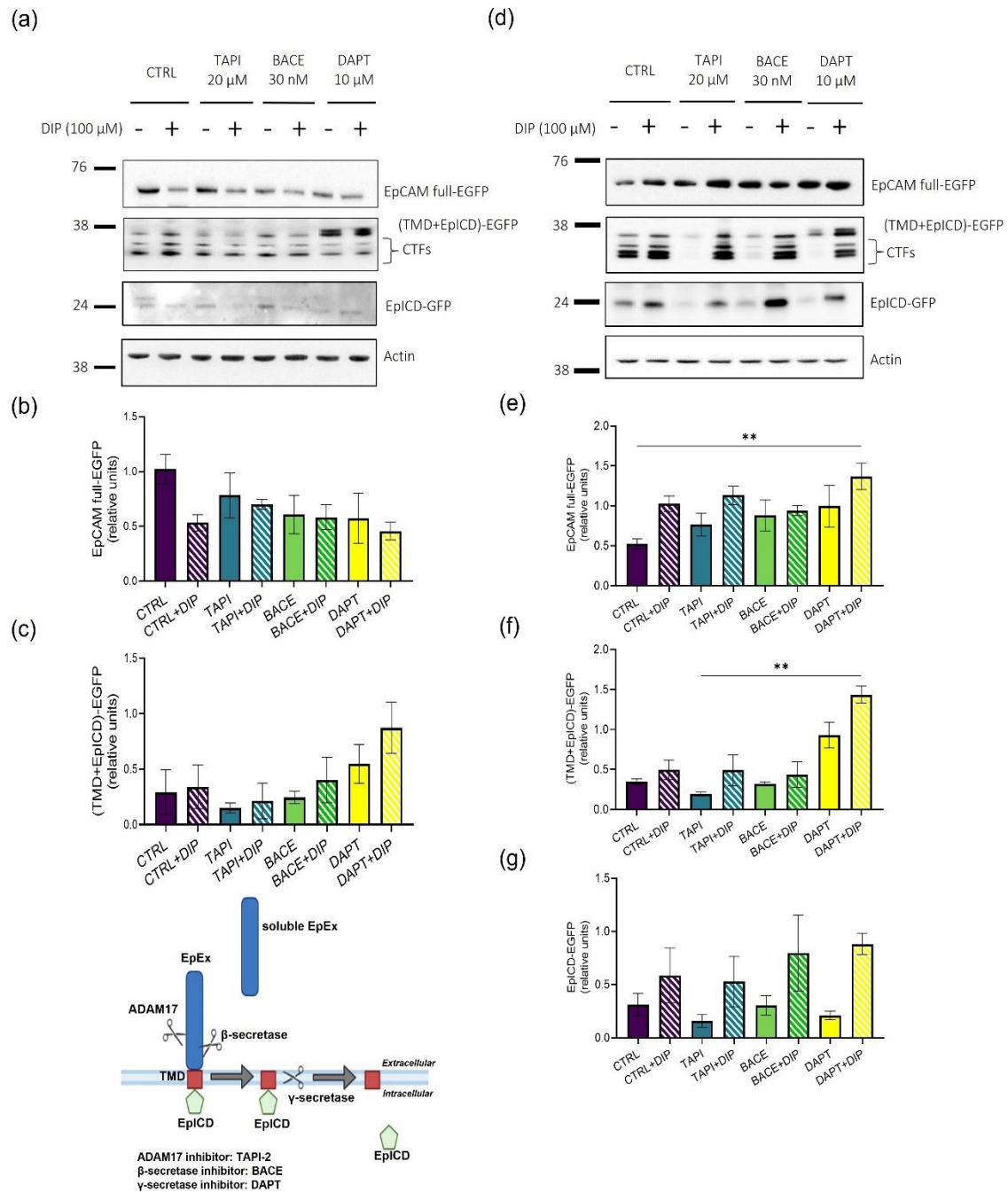


**Figure 13. Three main proteases (ADAM17,  $\beta$ -secretase and  $\gamma$ -secretase) are involved in EpCAM cleavages in FRO adherent cells. (a) Western Blot of protein extracts obtained from FRO adherent cells transfected with human EpCAM-EGFP and**

treated with TAPI-2 (20  $\mu$ M), BACE (30 nM) and DAPT (10  $\mu$ M). DIP (100  $\mu$ M) was also added to mimic pseudo-hypoxic condition. Relative quantification of EpCAM full length (b) and EpCAM TMD+ICD (c). (d) Western Blot of protein extracts obtained from HEK293T adherent cells transfected with human EpCAM-EGFP and treated with TAPI-2 (20  $\mu$ M), BACE (30 nM) and DAPT (10  $\mu$ M). DIP (100  $\mu$ M) was also added to mimic pseudo-hypoxic condition. Relative quantification of EpCAM full length (e), EpCAM TMD+ICD (f) and EpICD only (g). CTRL= untreated control transfected with human C-terminal EGFP. Statistical analysis: One way ANOVA followed by Tukey's multiple comparisons test. \*\*p < 0.01, n= 4.

From the quantification of the bands obtained in FRO, as expected, EpCAM full length decreased after DIP treatment respect to the control in basal condition. On the contrary, we didn't expect such high expression of full length EpCAM in the control in basal condition, since in this context all three proteases should be active and should cleave the full length, and a corresponding higher TMD+EpICD expression should be observed (Figure 13b, c). However, this trend could be due to the fact that, without any kind of stimulation, EpCAM remains intact in the plasma membrane and is not necessarily cleaved by proteases.

Considering each inhibitor alone, after inhibition of ADAM17 cleavage also  $\gamma$ -secretase is blocked and EpCAM should remain in its full length conformation, but  $\beta$ -secretase can still be active and able to cleave EpCAM, especially after DIP treatment. After inhibition of  $\beta$ -secretase alone, we observed a decrease of the full length respect to the control in basal conditions and a slight increase respect to the control under DIP treatment (Figure 13b). In this situation, ADAM17 and  $\gamma$ -secretase are active and their activity is increased by DIP, so they should cleave EpCAM more powerfully, but  $\beta$ -secretase cleavage is blocked and so a small portion of the full length can still be present. After inhibition of  $\gamma$ -secretase only, the full length is decreased respect to the control in basal condition since ADAM17 and  $\beta$ -secretase are both active and their activity is intensified after DIP treatment (Figure 13b). In this condition, the only part of the protein that is not cleaved is a small portion of the extracellular domain left after  $\beta$ -secretase cut, the TMD and the EpICD fragment. Indeed, in correspondence to a decreased EpCAM full length after DAPT treatment, we observed an increased expression of the TMD+EpICD, more pronounced after DIP treatment (Figure 13b, c).

Since the EpICD signal was hard to detect clearly, HEK293T easily transfectable cells were used to better identify the different bands obtained in FRO. After treating transfected cells with different inhibitors in the same way as FRO, we were able to visualize the full length, the TMD+EpICD and the EpICD fragment alone (Figure 13d). From the quantification of the different bands obtained in HEK293T, we observed an increased expression of EpCAM full length after DIP treatment (Figure 13e). This is quite unexpected since the full length should be more cleaved under pseudo-hypoxic condition induced by DIP, thus its expression should be lower. Moreover, differently than in FRO cells we also detected increased EpCAM full length expression after treatment with different inhibitors in normoxic conditions (Figure 13e).

After both ADAM17 and  $\beta$ -secretase inhibition, in correspondence to an increased EpCAM full length signal we observed a decreased TMD+EpICD expression, while after inhibition of  $\gamma$ -secretase we obtained a significant increase of TMD+EpICD expression, as expected, especially after DIP treatment (Figure 13e, f). In HEK293T transfected cells we were also able to better distinguish and quantify the EpICD-EGFP fragment alone (Figure 13g). As expected, EpICD expression increased in the control after DIP treatment respect to the control in basal condition, since the activity of the proteases is improved by DIP and they cleave EpCAM in all its domains (Figure 13g). After the inhibition of ADAM17, both without DIP and after DIP treatment, the EpICD signal is lower respect to the control, and this correlates to the increased EpCAM full expression (Figure 13g). After inhibition of  $\beta$ -secretase, the expression of EpICD is almost similar to the control in basal condition, but tend to increase after DIP treatment, probably suggesting that the block of  $\beta$ -secretase activity doesn't influence the proteolytic activity of  $\gamma$ -secretase, that is still active and cleaves EpICD fragment (Figure 13g).

At last, although the  $\gamma$ -secretase inhibition lead to an increase in the TMD+EpICD fragment, we didn't detected a corresponding decrease in the EpICD fragment alone (Figure 13g). This could be due either because the  $\gamma$ -secretase inhibition was only partially effective or because of in the case of artificially induced EpCAM overexpression in EpCAM negative cells, other degradation pathways different than canonically RIP ones may be activated.

## 1.6 EpCAM cleavage manipulation influences sphere-forming abilities of FRO cells

Given the complex pattern of EpCAM cleavages and the possibility to regulate it at many different levels we wanted to understand how this may influence the ability of cells with potential tumor-initiating properties to generate the 3D spheres. To do so, we performed two distinct experiments: in one experiment, adherent FRO were treated with selected concentrations of TAPI-2, BACE and DAPT; in the other one, adherent FRO were treated with increasing concentrations of DIP. After 24 hours of treatments, cells were then collected and seeded at clonal density as hanging-drops, and the ability to generate spheres was assessed after 7-10 days of culture. We observed that after the treatment with cleavages' inhibitors, the sphere-forming ability of cells in RPMI was slight increased after ADAM17 inhibition, decreased after beta-secretase inhibition and significantly increased after gamma-secretase inhibition (Figure 14a, left). We observed the same trend also in Sphere Medium, but the inhibition of gamma-secretase was not significant in this case (Figure 14a, right). On the other hand, the sphere-forming ability of cells was significantly compromised respect to the untreated control after increasing concentrations of DIP (Figure 14b). We observed the same trend both in RPMI (Figure 14b, left) and Sphere Medium (Figure 14b, right). Based on these results, we postulated that the integrity of EpCAM may be a crucial aspect for the initiation of 3D structures generation, at least in this specific *in vitro* setting, while EpCAM cleavage pattern may occur after the 3D spheres have been generated, in response to the more complex environment that exist in bigger spheres and in aggressive tumors.



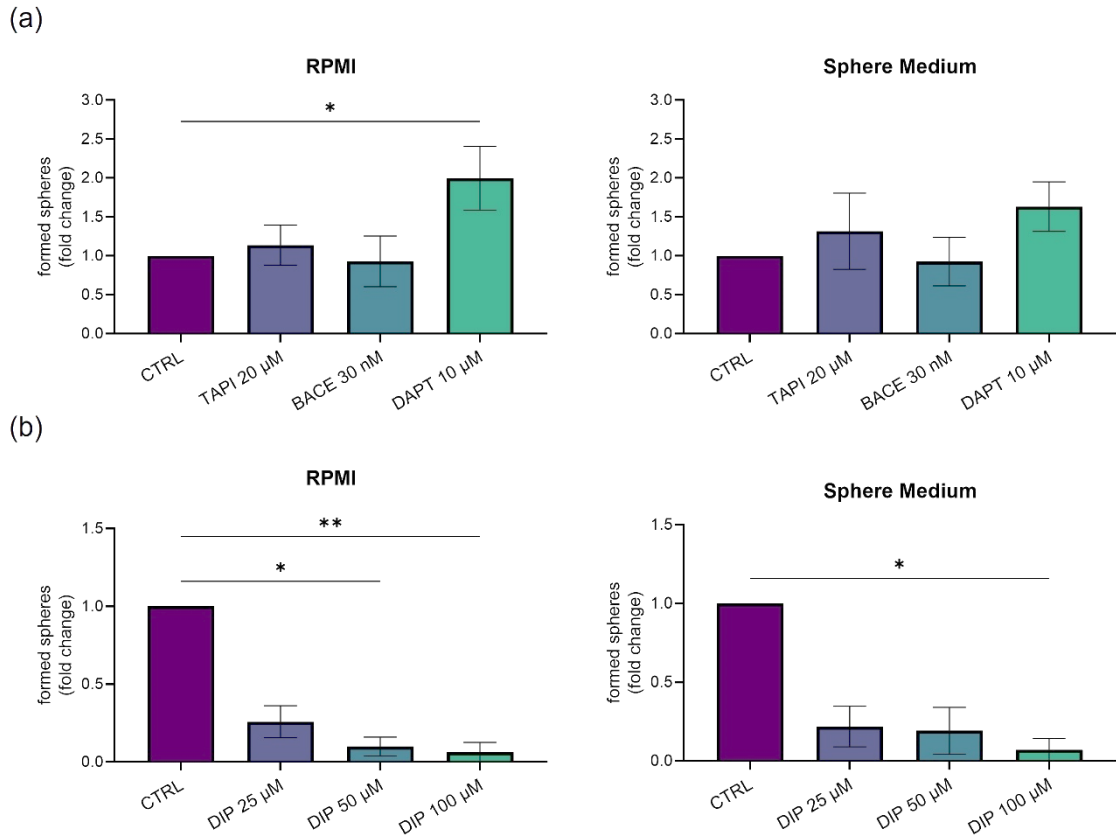


**Figure 14. Pseudo-hypoxic state, but not inhibition of EpCAM cleavages, significantly affects 3D sphere-generation ability in FRO.** (a) FRO were first seeded as adherent cells and treated with TAPI-2 (20  $\mu$ M), BACE (30 nM) and DAPT (10  $\mu$ M) after 48 h. Cells were then collected and seeded at clonal density as hanging-drops (10 cells per drop) in RPMI (left) and Sphere Medium (right) 24 h post treatments. The ability of cells to generate 3D spheres was assessed after 7-10 days of culture. (b) FRO were first seeded as adherent cells and treated with DIP (25  $\mu$ M, 50  $\mu$ M, 100  $\mu$ M) after 48 h. Cells were then collected and seeded at clonal density as hanging-drops (10 cells per drop) in RPMI (left) and Sphere Medium (right) 24 h post treatments. The ability of cells to generate 3D spheres was assessed after 7-10 days of culture. Statistical analysis: ANOVA Kruskal-Wallis test followed by Dunn's multiple comparisons test. \* $p < 0.05$ , \*\* $p < 0.01$ ,  $n = 4$ .

## 1.7 Vemurafenib (PLX-4032) treatments on FRO and HTCC3

Considering the results obtained, we tested if cells expressing EpCAM were resistant or sensitive to the effect of a well-known drug already used in clinical setting, Vemurafenib (PLX-4032), since it is known that tumor cells with tumor-initiating properties exert mechanisms of resistance toward pharmacological treatment (65,84–87). To evaluate whether the presence of EpCAM may be considered an additional factor to induce therapy resistance in tumor cells with tumor-initiating abilities, we treated adherent FRO and HTCC3 with increasing concentrations of PLX-4032. From cell proliferation curve obtained after MTT assay on FRO (Figure 15a) and HTCC3 (Figure 15b), we observed that both cell lines were responsive to PLX-4032 treatment but especially in FRO not all the data corresponded to the predicted sigmoidal dose-response curve. Since we demonstrated that EpCAM is expressed by both FRO and HTCC3 and they both present EpCAM+ and EpCAM- subpopulations, we hypothesized that this trend may be due to a different sensitivity of the two subpopulations to PLX-4032 treatment. One of the two might be more sensitive than the other, and the inhibitory effect of the drug is visible even at low concentrations, while the other one might be more resistant and responds to the drug at higher concentrations.

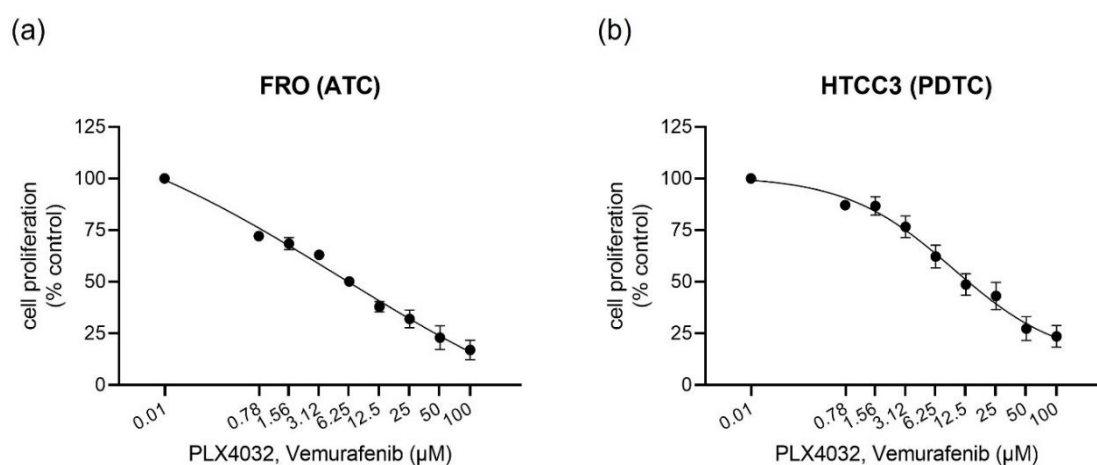


**Figure 15. Cell proliferation after PLX-4032 treatment on FRO and HTCC3 adherent cells.** Cells were seeded at the optimal density in 96-well plates and treated with increasing concentrations of PLX-4032 (0-100 µM) 24 h later. Cell proliferation curves of

FRO (a) and HTCC3 (b) were assessed with MTT assay (% control) 72 h after PLX-4032 treatment. n= 3.

To validate the hypothesis that EpCAM+ and EpCAM- subpopulation may present different sensitivity to PLX-4032, we performed Immunofluorescence on FRO adherent cells 72 h after the treatment with selected concentrations of PLX-4032 (IC50 and IC75), comparing them with untreated cells (Figure 16a). We clearly observed that the two subpopulations were fairly balanced in untreated cells (EpCAM+ 54,68%  $\pm$  6,47; EpCAM- 45,32%  $\pm$  6,47), while they tend to lose this balance upon treatment with PLX-4032 IC50 (EpCAM+ 76,22%  $\pm$  5,26; EpCAM- 23,78%  $\pm$  5,26) and IC75 (EpCAM+ 71,41%  $\pm$  14,50; EpCAM- 28,59%  $\pm$  14,50), characterized by a very significant decrease of EpCAM- subpopulation (Figure 16b). These results suggested that EpCAM+ cells appear to be more resistant than EpCAM- upon drug treatment, and this is a common feature of tumor cells that display tumor-initiating properties.

Knowing that the spatial organization of cells in the 3D spheres is a key factor to block drug penetration, as a next step we assessed the response of FRO-derived 3D spheres to PLX-4032. From the cell proliferation curve obtained in adherent cells, three concentrations were selected to be tested on 3D spheres and we observed that FRO-derived spheres seem to be non responsive to PLX-4032 treatment (Figure 16c), compared to FRO adherent cells.

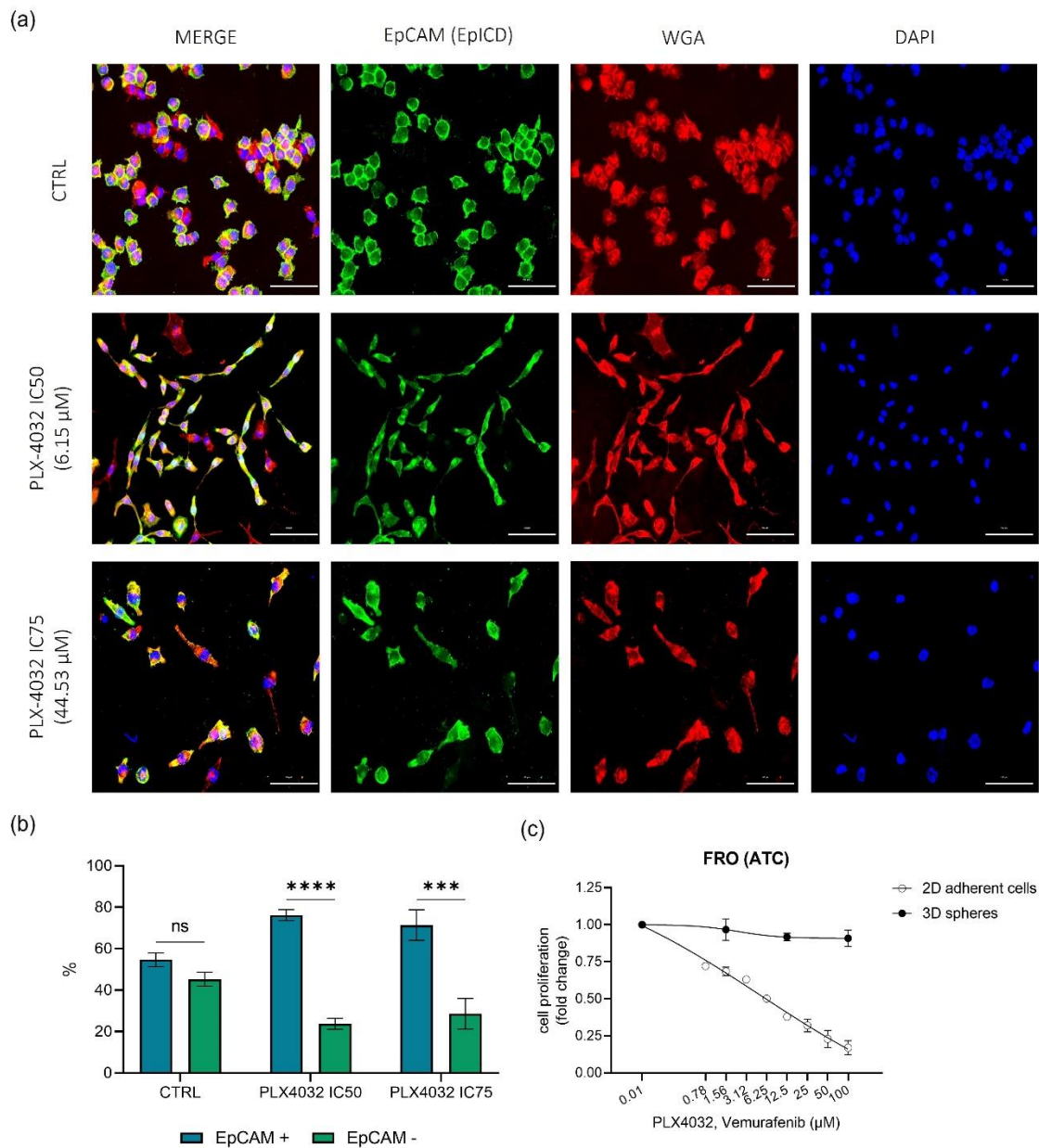


**Figure 16. EpCAM+ and EpCAM- cell subpopulations respond differently to PLX-4032 treatment on FRO adherent cells.** (a) Immunofluorescence experiments on FRO adherent cells were achieved respecting the same time points of the MTT assay: cells were seeded and treated with PLX-4032 IC50 (6.15  $\mu\text{M}$ ) and IC75 (44.53  $\mu\text{M}$ ) 24 h later, and Immunofluorescence was performed 72 h after treatment. EpICD in green, Wheat Germ Agglutinin (WGA) in red and DAPI staining for nuclei in blue. Scale bars represent 100  $\mu\text{M}$ . (b) Quantification as relative percentage of EpCAM+ and EpCAM- cells respect to the total number of cells. At least 10 different fields for each condition have been analyzed. CTRL= untreated cells. Statistical analysis: 2way-ANOVA followed by Šidák's multiple comparisons test. ns, not significant; \*\*\*\*p < 0.0001; \*\*\*p = 0.0001. n=3. (c) Cell proliferation curves of FRO-derived 3D spheres and FRO adherent cells. Selected concentrations of PLX-4032 were applied for treatment on 3D spheres (1.56, 12.5, 100

$\mu\text{M}$ ). White dots indicate FRO adherent cells relative proliferation (fold change), black dots indicate FRO-derived 3D spheres relative proliferation (fold change). For FRO-derived 3D spheres,  $n=3$ .

For further confirmation, the same Immunofluorescence experiments were carried out also on HTCC3 (Figure 17a) and we noticed a very significant imbalance of the two subpopulations toward the EpCAM+ one, even in untreated cells (EpCAM+ 76,51%  $\pm$  7,58; EpCAM- 23,49%  $\pm$  7,58). In cells treated with PLX-4032 IC50 we observed that EpCAM+ and EpCAM- were 82,98%  $\pm$  3,67 and 17,02%  $\pm$  3,67 respectively, and in cells treated with PLX-4032 IC75 were 100% and 0% respectively (Figure 17b). As for FRO, from the cell proliferation curve obtained in HTCC3 adherent cells, three concentrations were selected to be tested on 3D spheres and we observed that HTCC3-derived spheres seem to be more responsive to PLX-4032 treatment (Figure 17c), even at low concentrations, compared to FRO-derived 3D spheres.

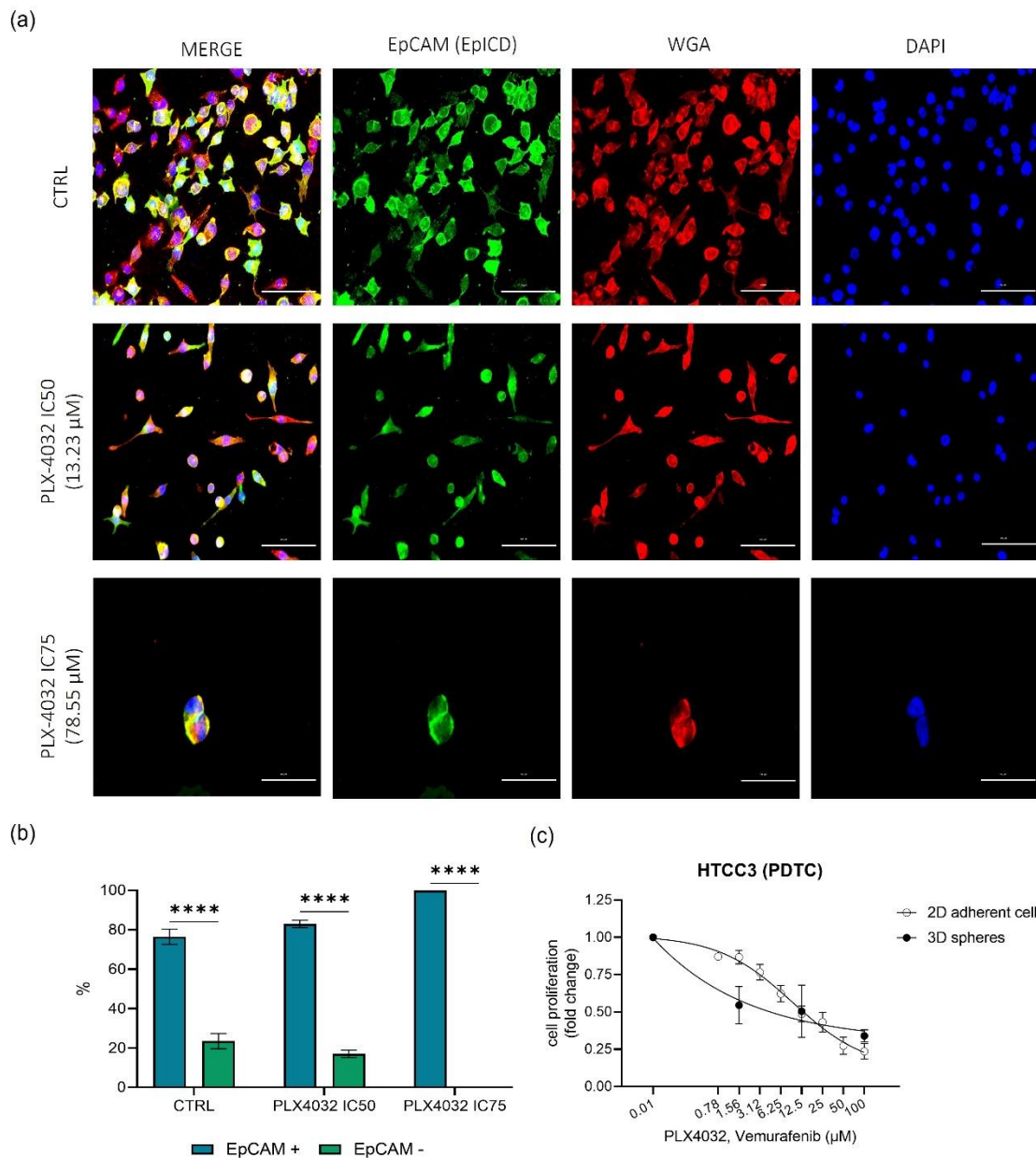


**Figure 17. EpCAM+ and EpCAM- cell subpopulations respond differently to PLX-4032 treatment on HTCC3 adherent cells.** (a) Immunofluorescence experiments on HTCC3 adherent cells were achieved respecting the same time points of the MTT assay: cells were seeded and treated with PLX-4032 IC50 (13.23  $\mu\text{M}$ ) and IC75 (78.55  $\mu\text{M}$ ) 24 h later, and Immunofluorescence was performed 72 h after treatment. EpICD in green, Wheat Germ Agglutinin (WGA) in red and DAPI staining for nuclei in blue. Scale bars represent 100  $\mu\text{M}$ . (b) Quantification as relative percentage of EpCAM+ and EpCAM- cells respect to the total number of cells. At least 10 different fields for each condition have been analyzed. CTRL= untreated cells. Statistical analysis: 2way-ANOVA followed by Šídák's multiple comparisons test. \*\*\*\* $p < 0.0001$ ,  $n = 3$ . (c) Cell proliferation curves of HTCC3-derived 3D spheres and HTCC3 adherent cells. Selected concentrations of PLX-4032 were applied for treatment on 3D spheres (1.56, 12.5, 100  $\mu\text{M}$ ). White dots

indicate HTCC3 adherent cells relative proliferation (fold change), black dots indicate HTCC3-derived 3D spheres relative proliferation (fold change). For HTCC3-derived 3D spheres, n= 3.

These results suggest that probably the subpopulation of EpCAM+ cells in FRO may have a greater role in inducing resistance to treatment, especially when cells are organized as 3D spheres, compared to HTCC3, that appear to be more sensitive when treated as 3D spheres. Different mechanisms of resistance or escape may occur in both FRO and HTCC3 when cells are organized in a 3D environment, but the presence of EpCAM+ cells seem to be effective in induce, at least partially, drug resistance in FRO.

# **Discussion and Conclusions**



Thyroid cancer (TC) is the most common Endocrine malignancy. Nowadays undifferentiated thyroid cancer are still a lethal disease, mostly because lack of effective therapeutic options. The insurgence of therapy resistance and disease relapse is believed to be caused by a subpopulation of cancer cells with a stem like phenotype and specific tumor initiating abilities, the so called tumor-initiating cells (TICs). Several markers have been identified and described over the years to detect TICs and allow the development of potential therapeutic approaches that could serve to specifically target these cells and promote the eradication of the tumor. In thyroid cancer, TICs have been identified using precise *in vitro* and *in vivo* assays (e.g. sphere-forming assays and tumor grafts), variations of enzymatic activities, expression of well-known stemness markers and expression of membrane markers.

In the present work we provide more insight into the role that Epithelial Cell Adhesion Molecule (EpCAM), a known TICs marker, may have in TC biology (93–95). This result was accomplished through the integration of TC tissues examination and *in vitro* 2D and 3D models.

Up to date, only a couple of studies, where TC-derived cell lines were used, investigated how EpCAM and its related molecules are involved in the pathological features of ATC: Shimamura et al (92) described that EpCAM appear to be a candidate marker only in FRO cells, showing that EpCAM<sup>high</sup> cell fraction alone or in combination with aldehyde dehydrogenase (ALDH) positive cells (ALDH<sup>pos</sup>) cells displayed higher sphere-forming ability respect to other anaplastic thyroid cancer (ATC) and differentiated thyroid cancer (DTC) cell lines, both *in vitro* and *in vivo*; Okada et al (163) observed that the expression levels of EpCAM, claudin-7 and ALDH in ATC-derived cells were significantly higher than those in DTC-derived cells, especially in FRO cell line. Nevertheless, *in vitro* studies on the possible involvement of EpCAM in TC pathology and tumor progression are generally few and do not investigate the role of protein cleavages' in tumor context, nor the tumorigenic potential of the intracellular portion of the protein, as occurs for other epithelial tumors in which EpCAM and its cleavages are studied more thoroughly (112,115,164,165). Indeed, most of the studies of

EpCAM in TC focus on evaluating its expression in patient-derived tissues by immunohistochemistry.

Our data demonstrated that EpCAM is subjected to an intense cleavage process in FRO-derived 3D tumor spheres (Figure 11a, b). FRO is a promising cell line for 3D spheres *in vitro* characterization of EpCAM, since this model is representative of the variability of EpCAM expression and cleavage that we found in patient-derived tissue samples (Figure 8a, b, c). We also demonstrated that the expression of EpCAM can be modulated by the regulation of its cleavages and that the integrity of the protein seem to be a crucial factor for the initial phase of the generation of the 3D spheres in FRO (Figure 14a, b). Moreover, we demonstrated that EpCAM+ and EpCAM- subpopulations respond differently to treatment with a well-known drug commonly used in clinical practice, Vemurafenib (PLX-4032), both in FRO and HTCC3 adherent cells (Figure 15a, b). Finally, we observed that the 3D sphere model is also a valid *in vitro* approach to assess cell response to PLX-4032 activity (Figure 16c and 17c). We will now discuss more in detail the accomplished results.

First of all, we evaluated the expression and cleavage of EpCAM on healthy and pathological patient-derived tissue samples. Quite recent studies have demonstrated that cytoplasmic and/or nuclear localization of EpCAM could be a useful marker for aggressive TC (132–134,166). At immunohistochemistry, Ralhan et al (132,133) demonstrated that the low-grade papillary thyroid cancers (PTCs) showed membranous expression of EpCAM (both extracellular, EpEx, and intracellular, EpICD, fragments), the follicular thyroid cancers (FTCs) showed a variable EpCAM signal, both membranous and cytoplasmic, but no detectable nuclear EpICD was reported in both PTCs and FTCs. On the other hand, loss of membranous expression and increased cytoplasmic and nuclear accumulation of EpICD fragment was observed in ATCs, correlating with tumor aggressiveness. We obtained similar results in our patient-derived tissue samples both at Western Blot and Immunofluorescence, where the variability in EpCAM expression in the healthy tissue and within the different TC histotypes is not due to a loss of protein expression, but to a differential cleavage pattern, where EpCAM is highly cleaved in UDTCs (Figure 8a, b, c). We hypothesized that these variations observed in

EpCAM cleavage could be associated with the distinct degree of differentiation of neoplastic cells within the tumor and/or with variations of microenvironment in specific areas of the tumor, as a support of the presence of tumor cells with tumor-initiating abilities and stem-like properties in certain niches of the tumor mass (61,63–65).

Having observed that EpCAM was predominantly expressed in FRO and in small amount in HTCC3 cell lines (Figure 9a, b), we decided to develop a proper tridimensional model based on these cells to study EpCAM modifications *in vitro*. We first analyzed the ability of the selected TC cell lines to generate 3D spheres when seeded at clonal density as hanging-drops, discriminating between cells seeded in their culture medium or in Sphere Medium. We applied the 3D spheres model since one of the main features of TICs is to self-renew and display anchorage-independent growth in form of spheroids, as described in different cancer types (167–170). Moreover, cells were seeded at clonal density in order to observe if even from a single clone, potentially capable of regenerating the tumor, 3D spheres were obtained; in this case, that cell could display self-renew ability and could grow in anchorage-independent way, thus being considered as a putative TIC.

Given that we observed an impairment in cells ability to generate 3D spheres when seeded in Sphere Medium, we postulated that, since they are immortalized cell lines, they are "pre-selected" to grow in their culture medium, so they may not be able to generate spheres in a serum-free environment. It is known that Sphere Medium is the ideal medium to isolate stem-like cells (142), however in recent years it has been observed that not all cells that are capable of regenerating the tumor are considered stem cells, but rather the term TIC has been applied, which represents a functional definition of the capacity of these tumor cells to induce tumor formation in xenotransplantation studies. TICs have only some common features with CSCs, so cells with stemness ability could still be present in immortalized cell lines, but they don't have such a degree of stemness that they can survive only in Sphere Medium, but could be selected through the seeding at clonal density or single clone seeding in their culture medium.

As a confirm, FRO presented the highest frequency of tumor cells with putative tumor-initiating ability within the 3D sphere cultures, as observed by Extreme Limiting Dilution Analysis (ELDA), when cells were seeded at clonal density in their culture medium (Figure 10d and Table 6a). Considering the preliminary results, we decided to deepen the studies on FRO for the characterization of EpCAM, applying the 3D spheres model with both their culture medium and Sphere Medium.

The same variations in the degree of EpCAM cleavage obtained in patient-derived tissues were also observed in FRO-derived 3D spheres (Figure 11a, b). The progressive increase in EpICD signal in opposite to a reduction of EpEx signal from the outer surface to the inner core of the spheres could indicate the existence of a radial gradient of EpCAM cleavage in FRO spheres, probably due to the radial gradient of nutrients and oxygen typical of 3D tumor spheres (64,77) and the consequent progressive loss of epithelial differentiation towards a more mesenchymal phenotype (171–174). Moreover, we noticed a slight expression of both E-Cadherin, typical epithelial marker, together with a strong expression of Vimentin, typical mesenchymal marker, in 3D spheres at Western Blot. The presence of both markers may be explained by the fact that the epithelial component is not completely lost when cells are organized as 3D spheres: indeed, cells forming the outer layer of the sphere are those that keep more epithelial-like phenotype, so E-Cadherin may still be expressed. However, Vimentin is also present in these spheres, characterized by a stronger expression, as observed at Western Blot, that may indicate that cells in an intermediate condition are more prone to change their phenotype based on metabolism and/or oxygen variations, which resembles what we observed in patient-derived tissues.

Therefore, we decided to evaluate whether the expression and cleavage of EpCAM could be modulated or influenced by some features occurring in solid tumors such as the presence of an hypoxic niche and the 3D organization of the tumor itself, since EpCAM is also involved in cell-cell adhesion, and we aimed to study this protein in a *in vitro* condition that is similar, as far as possible, to primary solid tumors. To evaluate the influence of 3D organization on EpCAM full expression, cells were treated with epidermal growth factor (EGF), being one of

the main growth factors for the maintenance of stem-like cells in 3D cultures, known to upregulate EpCAM expression in some tumors via ERK1/2 signaling (113,135). We expected to see an increase in full length protein expression correlated with increasing concentrations of EGF in culture; on the contrary, we didn't observe significant differences in EpCAM full length expression between treated and untreated conditions (Figure 12).

Although we used the same concentrations as for the maintenance of cells as 3D sphere cultures, where we observed an intense cleavage rate of EpCAM at Immunofluorescence, the presence of growth factors such as EGF in the culture medium may not influence the preservation of EpCAM in its full length form or induce its cleavage, but rather the fact that cells grow in a three-dimensional organization may have stronger effect on EpCAM expression and/or its cleavage. On the other hand, the presence of a condition of pseudo-hypoxia induced by 2,2'-Bipyridyl (DIP) treatment allowed us to demonstrate that the expression of the full length decreases as the concentration of DIP increases (Figure 12). This supports what is described in literature regarding DIP as an hypoxia-mimetic compound that increases the proteolytic activity of ADAM17, and consequently of  $\gamma$ -secretase, which are known to be among the major proteases involved in EpCAM cleavage (68,153–156). As a consequence, the more the pseudo-hypoxic condition is emphasized, the more the full length EpCAM is cleaved and potentially the intracellular portion of the protein is able to translocate from the membrane to the cytoplasm and/or nucleus.

To better understand the role of the different proteases involved in EpCAM cleavage, we performed Western Blots on both our cell line of interest (FRO) and on HEK293T (Figure 13), as they are an easily transfectable cell line already used in literature to characterize EpCAM cleavages (116). After having tested the cleavage activity of the different proteases (ADAM17,  $\beta$ -secretase and  $\gamma$ -secretase) through their inhibitors (TAPI-2, BACE and DAPT, respectively), we noticed that the inhibition of ADAM17 and  $\beta$ -secretase in FRO didn't play a predominant role in the regulation of EpCAM cleavage and eventually in the activation of intracellular signaling due to its shedding. Indeed, both in FRO, that normally express EpCAM, and in HEK293T cells, that presented overexpression of EpCAM after transient transfection, the protease  $\gamma$ -secretase seemed to have

a greater role, since the inhibition of its cleavage induced by DAPT led to an increased expression of transmembrane domain and intracellular domain of EpCAM (TMD+EpICD) portion, as observed at Western Blot. We weren't able to obtain great variations in the EpICD expression alone in FRO, since in these experimental conditions in immortalized cells is hard to perfectly recreate the conditions that exist in the primary tumor, and the use of the different inhibitors may alter the activity of co-factors that could stabilize the EpICD fragment and eventually prevent its degradation. Indeed, ADAM17 and  $\gamma$ -secretase in particular, are involved in the cleavage, and eventual activation, of membrane receptors involved in other well-known pathways in tumor context, such as Notch or Wnt/ $\beta$ -catenin, which are involved in maintenance of stemness and in promoting tumor-initiating abilities (85–87). Thus, ADAM17 and  $\gamma$ -secretase inhibitors may not only block EpCAM cleavage but may also induce inhibition or significant alteration of other pathways in which these proteases are involved. Nevertheless, we observed that EpCAM cleavage is present and occur in FRO cell line and that has a fundamental role, otherwise we wouldn't observe any changes following  $\gamma$ -secretase inhibition, as we did notice at Western Blot.

To further characterize the role of EpCAM cleavages, in particular of EpICD, we performed Western Blot experiments on FRO adherent cells treated with TAPI-2, BACE and DAPT, and observe the ability of treated and untreated cells to generate 3D spheres when seeded as hanging-drops (Figure 14a). We believed that protein cleavage in EpCAM-expressing cells was a necessary event to induce the generation of the 3D spheres, as the intracellular portion of EpCAM, if translocate into the nucleus, can regulate the transcription of genes associated with proliferation (109–111), stemness (112,115), and epithelial to mesenchymal transition (EMT)-associated factors (114). However, the inhibition of EpCAM cleavages by treating cells with the different proteases' inhibitors, led us to observe that the ability of FRO to generate 3D spheres when seeded at clonal density was not impaired, as we originally expected, but had the tendency to increase, even slightly significantly after  $\gamma$ -secretase inhibition with DAPT.

This result is fundamental, since suggests that the intracellular domain of EpCAM, when it is not cleaved but remains in the plasma membrane, can be associated with actin molecules of the cytoskeleton, and can contribute to the

stability of the connection between the protein itself and the cytoskeleton through alpha-actinin binding sites (104–106). The maintenance of this connection might then be necessary for the involvement of EpCAM in the generation of the 3D structures, as described in literature (104,105,175).

The manipulation of EpCAM cleavages in adherent cells, given that FRO are first treated as adherent cells and then seeded at clonal density as hanging-drops, can be considered an artificial attempt to reproduce the conditions occurring in the spheres, and that EpCAM cleavages can be promoted as the organization of the spheres increases, together with increase in dimensions. We believe that the integrity of EpCAM in the initial stages of sphere generation could be an advantage for cells that have to organize the 3D structure, especially in the very early stages and when the 3D aggregate is small, since EpCAM role as an adhesion molecule, that could promote and intensify cell-cell contact, is guaranteed when the protein is in its full length form. As the sphere grows and the 3D structure is more defined, EpCAM cleavage may then occur, as we have observed at Immunofluorescence on FRO-derived spheres (Figure 11b), induced by the ability of cells to adapt to variations in growth conditions and/or to the microenvironment within the spheres.

As a confirm, the results obtained after treating adherent cells with increasing concentrations of DIP, that improves proteolytic cleavage of ADAM17 and  $\gamma$ -secretase, showed that DIP-induced pseudo-hypoxic condition significantly compromise the ability of FRO to generate 3D spheres when seeded at clonal density (Figure 14b).

Given their identification and characterization in TC, TICs have emerged as possible fundamental players for the resistance to conventional therapies. Unlike the highly proliferating cells, TICs may not be eradicated by chemotherapy and radiotherapy, causing the relapse of the disease. Resistance of TICs to kinase inhibitors may be due to different mechanisms, including induction of EMT through the activation of EMT transcription factors (78,79,82,176), increased drug efflux efficiency through ATP-binding cassette (ABC) transporters (65,90), activation of the bypass pathways via overexpression of MAP3K8, after

BRAFV600E inhibition, that promotes survival of tumor cells (84), and deregulation of stem cell signaling pathways such as Hedgehog, Notch, JAK/STAT and Wnt/ $\beta$ -catenin (85–87).

Since we demonstrated that FRO-derived 3D spheres present a gradient of EpCAM cleavage and after manipulating these cleavages we obtained different sphere-forming abilities, we aimed to observe whether EpCAM<sup>+</sup> and EpCAM<sup>-</sup> subpopulations present in FRO and HTCC3 could express a different sensibility to the effect of Vemurafenib (PLX-4032), a well-known drug commonly used in clinical setting, upon treatment on adherent cells and on 3D spheres.

Giving the proliferation curves obtained after treating adherent cells with PLX-4032 (Figure 15a, b), we hypothesized that the two subpopulations present in FRO and HTCC3 may actually respond differently to the drug and that the trend observed is due to a different sensitivity of the two subpopulations to PLX-4032 treatment. Indeed, one might be more sensitive than the other, and the inhibitory effect of the drug is visible even at low concentrations, while the other one might be more resistant and responds to the drug at higher concentrations. Through Immunofluorescence experiments on adherent FRO and HTCC3 we actually confirmed that EpCAM<sup>+</sup> cells appear to be more resistant than EpCAM<sup>-</sup> cells (Figure 16 a, b and Figure 17 a, b). Through these experiments we also noticed that after the treatment with different concentrations of PLX-4032 (IC<sub>50</sub> and IC<sub>75</sub>) cells displayed a more elongated, “mesenchymal-like” morphology, especially the EpCAM<sup>+</sup> ones, respect to the untreated control (Figure 16a and 17a), in both cell lines.

We hypothesized that this morphological change may be due to the activation of mechanisms of resistance to the treatment, for example by promoting the induction of EMT which, as previously mentioned, is known to be one of the mechanisms of drug-resistance in TICs, or by activating some escape mechanisms via different pathways that lead them to change morphology. In literature is known that cells in response to signals that receive from their microenvironment may induce EMT, where changes in gene expression and post-translational mechanisms lead to the repression of the epithelial features



and induce the acquisition of mesenchymal ones, where cells display more elongated and fibroblast-like morphology and architecture (78,79,82,176). Certainly these results will have to be further investigated in the future, to observe whether in EpCAM+ cells the switch between expression of E-Cadherin or cytokeratins to vimentin occurs, or whether we are facing the phenomenon of epithelial-mesenchymal plasticity (EMP) (176), where cells assume both epithelial and mesenchymal features and interchange between intermediate epithelial/mesenchymal phenotype.

Knowing that the spatial organization of cells in the 3D spheres is a key factor to block drug penetration, concomitantly to the treatment on adherent cells and Immunofluorescence experiments, we assessed whether FRO-derived and HTCC3-derived 3D spheres respond differently to PLX-4032 treatment respect to 2D adherent cells (Figure 16c and 17c).

We noticed a differential response of the two cell lines in response to PLX-4032: FRO-derived 3D spheres seemed to be more resistant, since they didn't respond to the drug at any of the selected concentrations, while HTCC3-derived 3D spheres seemed to be more sensitive, even at low concentrations. Moreover, although we obtained a complete different response in treatment between adherent cells and 3D spheres in FRO, also in HTCC3 the survival of cells when treated as 3D spheres at higher concentrations of PLX-4032 is greater than when treated as adherent cells, and this reflects what we observed at Immunofluorescence on adherent cells, where the only cells that persisted after treatment with high concentrations of PLX-4032 were the EpCAM+ ones. Furthermore, 3D spheres are mostly constituted by EpCAM+ cells, at least as we demonstrated in FRO, and present a different degree of protein cleavage. The different domains of cleaved EpCAM could therefore be another important aspect that may be involved in inducing drug resistance. As observed at Western Blot in FRO-derived 3D spheres (Figure 11a), cells organized in 3D structures may induce higher cleavage of EpCAM full length, together with an increase in vimentin signal, and this could lead to the generation of a more "mesenchymal-like" phenotype, that is known to be another mechanism of resistance toward anticancer drugs.

Nevertheless, EpCAM alone may not be responsible for the induction of drug resistance, but could play a role in maintaining tumor cells with tumor-initiating abilities during pharmacological treatment. Indeed, other several factors may be implied to induce therapy resistance, such as problems with drug penetration that may occur in the inner core of the spheres, or the activation of drug efflux mechanisms and/or escape mechanisms. At the moment we cannot say with confidence that the difference we observed in PLX-4032 sensitivity is due to the actual presence of EpCAM+ subpopulation, and not due to other factors such as the genetic background of these cell lines.

Indeed, as future work it would be of interest to separate the two subpopulations through fluorescence-activated cell sorting (FACS), and confirm which one is actually resistant and which one is not, also evaluating the type of mutations that the two subpopulations have, as it is not certain that they both express the same genetic background. Upon cell sorting, it would be also interesting to characterize EpCAM+ and EpCAM- subpopulations in both adherent cells and 3D spheroids by studying the co-expression and possible correlation of the protein with stem cell markers (OCT-4, NANOG, SOX2, CD133) or with thyroid differentiation markers (thyroglobulin, TG, receptor of thyroid stimulating hormone, TSH-R, thyroid peroxidase, TPO) through Immunofluorescence, Western Blot and RT-PCR. It would be equally intriguing to assess if the contribution of only one or both subpopulations in FRO is required to create and maintain the 3D spheres structures, and to observe if these abilities are somehow improved or compromised after EpCAM silencing in FRO through siRNA or shRNA. In addition, once the EpICD fragment moves from the plasma membrane to the cytoplasm or nucleus, it would be useful to apply a high-resolution imaging technique, such as expansion microscopy (ExM), to better visualize its localization; this technique allows to generate valuable structural insights that would otherwise require more complex super-resolution methods.

Overall, we observed that FRO exhibit different biological behavior than the other cell lines used in the study, even compared with other cell lines with the same tumor origin. We hypothesize that one of the reasons may be due precisely to the properties associated with tumor-initiating ability that we found in this cell line, as previously mentioned; these properties suggest that FRO, better than the other

cell lines, may be able to reproduce the heterogeneity of the tumor of origin *in vitro*, as far as possible. Furthermore, in FRO EpCAM-expressing cells, the intense cleavage of the protein and the transfer of the EpICD portion from the plasma membrane to the cytoplasm and/or nucleus, as previously discussed, could play a key role in maintaining a more undifferentiated phenotype with respect to the other cell lines, which are totally negative for EpCAM, and respect to HTCC3, where the protein is expressed but is localized predominantly in the plasma membrane. In addition to EpCAM, FRO may also express other markers related to TICs, as already described in literature for other epithelial tumors. Certainly, a further comprehension of the properties of this cell line is needed.

In conclusion, in the present study we demonstrated that FRO is a promising cell line for the characterization of EpCAM through *in vitro* studies, both applying classical monolayer cultures and 3D sphere cultures, given that the 3D model is representative of the variability of EpCAM expression that we observed in patient-derived tissue samples, with the different gradient of EpCAM cleavages that corresponds to different areas of the tumor sections. We demonstrated that the 3D model was also manageable to perform experiments that better described EpCAM expression and cleavage pattern. In particular, the results obtained after the inhibition of EpCAM cleavages and after DIP treatments suggested that the integrity of EpCAM may be required for the initial phases of the generation of the 3D spheres, and that cleavage of the protein may occur in a second moment, induced by the ability of cells to adapt to variations in growth conditions and/or to the microenvironment within the spheres. Giving the proliferation curves obtained after treating cells with PLX-4032, we hypothesized that EpCAM<sup>+</sup> and EpCAM<sup>-</sup> subpopulations present in FRO and HTCC3 may respond differently to the drug, and Immunofluorescence performed after treatment on both cell lines confirmed that EpCAM<sup>+</sup> cells appeared to be more resistant. Finally, the treatment with PLX-4032 on FRO-derived and HTCC3-derived 3D spheres showed that FRO seemed to be more resistant than HTCC3-derived spheres. We believed that the presence of EpCAM and its cleavage in 3D spheres could be an additional factor for cells to induce therapy resistance, concomitantly to other mechanisms of resistance and/or escape that may occur.

To conclude, EpCAM expression and cleavage is playing a significant role in putative TC TICs biology and may partially explain the therapeutic failure observed in the more undifferentiated thyroid cancers. For these reasons we believe that EpCAM evaluation could play a role in the clinical decisions regarding patients therapy and further studies need to be performed in order to translate these findings in patient-derived primary tumors.

## **Acknowledgements**

*At the end of this experience, I would like to express my sincere gratitude to Prof. Luca Persani, my tutor, for giving me the opportunity to carry out the PhD in his research group, and a special thank to Elisa Grassi, my supervisor, for sharing her expertise, insights and encouragement in the development of this crazy work. I am also grateful to all my lab colleagues for providing support and friendship throughout these years. They immediately made me feel part of the group and have made this experience much more enjoyable.*

*I would also like to express my gratitude to the PhD program in Experimental Medicine and the fellowship supported by Università degli Studi di Milano, for providing me with the resources needed to pursue the research project.*

*A huge thank to my parents for their sacrifices and continuous support in any moment, without the need to ask, and to my lifetime friends, for being a constant in my life.*

*A special thank to Edo, for his resolute encouragement throughout this experience and his infinite patience and support in the moments of insecurity; dealing with me every day is not easy, so thanks for always being there.*

# **Bibliography**

1. <http://seer.cancer.gov/faststats> [Internet].
2. Vaccarella S, Franceschi S, Bray F, Wild CP, Plummer M, Dal Maso L. Worldwide Thyroid-Cancer Epidemic? The Increasing Impact of Overdiagnosis. *N Engl J Med*. 2016 Aug 18;375(7):614–7.
3. Pellegriti G, Frasca F, Regalbuto C, Squatrito S, Vigneri R. Worldwide Increasing Incidence of Thyroid Cancer : Update on Epidemiology and Risk Factors. 2013;2013.
4. Kilfoy BA, Zheng T, Holford TR, Han X, Ward MH, Sjodin A, et al. International patterns and trends in thyroid cancer incidence, 1973-2002. *Cancer Causes Control*. 2009 Jul;20(5):525–31.
5. Thyroid Cancer: Statistics | Cancer.Net [Internet]. Available from: <https://www.cancer.net/cancer-types/thyroid-cancer/statistics>
6. Smallridge RC, Ain KB, Asa SL, Bible KC, Brierley JD, Burman KD, et al. for Management of Patients with Anaplastic Thyroid Cancer. 2012;22(11):1104–39.
7. Haddad RI, Lydiatt WM, Ball DW, Busaidy NL, Byrd D, Callender G et al. Anaplastic Thyroid Carcinoma, Version 2.2015. *J Natl Compr Canc Netw*. 2015;13(1140–50).
8. Liu Y, Su L, Xiao H. Review of Factors Related to the Thyroid Cancer Epidemic. *Int J Endocrinol*. 2017;2017.
9. Williams D. Radiation carcinogenesis: lessons from Chernobyl. *Oncogene* 2009 272. 2009 Dec 3;27(2):S9–18.
10. Bumber B, Marjanovic Kavanagh M, Jakovcevic A, Sincic N, Prstacic R, Prgomet D. Role of matrix metalloproteinases and their inhibitors in the development of cervical metastases in papillary thyroid cancer. *Clin Otolaryngol*. 2020;45(1):55–62.
11. Guan H, Ji M, Bao R, Yu H, Wang Y, Hou P, et al. Association of high iodine intake with the T1799A BRAF mutation in papillary thyroid cancer. *J Clin Endocrinol Metab*. 2009;94(5):1612–7.
12. Almquist M, Johansen D, Björge T, Ulmer H, Lindkvist B, Stocks T, et al. Metabolic factors and risk of thyroid cancer in the Metabolic syndrome and Cancer project (Me-Can). *Cancer Causes Control*. 2011;22(5):743–51.
13. Yang SP, Ngeow J. Review S Peiling Yang and J Ngeow Familial non-

- medullary thyroid cancer review Familial non-medullary thyroid cancer: unraveling the genetic maze. 2016;
14. Tiedje V, Fagin JA. Therapeutic breakthroughs for metastatic thyroid cancer. *Nat Rev | Endocrinol.* 2020;16.
  15. Veschi V, Verona F, Lo Iacono M, D'Accardo C, Porcelli G, Turdo A, et al. Cancer Stem Cells in Thyroid Tumors: From the Origin to Metastasis. *Front Endocrinol (Lausanne).* 2020;11(August):1–18.
  16. Remick SC, Nagaiah G, Hossain A, Mooney CJ, Parmentier J. Anaplastic thyroid cancer: A review of epidemiology, pathogenesis, and treatment. Vol. 2011, *Journal of Oncology. J Oncol;* 2011.
  17. Perri F. Anaplastic thyroid carcinoma: A comprehensive review of current and future therapeutic options. *World J Clin Oncol.* 2011;2(3):150.
  18. Xing M. Molecular pathogenesis and mechanisms of thyroid cancer. *Nat Rev Cancer.* 2013 Mar;13(3):184–99.
  19. Tamhane S, Gharib H. Thyroid nodule update on diagnosis and management. 2016;
  20. Hsiao SJ, Nikiforov YE. Molecular approaches to thyroid cancer diagnosis.
  21. Tate JG, Bamford S, Jubb HC, Sondka Z, Beare DM, Bindal N, et al. COSMIC: the Catalogue Of Somatic Mutations In Cancer. *Nucleic Acids Res.* 2019 Jan 8;47(D1):D941–7.
  22. Pogliaghi Gabriele. Liquid biopsy in thyroid cancer: from circulating biomarkers to a new prospective of tumor monitoring and therapy. *Minerva Endocrinol.* 2021;46((1)):45–61.
  23. Mahmoudian-sani M-R, Mehri-Ghahfarrokhi A, Asadi-Samani M, Mobini G-R. Serum miRNAs as Biomarkers for the Diagnosis and Prognosis of Thyroid Cancer: A Comprehensive Review of the Literature. *Eur Thyroid J.* 2017;6(4):171–7.
  24. Nikiforov YE. Thyroid Carcinoma: Molecular Pathways and Therapeutic Targets. *Mod Pathol.* 2008;21(Suppl 2):S37.
  25. Aashiq M, Silverman DA, Na'ara S, Takahashi H, Amit M. Radioiodine-Refractory Thyroid Cancer: Molecular Basis of Redifferentiation Therapies, Management, and Novel Therapies. 2019;
  26. Prete A, Borges de Souza P, Censi S, Muzza M, Nucci N, Sponziello M.



- Update on Fundamental Mechanisms of Thyroid Cancer. *Front Endocrinol (Lausanne)*. 2020 Mar 13;11:102.
27. Tirrò E, Martorana F, Romano C, Vitale SR, Motta G, Di Gregorio S, et al. Molecular Alterations in Thyroid Cancer: From Bench to Clinical Practice. *Genes (Basel)*. 2019 Sep 1;10(9).
  28. Namba H, Rubin SA, Fagin JA. Point mutations of ras oncogenes are an early event in thyroid tumorigenesis. *Mol Endocrinol*. 1990;4(10):1474–9.
  29. Xing M. Genetic alterations in the phosphatidylinositol-3 kinase/Akt pathway in thyroid cancer. *Thyroid*. 2010;20(7):697–706.
  30. Sastre-Perona A, Santisteban P. Role of the Wnt Pathway in Thyroid Cancer. *Front Endocrinol (Lausanne)*. 2012;3(FEB).
  31. Nikiforov YE, Nikiforova MN. Molecular genetics and diagnosis of thyroid cancer. *Nat Publ Gr*. 2011;7:569–80.
  32. Agrawal N, Akbani R, Aksoy BA, Ally A, Arachchi H, Asa SL, et al. Integrated genomic characterization of papillary thyroid carcinoma. *Cell*. 2014 Oct 23;159(3):676–90.
  33. Solomon JP, Benayed R, Hechtman JF, Ladanyi M. Identifying patients with NTRK fusion cancer. *Ann Oncol Off J Eur Soc Med Oncol*. 2019 Nov 1;30 Suppl 8(Suppl\_8):viii16–22.
  34. Eberhardt NL, Grebe SKG, Mclver B, Reddi H V. The role of the PAX8/PPAR $\gamma$  fusion oncogene in the pathogenesis of follicular thyroid cancer. *Mol Cell Endocrinol*. 2010 May 28;321(1):50–6.
  35. Killela PJ, Reitman ZJ, Jiao Y, Bettegowda C, Agrawal N, Diaz LA, et al. TERT promoter mutations occur frequently in gliomas and a subset of tumors derived from cells with low rates of self-renewal.
  36. Liu X, Bishop J, Shan Y, Pai S, Liu D, Murugan K, et al. Highly prevalent TERT promoter mutations in aggressive thyroid cancers.
  37. Muzza M, Colombo C, Rossi S, Tosi D, Cirello V, Perrino M, et al. Telomerase in differentiated thyroid cancer: Promoter mutations, expression and localization. *Mol Cell Endocrinol*. 2015;399:288–95.
  38. Yang J, Gong Y, Yan S, Chen H, Qin S, Gong R. Association between TERT promoter mutations and clinical behaviors in differentiated thyroid carcinoma: a systematic review and meta-analysis. *Endocrine*. 2020 Jan 1;67(1):44.

39. Landa I, Ibrahimasic T, Boucai L, Sinha R, Knauf JA, Shah RH, et al. Genomic and transcriptomic hallmarks of poorly differentiated and anaplastic thyroid cancers. *J Clin Invest*. 2016 Mar 1;126(3):1052–66.
40. Schlumberger M, Leboulleux S. Current practice in patients with differentiated thyroid cancer. *Nat Rev Endocrinol*. 2021 Mar 1;17(3):176–88.
41. Haugen BR, Alexander EK, Bible KC, Doherty GM, Mandel SJ, Nikiforov YE, et al. 2015 American Thyroid Association Management Guidelines for Adult Patients with Thyroid Nodules and Differentiated Thyroid Cancer: The American Thyroid Association Guidelines Task Force on Thyroid Nodules and Differentiated Thyroid Cancer. *Thyroid*. 2016 Jan 1;26(1):1–133.
42. Michael Tuttle R, Ahuja S, Avram AM, Bernet VJ, Bourguet P, Daniels GH, et al. Controversies, Consensus, and Collaboration in the Use of 131I Therapy in Differentiated Thyroid Cancer: A Joint Statement from the American Thyroid Association, the European Association of Nuclear Medicine, the Society of Nuclear Medicine and Molecular Imaging, and the European Thyroid Association. *Thyroid*. 2019 Apr 1;29(4):461–70.
43. Tuttle RM. Distinguishing remnant ablation from adjuvant treatment in differentiated thyroid cancer. *lancet Diabetes Endocrinol*. 2019 Jan 1;7(1):7–8.
44. Mazzaferri EL, Kloos RT. CLINICAL REVIEW 128 Current Approaches to Primary Therapy for Papillary and Follicular Thyroid Cancer. 2001.
45. X Z, D C, S X, G B, M D. Doxorubicin fails to eradicate cancer stem cells derived from anaplastic thyroid carcinoma cells: characterization of resistant cells. *Int J Oncol*. 2010 Jun 23;37(2).
46. Friedman S, Lu M, Schultz A, Thomas D, Lin RY. CD133+ Anaplastic Thyroid Cancer Cells Initiate Tumors in Immunodeficient Mice and Are Regulated by Thyrotropin. *PLoS One*. 2009 Apr 30;4(4).
47. Fullmer T, Cabanillas ME, Zafereo M. Novel Therapeutics in Radioactive Iodine-Resistant Thyroid Cancer.
48. De Leo S, Trevisan M, Fugazzola L. Recent advances in the management of anaplastic thyroid cancer. *Thyroid Res* 2020 131. 2020 Nov 24;13(1):1–14.

49. Cabanillas ME, Ryder M, Jimenez C. Targeted Therapy for Advanced Thyroid Cancer: Kinase Inhibitors and Beyond. *Endocr Rev.* 2019 Dec 1;40(6):1573–604.
50. Saini S, Tulla K, Maker A V., Burman KD, Prabhakar BS. Therapeutic advances in anaplastic thyroid cancer: a current perspective. *Mol Cancer.* 2018 Oct 23;17(1).
51. Na KJ, Choi H. Immune landscape of papillary thyroid cancer and immunotherapeutic implications. *Endocr Relat Cancer.* 2018 May 1;25(5):523–31.
52. Mehnert JM, Varga A, Brose MS, Aggarwal RR, Lin CC, Prawira A, et al. Safety and antitumor activity of the anti-PD-1 antibody pembrolizumab in patients with advanced, PD-L1-positive papillary or follicular thyroid cancer. *BMC Cancer.* 2019 Mar 4;19(1).
53. Hardin H, Montemayor-Garcia C, Lloyd R V. Thyroid cancer stem-like cells and epithelial-mesenchymal transition in thyroid cancers. *Hum Pathol.* 2013 Sep;44(9):1707–13.
54. Hardin H, Helein H, Meyer K, Robertson S, Zhang R, Zhong W, et al. Thyroid cancer stem-like cell exosomes: regulation of EMT via transfer of lncRNAs. *Lab Investig.* 2018 Sep;98(9):1133–42.
55. Nikiforova MN, Wald AI, Roy S, Durso MB, Nikiforov YE. Targeted next-generation sequencing panel (ThyroSeq) for detection of mutations in thyroid cancer. *J Clin Endocrinol Metab.* 2013 Nov 1;98(11).
56. Takano T, Amino N. Fetal cell carcinogenesis: A new hypothesis for better understanding of thyroid carcinoma. *Thyroid.* 2005;15(5):432–8.
57. Colombo C, Muzza M, Proverbio MC, Tosi D, Soranna D, Pesenti C, et al. Impact of Mutation Density and Heterogeneity on Papillary Thyroid Cancer Clinical Features and Remission Probability. *Thyroid.* 2019;29(2):237–51.
58. Bonnet D, Dick JE. Human acute myeloid leukemia is organized as a hierarchy that originates from a primitive hematopoietic cell. *Nat Med.* 1997 Jul;3(7):730–7.
59. Lin RY. Thyroid cancer stem cells. *Nat Rev Endocrinol.* 2011;7(10):609–16.
60. Grassi ES, Ghiandai V, Persani L. Thyroid cancer stem-like cells: From

- microenvironmental niches to therapeutic strategies. *J Clin Med*. 2021;10(7).
61. Mcgranahan N, Swanton C. Review Clonal Heterogeneity and Tumor Evolution : Past , Present , and the Future. *Cell*. 2017;168(4):613–28.
  62. Baghban R, Roshangar L, Jahanban-esfahlan R, Seidi K, Ebrahimi-kalan A. Tumor microenvironment complexity and therapeutic implications at a glance. 2020;4:1–19.
  63. Borovski T, De Sousa E Melo F, Vermeulen L, Medema JP. Cancer stem cell niche: The place to be. *Cancer Res*. 2011;71(3):634–9.
  64. Schito L, Semenza GL. Hypoxia-Inducible Factors: Master Regulators of Cancer Progression. Vol. 2, *Trends in Cancer*. Cell Press; 2016. p. 758–70.
  65. Tirino V, Desiderio V, Paino F, De Rosa A, Papaccio F, La Noce M, et al. Cancer stem cells in solid tumors: An overview and new approaches for their isolation and characterization. *FASEB J*. 2013;27(1):13–24.
  66. Jolly LA, Novitskiy S, Owens P, Massoll N, Cheng N, Fang W, et al. Fibroblast-mediated collagen remodeling within the tumor microenvironment facilitates progression of thyroid cancers driven by BrafV600E and Pten loss. *Cancer Res*. 2016 Apr 4;76(7):1804.
  67. Xing M. BRAF mutation in papillary thyroid cancer: pathogenic role, molecular bases, and clinical implications. *Endocr Rev*. 2007 Dec;28(7):742–62.
  68. Johansson E, Grassi ESES, Pantazopoulou V, Tong B, Lindgren D, Berg TJTJTJ, et al. CD44 Interacts with HIF-2 $\alpha$  to Modulate the Hypoxic Phenotype of Perinecrotic and Perivascular Glioma Cells. *Cell Rep*. 2017 Aug;20(7):1641–53.
  69. Vesely MD, Kershaw MH, Schreiber RD, Smyth MJ. Natural innate and adaptive immunity to cancer. *Annu Rev Immunol*. 2011 Apr 23;29:235–71.
  70. Polyak K, Hahn WC. Roots and stems: stem cells in cancer. 2006;
  71. Wicha MS, Liu S, Dontu G. Cancer Stem Cells: An Old Idea-A Paradigm Shift. *Cancer Res*. 2006;66(4):1883–90.
  72. Sell S. Stem cell origin of cancer and differentiation therapy. *Crit Rev Oncol Hematol*. 2004 Jul 1;51(1):1–28.

73. Prieto-Vila M, Takahashi RU, Usuba W, Kohama I, Ochiya T. Drug Resistance Driven by Cancer Stem Cells and Their Niche. *Int J Mol Sci.* 2017 Dec 1;18(12).
74. Zhou HM, Zhang JG, Zhang X, Li Q. Targeting cancer stem cells for reversing therapy resistance: mechanism, signaling, and prospective agents. *Signal Transduct Target Ther* 2021 61. 2021 Feb 15;6(1):1–17.
75. Das PK, Islam F, Lam AK. The Roles of Cancer Stem Cells and Therapy Resistance in Colorectal Carcinoma. *Cells.* 2020;9(6):1–21.
76. Cirello V, Vaira V, Grassi ES, Vezzoli V, Ricca D, Colombo C, et al. Multicellular spheroids from normal and neoplastic thyroid tissues as a suitable model to test the effects of multikinase inhibitors. *Oncotarget.* 2017;8(6):9752–66.
77. Weiswald LB, Bellet D, Dangles-Marie V. Spherical Cancer Models in Tumor Biology. *Neoplasia (United States).* 2015;17(1):1–15.
78. Bidarra SJ, Oliveira P, Rocha S, Saraiva DP, Oliveira C, Barrias CC. A 3D in vitro model to explore the inter-conversion between epithelial and mesenchymal states during EMT and its reversion. *Sci Reports* 2016 61. 2016 Jun 3;6(1):1–14.
79. Gao YJU, Li BO, Wu XYU, Cui J, Han JK. Thyroid tumor-initiating cells: Increasing evidence and opportunities for anticancer therapy (Review). *Oncol Rep.* 2014;31(3):1035–42.
80. Hadnagy A, Gaboury L, Beaulieu R, Balicki D. SP analysis may be used to identify cancer stem cell populations. Vol. 312, *Experimental Cell Research.* Academic Press Inc.; 2006. p. 3701–10.
81. Mitsutake N, Iwao A, Nagai K, Namba H, Ohtsuru A, Saenko V, et al. Characterization of side population in thyroid cancer cell lines: Cancer stem-like cells are enriched partly but not exclusively. *Endocrinology.* 2007;148(4):1797–803.
82. LAN L, LUO Y, CUI D, SHI B-Y, DENG W, HUO L-L, et al. Epithelial-mesenchymal transition triggers cancer stem cell generation in human thyroid cancer cells. *Int J Oncol.* 2013 Jul;43(1):113–20.
83. Todaro M, Iovino F, Eterno V, Cammareri P, Gambarà G, Espina V, et al. Tumorigenic and metastatic activity of human thyroid cancer stem cells. *Cancer Res.* 2010;70(21):8874–85.

84. Giani`1 F, Giani`1 G, Russo G, Pennisi M, Sciacca L, Frasca F, et al. Computational modeling reveals MAP3K8 as mediator of resistance to vemurafenib in thyroid cancer stem cells. *Bioinformatics*. 2019;35(13):2267–75.
85. Kamran MZ, Patil P, Gude RP. Role of STAT3 in cancer metastasis and translational advances. *Biomed Res Int*. 2013;2013.
86. Wang ML, Chiou SH, Wu CW. Targeting cancer stem cells: emerging role of Nanog transcription factor. *Onco Targets Ther*. 2013;6:1207.
87. Giani F, Vella V, Nicolosi ML, Fierabracci A, Lotta S, Malaguarnera R, et al. Thyrospheres From Normal or Malignant Thyroid Tissue Have Different Biological, Functional, and Genetic Features. *J Clin Endocrinol Metab*. 2015 Sep 1;100(9):E1168–78.
88. Zhao W, Ji X, Zhang F, Li L, Ma L. Embryonic Stem Cell Markers. *Molecules*. 2012;17(6):6196–236.
89. Monk M, Holding C. Human embryonic genes re-expressed in cancer cells. *Oncogene*. 2001;20(56):8085–91.
90. Tseng LM, Huang PI, Chen YR, Chen YC, Chou YC, Chen YW, et al. Targeting signal transducer and activator of transcription 3 pathway by cucurbitacin I diminishes self-renewing and radiochemoresistant abilities in thyroid cancer-derived CD133 + cells. *J Pharmacol Exp Ther*. 2012;341(2):410–23.
91. Ahn SH, Henderson YC, Williams MD, Lai SY, Clayman GL. Detection of thyroid cancer stem cells in papillary thyroid carcinoma. *J Clin Endocrinol Metab*. 2014;99(2):536–44.
92. Shimamura M, Nagayama Y, Matsuse M, Yamashita S, Mitsutake N. Analysis of multiple markers for cancer stem-like cells in human thyroid carcinoma cell lines. *Endocr J*. 2014;61(5):481–90.
93. Huang L, Yang Y, Yang F, Liu S, Zhu Z, Lei Z, et al. Functions of EpCAM in physiological processes and diseases (Review). *Int J Mol Med*. 2018;42(4):1771–85.
94. van der Gun BTF, Melchers LJ, Ruiters MHJ, de Leij LFMH, McLaughlin PMJ, Rots MG. EpCAM in carcinogenesis: The good, the bad or the ugly. *Carcinogenesis*. 2010;31(11):1913–21.
95. Baeuerle PA, Gires O. EpCAM (CD326) finding its role in cancer. *Br J*

- Cancer. 2007 Feb 12;96(3):417–23.
96. Herlyn M, Steplewski Z, Herlyn D, Koprowski H. Colorectal carcinoma-specific antigen: detection by means of monoclonal antibodies. *Proc Natl Acad Sci U S A*. 1979;76(3):1438–42.
  97. Schnell U, Cirulli V, Giepmans BNG. EpCAM: Structure and function in health and disease. *Biochim Biophys Acta - Biomembr*. 2013;1828(8):1989–2001.
  98. J Strnad 1, A E Hamilton, L S Beavers, G C Gamboa, L D Apelgren, L D Taber, J R Sportsman, T F Bumol, J D Sharp RAG. Molecular cloning and characterization of a human adenocarcinoma/epithelial cell surface antigen complementary DNA. *Cancer Res*. 1989;49(2):314-.
  99. Aiman Mohtar M, Syafruddin SE, Nasir SN, Yew LT. Revisiting the roles of pro-metastatic epcam in cancer. *Biomolecules*. 2020;10(2).
  100. Pauli C, Münz M, Kieu C, Mack B, Breinl P, Wollenberg B, et al. Tumor-specific glycosylation of the carcinoma-associated epithelial cell adhesion molecule EpCAM in head and neck carcinomas. *Cancer Lett*. 2003 Apr 10;193(1):25–32.
  101. Nü Bel T, Preobraschenski J, Seyin Tuncay H, Weiss T, Kuhn S, Ladwein M, et al. Claudin-7 Regulates EpCAM-Mediated Functions in Tumor Progression. 2009;
  102. Balzar M, Prins FA, Bakker HAM, Fleuren GJ, Warnaar SO, Litvinov S V. The Structural Analysis of Adhesions Mediated by Ep-CAM. *Exp Cell Res*. 1999 Jan 10;246(1):108–21.
  103. Litvinov S V., Velders MP, Bakker HAM, Fleuren GJ, Warnaar SO. Ep-CAM: a human epithelial antigen is a homophilic cell-cell adhesion molecule. *J Cell Biol*. 1994;125(2):437–46.
  104. Balzar M, Bakker HAM, Briaire-de-Bruijn IH, Fleuren GJ, Warnaar SO, Litvinov S V. Cytoplasmic Tail Regulates the Intercellular Adhesion Function of the Epithelial Cell Adhesion Molecule. *Mol Cell Biol*. 1998;18(8):4833–43.
  105. Balzar M, Briaire-de Bruijn IH, Rees-Bakker HAM, Prins FA, Helfrich W, de Leij L, et al. Epidermal growth factor-like repeats mediate lateral and reciprocal interactions of Ep-CAM molecules in homophilic adhesions. *Mol Cell Biol*. 2001 Apr;21(7):2570–80.

106. Litvinov S V., Balzar M, Winter MJ, Bakker HAM, Briaire-De Bruijn IH, Prins F, et al. Epithelial cell adhesion molecule (Ep-CAM) modulates cell-cell interactions mediated by classic cadherins. *J Cell Biol.* 1997 Dec 1;139(5):1337–48.
107. Lei Z, Maeda T, Tamura A, Nakamura T, Yamazaki Y, Shiratori H, et al. EpCAM contributes to formation of functional tight junction in the intestinal epithelium by recruiting claudin proteins. *Dev Biol.* 2012 Nov 15;371(2):136–45.
108. Gires O, Pan M, Schinke H, Canis M, Baeuerle PA. Expression and function of epithelial cell adhesion molecule EpCAM: where are we after 40 years? *Cancer Metastasis Rev.* 2020;39(3):969–87.
109. Munz M, Kieu C, Mack B, Schmitt BB, Zeidler R, Gires O. The carcinoma-associated antigen EpCAM upregulates c-myc and induces cell proliferation. *Oncogene.* 2004;23:5748–58.
110. Chaves-Pérez A, Mack B, Maetzel D, Kremling H, Eggert C, Harréus U, et al. EpCAM regulates cell cycle progression via control of cyclin D1 expression. *Oncogene.* 2013 Jan 31;32(5):641–50.
111. Wenqi D, Li W, Shanshan C, Bei C, Yafei Z, Feihu B, et al. EpCAM is overexpressed in gastric cancer and its downregulation suppresses proliferation of gastric cancer. *J Cancer Res Clin Oncol.* 2009;135:1277–85.
112. Maetzel D, Denzel S, Mack B, Canis M, Went P, Benk M, et al. Nuclear signalling by tumour-associated antigen EpCAM. *Nat Cell Biol.* 2009;11(2):162–71.
113. Pan M, Schinke H, Luxenburger E, Kranz G, Shakhtour J, Libl D, et al. EpCAM ectodomain EpEX is a ligand of EGFR that counteracts EGF-mediated epithelial-mesenchymal transition through modulation of phospho-ERK1/2 in head and neck cancers. Vol. 16, *PLoS Biology.* 2018. 1–36 p.
114. Hsu YT, Osmulski P, Wang Y, Huang YW, Liu L, Ruan J, et al. EpCAM-Regulated Transcription Exerts Influences on Nanomechanical Properties of Endometrial Cancer Cells that Promote Epithelial-to-Mesenchymal Transition. *Cancer Res.* 2016 Nov 11;76(21):6171.
115. Huang HP, Chen PH, Yu CY, Chuang CY, Stone L, Hsiao WC, et al.



- Epithelial Cell Adhesion Molecule (EpCAM) Complex Proteins Promote Transcription Factor-mediated Pluripotency Reprogramming. *J Biol Chem.* 2011 Sep 9;286(38):33520.
116. Schnell U, Kuipers J, Giepmans BNG. EpCAM proteolysis: New fragments with distinct functions? *Biosci Rep.* 2013;33(2):321–32.
  117. Shimizu H, Tosaki A, Kaneko K, Hisano T, Sakurai T, Nukina N. Crystal Structure of an Active Form of BACE1, an Enzyme Responsible for Amyloid  $\beta$  Protein Production. *Mol Cell Biol.* 2008 Jun;28(11):3663.
  118. Warneke VS, Behrens HM, Haag J, Krüger S, Simon E, Mathiak M, et al. Members of the EpCAM signalling pathway are expressed in gastric cancer tissue and are correlated with patient prognosis. *Br J Cancer.* 2013;109(8):2217–27.
  119. M. Balzar · M.J. Winter · C.J. de Boer · S.V. Litvinov. The biology of the 17–1A antigen (Ep-CAM). *J Mol Med.* 1999;77:699–712.
  120. Went PT, Lugli A, Meier S, Bundi M, Mirlacher M, Sauter G, et al. Frequent EpCam Protein Expression in Human Carcinomas. *Hum Pathol.* 2004;35(1):122–8.
  121. carla j.de boer, johan h.j.m.van kriecken connie m. janssen-va. rhijn and sergey v. litvino. Expression of EpCAM in normal, regenerating, metaplastic and neoplastic liver. *J Pathol.* 1999;188:201–6.
  122. Ng VY, Ang SN, Chan JX, Choo ABH. Characterization of epithelial cell adhesion molecule as a surface marker on undifferentiated human embryonic stem cells. *Stem Cells.* 2010 Jan;28(1):29–35.
  123. Lu TY, Lu RM, Liao MY, Yu J, Chung CH, Kao CF, et al. Epithelial Cell Adhesion Molecule Regulation Is Associated with the Maintenance of the Undifferentiated Phenotype of Human Embryonic Stem Cells. *J Biol Chem.* 2010 Mar 3;285(12):8719.
  124. Fong D, Moser P, Kasal A, Seeber A, Gastl G, Martowicz A, et al. Loss of membranous expression of the intracellular domain of EpCAM is a frequent event and predicts poor survival in patients with pancreatic cancer. *Histopathology.* 2014;64(5):683–92.
  125. Seeber A, Untergasser G, Spizzo G, Terracciano L, Lugli A, Kasal A, et al. Predominant expression of truncated EpCAM is associated with a more aggressive phenotype and predicts poor overall survival in

- colorectal cancer. *Int J cancer*. 2016 Aug 1;139(3):657–63.
126. Spizzo G, Went P, Dirnhofer S, Obrist P, Simon R, Spichtin H, et al. High Ep-CAM expression is associated with poor prognosis in node-positive breast cancer. *Vol. 86, Breast Cancer Research and Treatment*. 2004.
  127. Spizzo G, Went P, Dirnhofer S, Obrist P, Moch H, Baeuerle PA, et al. Overexpression of epithelial cell adhesion molecule (Ep-CAM) is an independent prognostic marker for reduced survival of patients with epithelial ovarian cancer. *Gynecol Oncol*. 2006;103(2):483–8.
  128. Massoner P, Thomm T, Mack B, Untergasser G, Martowicz A, Bobowski K, et al. EpCAM is overexpressed in local and metastatic prostate cancer, suppressed by chemotherapy and modulated by MET-associated miRNA-200c/205. *Br J Cancer*. 2014;111(5):955–64.
  129. Philip Went 1, Stephan Dirnhofer, Tiziana Salvisberg, Mahul B Amin, So D Lim, Pierre-André Diener HM. Expression of epithelial cell adhesion molecule (EpCam) in renal epithelial tumors. *Am J Surg Pathol*. 2005;29((1)):83–8.
  130. Baumeister P, Hollmann A, Kitz J, Afthonidou A, Simon F, Shakhtour J, et al. High Expression of EpCAM and Sox2 is a Positive Prognosticator of Clinical Outcome for Head and Neck Carcinoma. *Sci Rep*. 2018 Dec 1;8(1).
  131. Ensinger C, Kremser R, Prommegger R, Spizzo G, Schmid KW. EpCAM overexpression in thyroid carcinomas: A histopathological study of 121 cases. *J Immunother*. 2006;29(5):569–73.
  132. Ralhan R, Cao J, Lim T, MacMillan C, Freeman JL, Walfish PG. EpCAM nuclear localization identifies aggressive Thyroid Cancer and is a marker for poor prognosis. *BMC Cancer*. 2010;10:14–6.
  133. Ralhan R, He HCH, So AKC, Tripathi SC, Kumar M, Hasan MR, et al. Nuclear and cytoplasmic accumulation of Ep-ICD is frequently detected in human epithelial cancers. *PLoS One*. 2010;5(11).
  134. Kunavisarut T, Kak I, MacMillan C, Ralhan R, Walfish PG. Immunohistochemical analysis based Ep-ICD subcellular localization index (ESLI) is a novel marker for metastatic papillary thyroid microcarcinoma. *BMC Cancer*. 2012;12:1–9.
  135. Sankpal N V, Fleming TP, Sharma PK, Wiedner HJ, Gillanders WE. A

- double-negative feedback loop between EpCAM and ERK contributes to the regulation of epithelial&ndash;mesenchymal transition in cancer. *Oncogene*. 2017;36:3706–17.
136. Lin CW, Liao MY, Lin WW, Wang YP, Lu TY, Wu HC. Epithelial Cell Adhesion Molecule Regulates Tumor Initiation and Tumorigenesis via Activating Reprogramming Factors and Epithelial-Mesenchymal Transition Gene Expression in Colon Cancer. *J Biol Chem*. 2012 Nov 11;287(47):39449.
137. Hoe SLL, Tan LP, Abdul Aziz N, Liew K, Teow SY, Abdul Razak FR, et al. CD24, CD44 and EpCAM enrich for tumour-initiating cells in a newly established patient-derived xenograft of nasopharyngeal carcinoma. *Sci Rep*. 2017 Dec 1;7(1).
138. Han M-E, Jeon T-Y, Hwang S-H, Lee Y-S, Kim H-J, Shim H-E, et al. Cancer spheres from gastric cancer patients provide an ideal model system for cancer stem cell research.
139. Pacini F, Basolo · F, Bellantone · R, Boni · G, Cannizzaro · M A, De Palma · M, et al. Italian consensus on diagnosis and treatment of differentiated thyroid cancer: joint statements of six Italian societies. 2018;41:849–76.
140. Amin MB, Frederick ;, Greene L, Edge SB, Compton CC, Gershewald JE, et al. The Eighth Edition AJCC Cancer Staging Manual: Continuing to Build a Bridge From a Population-Based to a More “Personalized” Approach to Cancer Staging.
141. Iñigo Landa, Nikita Pozdeyev, Christopher Korch, Laura A. Marlow, Robert C. Smallridge, John A. Copland, Ying C. Henderson, Stephen Y. Lai, Gary L. Clayman, Naoyoshi Onoda, Aik Choon Tan, Maria E.R. Garcia-Rendueles, Jeffrey A. Knauf, Bryan R. Haugen, Jam and RES. Comprehensive genetic characterization of human thyroid cancer cell lines: a validated panel for preclinical studies. *Clin Cancer Res*. 2019;25(10):3141–51.
142. REYNOLDS, B. A and SW. Generation of Neurons and Astrocytes from Isolated Cells of the Adult Mammalian Central Nervous System. *Sci (American Assoc Adv Sci)*. 1992;255(5052):1707–1710.
143. Minett TW, Tighe BJ, Lydon MJ, Rees DA. Requirements for cell

- spreading on polyHEMA coated culture substrates. *Cell Biol Int Rep*. 1984;8(2):151–9.
144. Al Habyan S, Kalos C, Szymborski J, McCaffrey L. Multicellular detachment generates metastatic spheroids during intra-abdominal dissemination in epithelial ovarian cancer. *Oncogene*. 2018;37(37):5127–35.
  145. Hu Y, Smyth GK. ELDA: Extreme limiting dilution analysis for comparing depleted and enriched populations in stem cell and other assays. *J Immunol Methods*. 2009 Aug 15;347(1–2):70–8.
  146. ELDA: Extreme Limiting Dilution Analysis [Internet]. Available from: <https://bioinf.wehi.edu.au/software/elda/>
  147. Winter MJ, Cirulli V, Briaire-de Bruijn IH, Litvinov S V. Cadherins are regulated by Ep-CAM via phosphatidylinositol-3 kinase. *Mol Cell Biochem*. 2007 Aug;302(1–2):19–26.
  148. Brown TC, Sankpal N V., Gillanders WE. Functional implications of the dynamic regulation of EpCAM during epithelial-to-mesenchymal transition. *Biomolecules*. 2021;11(7):1–22.
  149. Fan Q, Cheng JC, Qiu X, Chang HM, Leung PCK. EpCAM is up-regulated by EGF via ERK1/2 signaling and suppresses human epithelial ovarian cancer cell migration. *Biochem Biophys Res Commun*. 2015;457(3):256–61.
  150. Davis CK, Jain SA, Bae ON, Majid A, Rajanikant GK. Hypoxia mimetic agents for ischemic stroke. *Front Cell Dev Biol*. 2019;6(January):1–12.
  151. Martens LK, Kirschner KM, Warnecke C, Scholz H. Hypoxia-inducible factor-1 (HIF-1) is a transcriptional activator of the TrkB neurotrophin receptor gene. *J Biol Chem*. 2007;282(19):14379–88.
  152. Sulser P, Pickel C, Günter J, Leissing TM, Crean D, Schofield CJ, et al. HIF hydroxylase inhibitors decrease cellular oxygen consumption depending on their selectivity. *FASEB J*. 2020;34(2):2344–58.
  153. Charbonneau M, Harper K, Grondin F, Pelmus M, McDonald PP, Dubois CM. Hypoxia-inducible factor mediates hypoxic and tumor necrosis factor  $\alpha$ -induced increases in tumor necrosis factor- $\alpha$  converting enzyme/ADAM17 expression by synovial cells. *J Biol Chem*. 2007;282(46):33714–24.

154. Le Moan N, Houslay DM, Christian F, Houslay MD, Akassoglou K. Oxygen-dependent cleavage of the p75 neurotrophin receptor triggers stabilization of HIF-1 $\alpha$ . *Mol Cell*. 2011;44(3):476–90.
155. Wang XJ, Feng CW, Li M. ADAM17 mediates hypoxia-induced drug resistance in hepatocellular carcinoma cells through activation of EGFR/PI3K/Akt pathway. *Mol Cell Biochem*. 2013;380(1–2):57–66.
156. Li R, Uttarwar L, Gao B, Charbonneau M, Shi Y, Chan JSD, et al. High glucose up-regulates ADAM17 through HIF-1 $\beta$  in mesangial cells. *J Biol Chem*. 2015;290(35):21603–14.
157. Kirkegaard T, Yde CW, Kveiborg M, Lykkesfeldt AE. The broad-spectrum metalloproteinase inhibitor BB-94 inhibits growth, HER3 and Erk activation in fulvestrant-resistant breast cancer cell lines. *Int J Oncol*. 2014;45(1):393–400.
158. Seifert A, Düsterhöft S, Wozniak J, Koo CZ, Tomlinson MG, Nuti E, et al. The metalloproteinase ADAM10 requires its activity to sustain surface expression. *Cell Mol Life Sci*. 2021;78(2):715–32.
159. Ghosh AK, Brindisi M, Tang J. Developing  $\beta$ -secretase inhibitors for treatment of Alzheimer's disease. *J Neurochem*. 2012;120(SUPPL. 1):71–83.
160. Jämsä A, Belda O, Edlund M, Lindström E. BACE-1 inhibition prevents the -secretase inhibitor evoked A rise in human neuroblastoma SH-SY5Y cells. *J Biomed Sci*. 2011;18(1):1–9.
161. Sakai-Takemura F, Nogami K, Elhussieny A, Kawabata K, Maruyama Y, Hashimoto N, et al. Prostaglandin EP2 receptor downstream of Notch signaling inhibits differentiation of human skeletal muscle progenitors in differentiation conditions. *Commun Biol*. 2020;3(1):1–13.
162. Huang Y, Chanou A, Kranz G, Pan M, Kohlbauer V, Ettinger A, et al. Membrane-associated epithelial cell adhesion molecule is slowly cleaved by -secretase prior to efficient proteasomal degradation of its intracellular domain. *J Biol Chem*. 2019;294(9):3051–64.
163. Okada T, Nakamura T, Watanabe T, Onoda N, Ashida A, Okuyama R, et al. Coexpression of EpCAM, CD44 variant isoforms and claudin-7 in anaplastic thyroid carcinoma. *PLoS One*. 2014;9(4):1–13.
164. Tsaktanis T, Kremling H, Pavšič M, Von Stackelberg R, Mack B,

- Fukumori A, et al. Cleavage and cell adhesion properties of human epithelial cell adhesion molecule (HEPCAM). *J Biol Chem.* 2015;290(40):24574–91.
165. Lin CW, Liao MY, Lin WW, Wang YP, Lu TY, Wu HC. Epithelial cell adhesion molecule regulates tumor initiation and tumorigenesis via activating reprogramming factors and epithelial-mesenchymal transition gene expression in colon cancer. *J Biol Chem.* 2012;287(47):39449–59.
  166. Lin Z, Lu X, Li W, Sun M, Peng M, Yang H, et al. Association of cancer stem cell markers with aggressive tumor features in papillary thyroid carcinoma. *Cancer Control.* 2015;22(4):508–14.
  167. Fang D, Nguyen TK, Leishear K, Finko R, Kulp AN, Hotz S, Van Belle PA, Xu X, Elder DE HM. A tumorigenic subpopulation with stem cell properties in melanomas. *Cancer Res.* 2005;65(20):9328–37.
  168. Hermann PC, Huber SL, Herrler T, Aicher A, Ellwart JW, Guba M, Bruns CJ HC. Distinct populations of cancer stem cells determine tumor growth and metastatic activity in human pancreatic cancer. *Cell Stem Cell.* 2007;1(3):313-23.
  169. Singh SK, Hawkins C, Clarke ID, Squire JA, Bayani J, Hide T, Henkelman RM, Cusimano MD DP. Identification of human brain tumour initiating cells. *Nature.* 2004;432(7015):396–401.
  170. Qureshi-Baig K, Ullmann P, Haan S, Letellier E. Tumor-Initiating Cells: A criTICal review of isolation approaches and new challenges in targeting strategies. *Mol Cancer.* 2017;16(1):1–16.
  171. Nabhan F, Dedhia PH, Ringel MD. Thyroid cancer, recent advances in diagnosis and therapy. *Int J cancer.* 2021 Sep 1;149(5):984–92.
  172. Shakib H, Rajabi S, Dehghan MH, Mashayekhi FJ, Safari-Alighiarloo N, Hedayati M. Epithelial-to-mesenchymal transition in thyroid cancer: a comprehensive review. *Endocrine.* 2019;66(3):435–55.
  173. Zeisberg M, Neilson EG. Review series personal perspective Biomarkers for epithelial-mesenchymal transitions. 2009;119(6):1429–37.
  174. Mani SA, Guo W, Liao MJ, Eaton EN, Ayyanan A, Zhou AY, et al. The Epithelial-Mesenchymal Transition Generates Cells with Properties of Stem Cells. *Cell.* 2008 May;133(4):704–15.
  175. Gisina AM, Kim YS, Gabashvili AN, Tsvetkova A V., Vakhrushev I V.,

- Yarygin KN, et al. Expression of Epithelial Cell Adhesion Molecule (EpCAM) in Tumor Spheroids of Human Colorectal Adenocarcinoma Cells. *Bull Exp Biol Med.* 2020;170(1):135–41.
176. Yang J, Antin P, Berx G, Blanpain C, Brabletz T, Bronner M, et al. Guidelines and definitions for research on epithelial–mesenchymal transition. *Nat Rev Mol Cell Biol.* 2020;21(6):341–52.

## List of figures and tables

### List of figures

|  |    |
|--|----|
| Figure 1. SEER incidence rates by age at diagnosis, years 2015-2019.....   | 7  |
| Figure 2. Molecular pathogenesis of TC.....  | 11 |
| Figure 3. Distribution and frequency of known somatic mutations in the different histotypes of thyroid cancer. ....                              | 13 |
| Figure 4. TC carcinogenesis models. ....   | 17 |
| Figure 5. Stem cell niche in TC. ....  | 19 |
| Figure 6. EpCAM and regulated intramembrane proteolysis (RIP).....   | 27 |
| Figure 7. Hanging-drop technique for the generation of 3D spheres when cells were seeded at clonal density.....                                  | 37 |
| Figure 8. EpCAM is subjected to differential expression and cleavage pattern in patient-derived tissue samples.....                              | 54 |
| Figure 9. EpCAM is mainly expressed by FRO and HTCC3 cell lines. ....  | 56 |
| Figure 10. 3D sphere-forming abilities in TC cell lines.....   | 58 |
| Figure 11. FRO-derived 3D spheres are representative of the variability of EpCAM cleavage. ....  | 61 |
| Figure 12. Pseudo-hypoxic state induced by DIP significantly affects EpCAM full length expression in FRO adherent cells. ....                    | 63 |
| Figure 13. Three main proteases (ADAM17, $\beta$ -secretase and $\gamma$ -secretase) are involved in EpCAM cleavages in FRO adherent cells. .... | 64 |
| Figure 14. Pseudo-hypoxic state, but not inhibition of EpCAM cleavages, significantly affects 3D sphere-generation ability in FRO.....           | 68 |
| Figure 15. Cell proliferation after PLX-4032 treatment on FRO and HTCC3 adherent cells.....  | 69 |
| Figure 16. EpCAM+ and EpCAM- cell subpopulations respond differently to PLX-4032 treatment on FRO adherent cells. ....                           | 71 |
| Figure 17. EpCAM+ and EpCAM- cell subpopulations respond differently to PLX-4032 treatment on HTCC3 adherent cells.....                          | 73 |



## List of tables

|  |    |
|--|----|
| <b>Table 1. Classification of thyroid tumors of epithelial origin with prevalence (%), morphological features, and 10-year mortality (%).</b> .....  | 10 |
| <b>Table 2. Cell lines.</b> .....  | 36 |
| <b>Table 3. Primary antibodies applied for Western Blot experiments with respective dilutions and molecular weight.</b> .....  | 42 |
| <b>Table 4. Primary (a) and secondary (b) antibodies applied for Immunofluorescence experiments with respective dilutions and conjugated fluorophores.</b> .....                                   | 45 |
| <b>Table 5. Cohort of TC patients representative of the different histotypes. PTC= papillary thyroid cancer; FTC= follicular thyroid cancer; PDTC= poorly differentiated thyroid cancer.</b> ..... | 53 |
| <b>Table 6. Extreme Limiting Dilution Analysis.</b> .....  | 60 |

## **Dissemination of results**

The transfer of my work to the scientific community and the sharing and integration among researchers have been pursued thanks to the participation to national and international congresses and seminars, through which I had the opportunity to present part of the data described in the present thesis. In particular, I had the opportunity to present part of my work as a poster presentation at:

- 44<sup>th</sup> Annual Meeting of the ETA (European Thyroid Association) 2022, held in Brussels, Belgium;
- 43<sup>rd</sup> Annual Meeting of the ETA 2021, Virtual Conference;
- 6<sup>th</sup> BIOMETRA Department annual workshop 2022, Milan;
- 5<sup>th</sup> BIOMETRA Department annual workshop 2021, Milan.

I also had the opportunity to present part of my data as an oral presentation at a national congress:

- 41<sup>st</sup> National Congress of SIE (Società Italiana di Endocrinologia) 2021, held in Rome, Italy.

The manuscript of the data reported in the present thesis is currently under writing and will be submitted for publication in indexed journal.

## **Summary of the research**

English version:

The present thesis investigates some features concerning the biology of the most aggressive thyroid cancers, classified as poorly differentiated and anaplastic tumors. Although they are extremely rare, patients with these types of tumor have a poor chance of survival as nowadays there is still the lack of specific therapeutic approaches capable of counteracting the extremely rapid and malignant progression of these tumors. Indeed, they are known to be resistant to common radiotherapy and chemotherapy. In literature is reported that a very small part of

the complex mixture of cells within the tumor mass has some specific factors that distinguish them from the other tumor cells and may improve aggressiveness of the tumor. In my thesis I've studied one of these possible factors, i.e. a protein expressed on cell membrane, to understand if its expression and role could be associated with these tumor cells, and eventually consider this protein as a new therapeutic target in the context of undifferentiated thyroid cancer.

Italian version:

La presente tesi approfondisce alcune caratteristiche riguardanti la biologia dei tumori tiroidei più aggressivi, classificati come tumori scarsamente differenziati e tumori anaplastici. Nonostante questi tumori siano estremamente rari, le possibilità di sopravvivenza sono scarse, in quanto ad oggi non esistono ancora terapie specifiche che riescano a contrastare la progressione estremamente rapida e maligna di questi tumori, che sono noti essere resistenti ai comuni trattamenti con radioterapia e chemioterapia. In letteratura è riportato che una piccolissima parte delle cellule tumorali che fanno parte del complesso mix di cellule all'interno della massa tumorale, presenta alcuni fattori specifici che le distinguono dalle altre cellule e possono promuovere l'aggressività del tumore. Nella mia tesi ho studiato uno di questi possibili fattori, ovvero una proteina espressa sulle membrana cellulare, per capire se la sua espressione e il suo ruolo possano essere associati a queste cellule aggressive, ed eventualmente considerare questa proteina come un nuovo target terapeutico nel contesto dei tumori tiroidei scarsamente differenziati.

# Appendix



Review

# Thyroid Cancer Stem-Like Cells: From Microenvironmental Niches to Therapeutic Strategies

Elisa Stellaria Grassi <sup>1,\*</sup> , Viola Ghiandai <sup>1</sup> and Luca Persani <sup>1,2</sup>

<sup>1</sup> Department of Medical Biotechnology and Translational Medicine, University of Milan, 20129 Milan, Italy; viola.ghiandai@unimi.it (V.G.); luca.persani@unimi.it (L.P.)

<sup>2</sup> Laboratory of Endocrine and Metabolic Research, Istituto Auxologico Italiano IRCCS, 20149 Milan, Italy

\* Correspondence: elehisie.rfm@gmail.com; Tel.: +39-02-619112432

**Abstract:** Thyroid cancer (TC) is the most common endocrine malignancy. Recent progress in thyroid cancer biology revealed a certain degree of intratumoral heterogeneity, highlighting the coexistence of cellular subpopulations with distinct proliferative capacities and differentiation abilities. Among those subpopulations, cancer stem-like cells (CSCs) are hypothesized to drive TC heterogeneity, contributing to its metastatic potential and therapy resistance. CSCs principally exist in tumor areas with specific microenvironmental conditions, the so-called stem cell niches. In particular, in thyroid cancer, CSCs' survival is enhanced in the hypoxic niche, the immune niche, and some areas with specific extracellular matrix composition. In this review, we summarize the current knowledge about thyroid CSCs, the tumoral niches that allow their survival, and the implications for TC therapy.

**Keywords:** thyroid cancer; cancer stem cells; tumor microenvironment; CSCs niche; targeted therapy



**Citation:** Grassi, E.S.; Ghiandai, V.; Persani, L. Thyroid Cancer Stem-Like Cells: From Microenvironmental Niches to Therapeutic Strategies. *J. Clin. Med.* **2021**, *10*, 1455. <https://doi.org/10.3390/jcm10071455>

Academic Editor: Laura Fugazzola

Received: 23 February 2021

Accepted: 29 March 2021

Published: 1 April 2021

**Publisher's Note:** MDPI stays neutral with regard to jurisdictional claims in published maps and institutional affiliations.



**Copyright:** © 2021 by the authors. Licensee MDPI, Basel, Switzerland. This article is an open access article distributed under the terms and conditions of the Creative Commons Attribution (CC BY) license (<https://creativecommons.org/licenses/by/4.0/>).

## 1. Introduction

Thyroid cancer (TC) is the most common endocrine malignancy [1]. The thyroid gland is a complex endocrine organ that is potentially affected by a variety of cancers that differ in molecular profile, morphology, tumorigenicity, and invasiveness [1]. Follicular cells can give rise to three different subtypes of thyroid carcinoma: papillary thyroid carcinoma (PTC), follicular thyroid carcinoma (FTC), poorly differentiated thyroid carcinoma (PDTC) and anaplastic thyroid carcinoma (ATC) [2]. PTCs and FTCs account for 80–85% and 10–15% of all TCs, respectively, and usually have a good prognosis. In contrast, ATCs are rare but are characterized by an aggressive phenotype and a poor prognosis [2]. Although ATCs represent only 1% of all thyroid cancers, they account for >50% of the mortality, as they often acquire therapy resistance [3,4]. TCs have a complex genetic background, with the acquisition of hyperactivating mutations in the BRAF, RAS, and PI3K pathways, together with the loss of function and suppression of PTEN, p53, and b-catenin in the less differentiated forms [5,6].

Recent progress in thyroid cancer biology revealed a certain degree of intratumoral heterogeneity [7–10], highlighting the coexistence of cellular subpopulations with distinct proliferative capacities and differentiation abilities, whose hierarchical organization is fundamental to the maintenance of the malignant phenotype [11]. Similarly to other solid tumors [12–17], a rare subpopulation of cells called cancer stem-like cells (CSCs) is hypothesized to drive the TC heterogeneity and contribute to the metastatic potential and therapy resistance [18–21]. CSCs exist predominantly in different specific tumor niches, where the dynamic equilibrium within cell-intrinsic and cell-extrinsic factors derived by the tumor microenvironment allow for the maintenance of the stem-like phenotype, which is characterized by a lack of tissue-specific differentiation, slow-cycling rate, quiescence, and theoretically unlimited self-renewal abilities [13,22,23].

In recent years, the discovery of thyroid CSCs uncovered the inadequacy of the “classical” carcinogenesis model and prompted further knowledge on the TC complex microenvironment.

## 2. Thyroid Cancer and CSCs

### 2.1. Thyroid Carcinogenesis and CSCs Origins

According to the classic multistep carcinogenesis model (Figure 1A), TC cells arise from the gradual accumulation of genetic alterations within normal thyroid epithelial cells, leading to uncontrolled proliferation and an invasive phenotype [24,25]. Thus, PTC and FTC are the results of randomly occurring genetic alterations, such as *BRAF* and *RAS* point mutations or the more complex *RET/PTC* and *PAX8/PPAR $\gamma$*  rearrangements. The sequential accumulation of further genetic alterations, particularly the inactivating mutations of *TP53* and *CTNNB1*, can then give rise to ATC [26]. These events come with the dedifferentiation process that occurs as the cancer cells acquire the neoplastic phenotype, with a marked epithelial-to-mesenchymal transition (EMT), which is a process that finally results in CSCs' phenotype acquisition [27,28]. Nevertheless, this model has some intrinsic limitations. While the mature thyroid follicular cells have a low proliferation rate, intrinsically limiting the accumulation of multiple mutations [29], the introduction of large-scale genome sequencing techniques revealed that PTC and FTC already have much more complex genetic alterations than what the classical multistep model can explain [30–32].

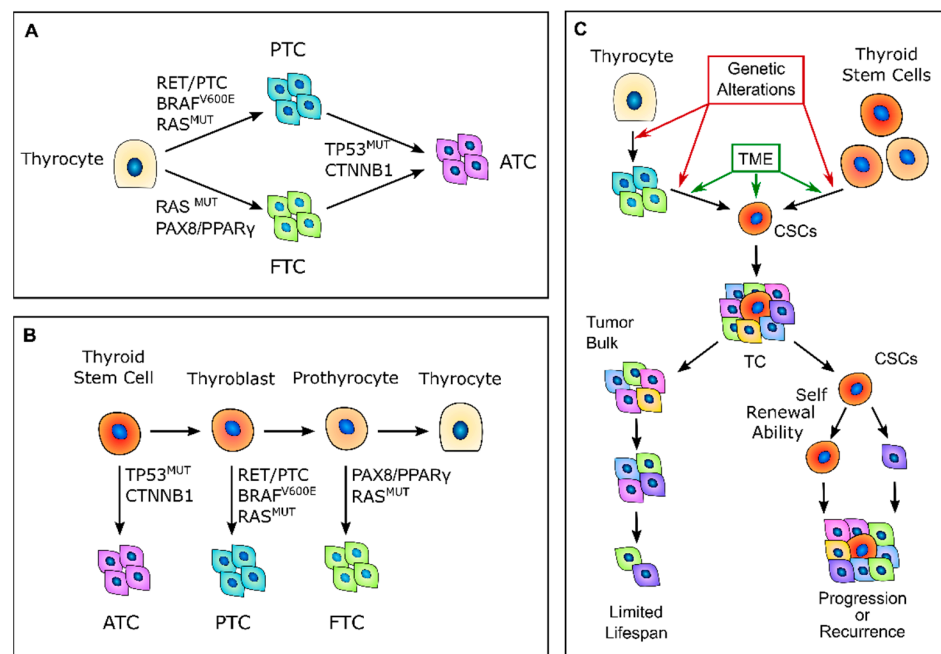


**Figure 1.** Thyroid carcinogenesis models. (A) Description of the classic multistep carcinogenesis model: the gradual accumulation of genetic alterations in normal thyrocytes leads to the transformation into cancer cells and to the acquisition of subsequently less differentiated and more aggressive phenotypes. Mutations in driver genes, such as *BRAF* and *RAS* or *RET/PTC* and *PAX8/PPAR $\gamma$*  rearrangements, give rise to the well-differentiated papillary thyroid cancers (PTCs) and follicular thyroid cancers (FTCs), while the acquisition of *TP53* and *CTNNB1* mutations leads to the transformation in anaplastic thyroid cancers (ATCs). (B) Fetal stem cells' origin model: thyroid cancer cells are derived from normal stem cells or precursor cells of fetal origin that acquire transforming mutations. These genetic alterations confer proliferative advantages and prevent fetal thyroid cells from differentiating. Less differentiated stem cells give rise to ATCs, while the more differentiated thyroblasts and prothyrocytes give rise to PTCs and FTCs, respectively. (C) Cancer stem-like cells' (CSCs) origin model: CSCs with high tumorigenic activity and increased ability to self-renew originate from either normal stem cells through a transformation process or from differentiated cancer cells as the result of a dedifferentiation process. The transition of stem cells into mature cancer cells is stimulated by the different tumor environment that is present outside the stem niches. Mature cells cannot sustain tumor progression, while CSCs can reconstitute and sustain tumor growth. TME, tumor microenvironment; TC, thyroid cancer.

In 2005, Takano et al. [26] proposed that TC cells are derived from normal stem cells or precursor cells of fetal origin that survive in the mature gland rather than from differentiated thyroid follicular cells [26,33] (Figure 1B). According to this model, normal fetal thyroid stem cells, which express oncofetal fibronectin but none of the markers that are typical of differentiated thyroid cells, give rise to ATC. Thyroblasts, which express both oncofetal fibronectin and the differentiation marker thyroglobulin (Tg), give rise to PTC. Finally, prothyrocytes, which are the more differentiated cell type, should give rise to FTC and follicular adenoma [33]. In this model, genetic alterations confer proliferative advantages and prevent fetal thyroid cells from differentiating. However, there is no explanation regarding how quiescent thyroid stem cells acquire such genetic alterations or about the coexistence of cellular subpopulations with different degrees of differentiation. The evidence that a cancer cell population is heterogeneous and that molecular alterations are not present in the whole tumor bulk finally brought about the CSC hypothesis for TC. This hypothesis was first established by the previous observation that leukemia may contain hierarchical multi-lineage cells [34]. In this perspective, some authors hypothesized that TC may be a CSC-driven disease [26,35,36], with only a subset of cancer cells that possess high tumorigenic activity, with increased ability to self-renew and produce progenitor cells that can reconstitute and sustain tumor growth [1] (Figure 1C). The transition of stem cells into mature cells is stimulated by growth factors and cytokines present in the microenvironment outside the stem niche [25]. According to this view, CSCs may originate from either normal stem cells through a transformation process or from differentiated cancer cells as the result of a dedifferentiation process [35]. The clinical implication of the CSC model may give rise to important effects for both the diagnosis and treatment of TC, especially for the management of poorly differentiated, recurrent, or rapidly growing diseases that are refractory to radioactive iodine (RAI) therapy. In this view, the eradication of all CSCs may arrest tumor growth, whereas the failure to eliminate CSCs will eventually lead to tumor relapse [37].

## 2.2. Thyroid CSC Identification

Nowadays, CSC identification relies mostly on the identification of stemness biomarkers, together with specific *in vitro* and *in vivo* assays (Table 1).

*In vitro* assays aim to demonstrate the self-renewal abilities of the CSCs and comprise thyrosphere formation assays, limiting–diluting assay, serial colony formation, and differentiation assays. Because normal thyroid stem cells can be grown as sphere-like cellular aggregates in a specialized stem cell culture medium, the multicellular three-dimensional (3D) spheroids assay is the best-studied methodology to determine the clonality and multipotency of putative thyroid CSCs [1,38]. Indeed, the ability to generate spheres in serum-free medium, even after serial passages, indicates that the cells have an extensive capacity for self-renewal and should be able to recreate a heterogeneous tumor cell population and recapitulate the primary tumor morphology [39]. Moreover, different from two-dimensional monolayer cultures, tumor spheroids create intercellular contacts and usually display low values of nutrients, oxygen, and glucose, generating a hypoxic core in the center of the 3D structure, thereby imitating the natural environment of solid tumors [40]. Researchers have also established a colony-forming assay in which cells are cultured in a semisolid methylcellulose medium that recapitulates the extracellular matrix (ECM). This assay allows the clonal progeny of a single cell to grow as a distinct cluster or colony and monitors anchorage-independent growth, which is a key property of cancer cells.

The most definitive way to assess putative CSCs is to inject these cells into immunocompromised mice to verify their ability to develop tumors over time [41]. In particular, the serial transplantations of cells that were isolated from secondary and tertiary xenografts allow for defining their long-term tumorigenic potential, as well as their self-renewing ability [42]. A further enhancement of this approach involves combining these serial transplantations with limiting–dilution assays to determine the minimum number of cancer stem cells that are required for tumor formation and to confirm that tumor size is positively

correlated with the number of cells injected [1]. Moreover, the ability of tumor initiation can be more accurately evaluated using an orthotopic transplantation to mimic the tumor environment as closely as possible [39].

**Table 1.** Markers that are used to identify thyroid CSCs.

| Markers   | Functions  | References          |
|---|--|---------------------|
| aldehyde dehydrogenase (ALDH) activity (ALDEFLUOR)                      | Used to isolate CSCs based on their elevated ALDH activity via positive flow cytometry selection   | [21,41,43–47]       |
| CD133 (prominin-1)  | CD133 <sup>+</sup> cells express stemness genes ( <i>POU5F1</i> , <i>SOX2</i> , and <i>NANOG1</i> ), drug-resistance genes ( <i>ABCG2</i> , <i>MDR1</i> , and <i>MRP</i> ), and a low expression of thyroid differentiation markers. | [47–49]             |
| CD44 <sup>+</sup> /CD24 <sup>−</sup> phenotype                          | CD44 <sup>+</sup> /CD24 <sup>−</sup> subpopulation of cells with tumorigenic potential identified by flow cytometry positive selection   | [47,48,50]          |
| Side population (SP) cells  | Ability to exclude DNA-binding dye Hoechst 33342 via ABC family of transporters; they export anticancer drugs when overexpressed in tumor cells  | [15,51,52]          |
| Stem cell transcription factors (OCT-4, SOX2, NANOG)                    | Highly enriched markers in cell populations with stemness properties   | [32,39,48,49,52–54] |
| EMT-promoting pathways (Notch-1, Wnt signaling, Sonic hedgehog protein) | Pathways involved in promoting self-renewal ability and tumorigenic potential  | [39,53,54]          |

Many studies have been carried out to identify the specific biomarkers of thyroid CSCs in the three histopathological TC variants.

Evaluating the enzymatic activity of aldehyde dehydrogenase (ALDH) is a well-known approach for identifying putative CSCs. Indeed, high levels of ALDH activity are present in stem and progenitor cells and seem to be related to their resistance to chemotherapy. Todaro et al. [21] were the first to isolate CSCs from primary thyroid tumors using ALDH activity. They demonstrated that the three histopathological TC variants expressed a small population of cells with tumorigenic potential, elevated ALDH activity, and unlimited replication ability [21]. This subpopulation of cells (1.2–3.5%) of the whole tumor was ALDH<sup>high</sup> and was able to form thyroid spheres when expanded in vitro in serum-free conditions, as well as create sequential tumor xenografts in immunocompromised mice model [21]. Another putative CSCs marker is prominin-1, also called CD133, which is a five transmembrane domain glycoprotein with unknown function that behaves as a stemness marker in many normal and tumor cells. In TC, Tseng et al. [49] isolated CD133<sup>+</sup> cells from ATC primary tumors and ATC cell lines. The CD133<sup>+</sup> cells expressed stemness genes, such as POU class 5 homeobox 1 (*POU5F1*), sex-determining region Y-box 2 (*SOX2*), and *NANOG1*, as well as drug-resistance genes (*ABCG2*, *MDR1*, and *MRP*). These cells were also chemoresistant and formed thyrospheres in vitro and tumors in vivo [49].

Ahn et al. [50] identified CD44 and CD24 expression in a small percentage of cells with tumorigenic potential in PTC cell lines and human primary samples. They observed that this subset of cells with tumorigenic capability expressed high levels of CD44, but no expression was detected for CD24 (CD44<sup>+</sup>/CD24<sup>−</sup>) [50]. Moreover, these CD44<sup>+</sup>/CD24<sup>−</sup> cells expressed the stem cell markers OCT4 and *POU5F1* and had a low expression of differentiation markers [50].

To further identify specific thyroid CSCs markers, Shimamura et al. [47] performed a comprehensive analysis of multiple markers (CD13, CD15, CD24, CD44, CD90, CD117, CD133, CD166, CD326, and ALDH activity) on eight thyroid cancer cell lines and then evaluated their ability to form thyrospheres in vitro and tumors in vivo. Their results suggest that ALDH<sup>pos</sup> and CD326<sup>high</sup> subpopulation of cells showed higher sphere-forming ability and both self-renewal and differentiation capability, generating homogeneous and heterogeneous cell populations. However, even if ALDH activity and CD326 expression are reliable candidates for detecting thyroid CSCs, they are not universal [47].



Another method to detect CSCs is the side population (SP) assay. This identifies a small subpopulation of cancer cells that is able to exclude the DNA binding dye Hoechst 33342 through the adenosine triphosphate-binding cassette (ABC) family of membrane transporters, which is also responsible for the anticancer drug export and therapy resistance of CSCs [15].

SP cells have been identified in different TCs: they presented a primitive morphology, with a high nuclear-to-cytoplasmic ratio, the ability to undergo thysosphere formation, and expressed typical stem cell markers, such as OCT-4, NANOG, and SOX2, but no markers of thyroid differentiation [51,52].

Mitsutake et al. [54] also found a very small portion of SP cells in human thyroid cancer cell lines. The detection of putative thyroid CSCs can also be supported by the evaluation of the expression of biomarkers belonging to self-renewing control pathways, such as Wnt/ $\beta$ -catenin, Sonic hedgehog protein, and Notch1, which are also responsible for the EMT process regulation [54]. Indeed, there is a strong correlation between EMT markers' expression and the presence of CSCs in TC [28,55]. For example, a loss of E-cadherin is associated with the expression of CD44, CD133, and Nestin, while Snail1 and vimentin upregulation is associated with ALDH expression [56–58].

### 3. Tumor Microenvironment and CSC Maintenance

Cancer stem cells are a small subpopulation that principally exists in tumor areas with specific microenvironmental conditions, the so-called stem cell niches, which are constituted by different stromal cell types, including a vascular system, mesenchymal and immune cells, the ECM, and soluble factors [13,59] (Figure 2 and Table 2). The stromal cells and the substances that they secrete are fundamental to maintaining the CSCs in a quiescent state and regulating their self-renewal and differentiation through the modulation of several signaling pathways [59]. The principal regulators of thyroid CSCs are the cancer-associated fibroblasts (CAFs) and the matrix secreted from them, the local variations in nutrients and oxygen distribution, mainly due to tumor fibrosis and altered vasculature growth that may create specific hypoxic niches, and immune cells, such as tumor-associated macrophages (TAMs) and mast cells (MCs), which secrete important paracrine factors.

**Table 2.** Secreted factors that promote CSCs' phenotypes and survival.

| Factors | Cell Type  | Action/Function  | Pathways Involved             | Other Cancers   | References    |
|---------|------------|--|-------------------------------|---|---------------|
| CCL-2   | CAFs, TAMs | Stimulates CSCs survival                               | Notch, NF- $\kappa$ B         | Breast cancer   | [60,61]       |
| CCL-15  | TCs        | Recruit TAMs<br>Promotes therapy resistance            | CCR1                          |   | [62]          |
| CXCL-1  | CAFs       | Promotes cancer cell stemness                          | IL-1a/JAK/STAT                | Pancreatic ductal adenocarcinoma  | [63–65]       |
| CXCL-12 | CAFs       | Induces CSC markers expression                         | Wnt, PI3K/Akt                 | Colorectal cancer   | [66–70]       |
| CXCL-2  | CAFs       | Promotes cancer cell stemness                          | IL-1a/JAK/STAT                | Pancreatic ductal adenocarcinoma  | [65,71]       |
| CXCL-8  | TAMs, TCs  | Promotes and maintains CSCs phenotype and induces EMT. | NF- $\kappa$ B, EGFR/RAS      | Melanoma, ovarian cancer<br>Colorectal cancer, non-small cell lung cancer | [71–79]       |
| HGF     | CAFs       | Induces CSC markers expression                         | PI3K, Met                     | Colorectal cancer   | [70,80]       |
| IGF-2   | CAFs       | Promotes acquisition of stem-like phenotype            | PI3K, TGF- $\beta$ , Wnt, SHH | Non-small cell lung cancer  | [48,81,82]    |
| IL-6    | CAFs, MCs  | Promotes and maintains CSCs phenotype and induces EMT. | JAK/STAT, NF- $\kappa$ B      | Breast cancer, pancreatic ductal adenocarcinoma                           | [65,79,83–88] |
| IL-8    | CAFs, MCs  | Promotes and maintains CSCs phenotype                  | FAK/AKT, Akt/Slug             | Breast cancer, pancreatic ductal adenocarcinoma                           | [89–93]       |

Table 2. Cont.

| Factors | Cell Type       | Action/Function   | Pathways Involved   | Other Cancers                       | References |
|---------|-----------------|---|---------------------|-------------------------------------|------------|
| OPN     | CAFs, TCs       | Supports the clonogenic capacity of CSCs<br>Induces CSCs markers expression | Wnt, PI3K           | Colorectal cancer                   | [70,94–96] |
| TGF-β   | CAFs, TAMs, TCs | Induces CSCs markers expression   | Wnt, PI3K           | Colorectal cancer                   | [70,97]    |
| TNF-α   | MCs             | Stimulate immune tolerance  | CCL20<br>CXCL8/EGFR | Breast cancer,<br>colorectal cancer | [93,98,99] |

MCs: mast cells.

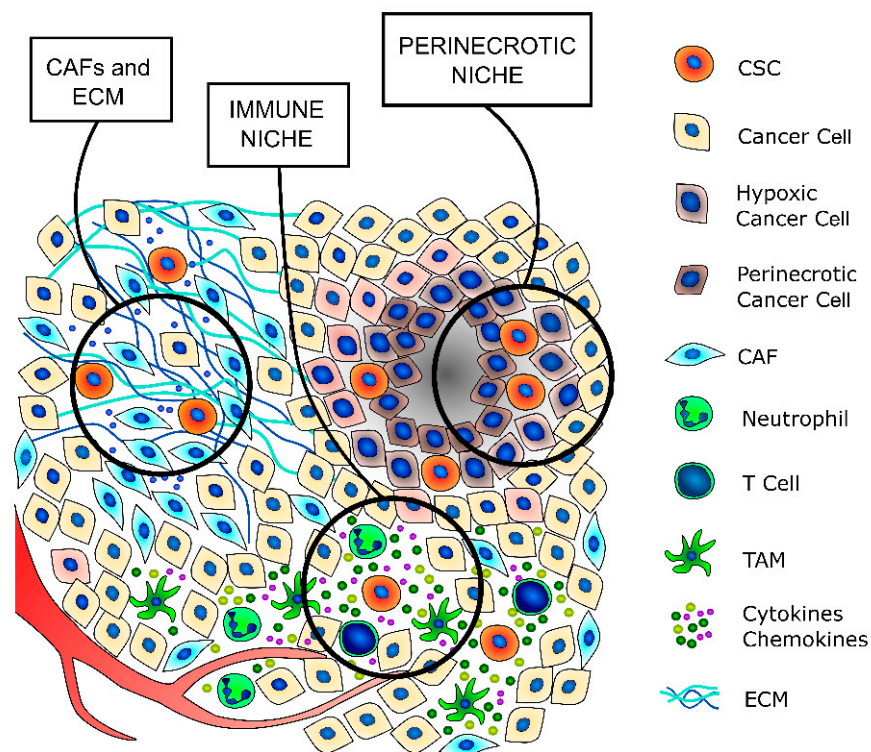


**Figure 2.** TC stem cell niches. CSCs principally exist in tumor areas with specific microenvironmental conditions, the so-called stem cell niches. The cancer-associated fibroblasts (CAFs) secrete a thicker extracellular matrix (ECM) and different prostemness soluble factors that induce the acquisition of a stem-like phenotype by cancer cells and promote and support the survival and self-renewal abilities of already existing CSCs. The immune niche is composed of all the different immune cells that contribute to regulate the CSCs’ phenotypes, such as T lymphocytes, tumor-associated macrophages (TAMs) and neutrophils. Indeed, immune cells secrete a wide variety of cytokines and chemokines that support the maintenance of the stem-like phenotype. The hypoxic niche contributes to CSCs’ phenotype maintenance, mainly through the induction of hypoxia-inducible factors (HIFs), whose activation deeply influences the parapsychological adaptations to the changes of the tumor microenvironment. Indeed, increasing evidence indicates that HIFs are one of the main regulators of CSC subpopulation maintenance, not only by stimulating an increase in the number of CSCs but also by enhancing the stem-like phenotype of dedifferentiated cancer cells.

### 3.1. CAFs, Extracellular Matrix, and Desmoplastic Reaction in TC

As with many other solid tumors of glandular origin, the more aggressive thyroid cancers are characterized by a pronounced desmoplastic stromal reaction [100–108], whose major components are CAFs and the ECM that they secrete (Figure 2) [107,109,110].

Indeed, different studies revealed that CAFs often secrete an ECM that is rich in collagen 1, which has been associated with tumor progression, metastatization, and therapy resistance [32,92,107,111–116].

In many cancer types, the crosstalk between the tumor and stromal components is fundamental for the establishment and maintenance of permissive niches that promote cancer progression and therapy resistance [117,118]. In fact, the interactions between cancer cells and CAFs often involve molecules such as CD44, thrombospondin-1, osteopontin, fibronectin, and integrins that are also involved in the induction and maintenance of CSCs' phenotypes [50,95,96,109,110,119–123] (Table 2). Moreover, a specific subpopulation of CAFs that effectively secrete pro-stemness factors have recently been identified [61,82,87,88,124–126]; these pro-stemness factors can induce the acquisition of a stem-like phenotype by cancer cells in normal conditions and promote and support the survival and self-renewal abilities of already existing CSCs after different stresses, such as anticancer therapies [127–130].

Although in recent years, the relationships between CSCs, CAFs, and the ECM have been deeply explored, only a few studies have investigated this topic regarding thyroid cancer.

In 2010, Nucera et al. demonstrated that the downstream pathways activated by BRAFV600E are crucial for ECM remodeling, where they identified thrombospondin 1 as one of the main effectors, together with CD44, fibronectin cathepsin B, and TGF $\beta$ 1 [131].

Further studies revealed that collagen 1 and lysyl-oxidase (LOX, a collagen fiber crosslinker) expressions are associated with less differentiated TC types and a poor overall survival rate; these alterations are the result of BRAF activation and/or PTEN loss, which promote the formation of a fibrotic tumor stroma that is rich in CAFs and collagen 1, facilitating tumor progression [117,132]. All these effects are mostly due to the fact that TC cells with specific genetic alterations secrete peculiar soluble factors that are able to activate the nearby fibroblast, inducing the changes in metabolism and phenotype that are typical of CAFs [131,133]. In turn, activated CAFs secrete soluble factors that modulate TC cells' proliferative and invasion potentials [133].

Thus, it seems that the well-characterized paracrine loop between CAFs and cancer cells that is definitely important for the definition of specific niches in which CSCs are mainly localized also exists in TC; further studies are, however, needed in this direction.

### 3.2. Hypoxic Niche

In many cancer types, hypoxia is a hallmark of malignancy and progression, as solid tumors often outgrow the vasculature, and the vasculature itself can be aberrant [134,135] (Figure 2). At the cellular level, hypoxia induces a complex coordinated response that deeply influences the paraphysiological adaptations to the changes in the tumor microenvironment, which are modifications that are often also responsible for therapy resistance [136–138].

The main players in the hypoxia response are two transcription factors, namely, hypoxia-inducible factors 1 and 2 (HIF-1 and HIF-2, respectively). HIF protein activity is finely regulated by the turnover of its oxygen-dependent alpha subunits (HIF-1 $\alpha$ , HIF-2 $\alpha$ , and HIF-3 $\alpha$ ) [135,139]. Upon exposure of the cells to hypoxia, the HIF $\alpha$  subunits are stabilized, translocate in the nucleus, and induce the transcription of different target genes that regulate cell metabolism, proliferation, invasive potential, and therapy resistance [140–142].

Indeed, increasing evidence indicates that HIFs are one of the main regulators of CSCs subpopulation maintenance, not only by stimulating an increase in the number of CSCs but also by enhancing the stem-like phenotype of dedifferentiated cancer cells [119,134,143–145]. HIF-1 $\alpha$  or HIF-2 $\alpha$  overexpression and their interplay in CSC maintenance have been observed in many cancer types, such as glioblastoma, colon, breast, lung, pancreatic, and ovarian cancers [22,146–152].

Although necrotic or hypoxic areas are uncommon in well-differentiated thyroid cancers, they are frequently found in the more aggressive anaplastic ones [3,153]. Moreover,

it is known that HIF1 $\alpha$  activity is also induced in non-hypoxic conditions by the hyperactivation of PI3K and RAS/RAF/ERK pathways, which is a direct consequence of genetic alterations that are common in thyroid cancer, such as PTEN deletion and RAS and BRAF mutations [154–158]. Overexpression of HIFs has been associated with an advanced tumor grade and distant metastasis in thyroid cancer [155,159].

Different studies demonstrated that the expression of HIF1 and its target genes, GLUT1 and VEGF, correlate with the TC grade and type [160–164]. While PTC and FTC showed only focal HIFs expression, PDTC and ATC presented a diffuse expression, which may be the result of a specific combination of tumor genotype and microenvironment alterations induced by diffusion-limited chronic hypoxia [155]. Up till now, no data exists on HIF2 expression in TC, but in vitro experiments demonstrated that HIF2 activation may be induced by the same stimuli that regulate HIF1, and its inhibition greatly affects thyroid cancer cell proliferation in hypoxic conditions [159,165].

### 3.3. Immune Niche

CSCs have a dual relationship with the immune components of the microenvironment. On one side, they are able to escape the attacks of immune cells against bulk cancer thanks to their quiescent state, low immunogenicity, and ability to recruit immunosuppressive cells [166,167]. On the other hand, immune cells secrete a wide variety of cytokines and chemokines that support the maintenance of the stem-like phenotype [168,169] (Figure 1 and Table 2). All the different immune cells that contribute to regulating the CSCs phenotype maintenance, such as T regulatory lymphocytes (T-regs), TAMs, and MCs, compose the so-called immune niche.

The immune evasion mechanism of TC cells is mainly based on the downregulation of MHC class I molecules, the upregulation of B7 homolog I (B7-H1), and the upregulation of HIF-1 $\alpha$ . Angell et al. [170] found that the expression of human histocompatibility antigen (HLA)-ABC and  $\beta$ 2-microglobulin in PTC was significantly reduced compared with normal thyroid tissue, and the proportion of tumor-infiltrating lymphocytes (TILs) was also decreased. In PTC, the B7-H1 protein and mRNA levels are strongly associated with tumor aggressiveness: the higher the B7-H1 expression level, the stronger the tumor aggressiveness [171]. Moreover, the hypoxic-like environment characterized by HIF-1 activation, which promotes CSC maintenance, also possesses an immune-suppressive effect that enhances tumor escape [172].

T-regs are highly enriched in the tumor microenvironment (TME), where they reduce the antitumor immune response. Some studies have suggested that T-regs can efficiently migrate into tumors in response to chemokines (e.g., chemokine receptor 4 (CCR4)-CC motif ligand 17/22 (CCL17/22), CCR10-CCL28, and CXC chemokine receptor 4 (CXCR4)-CXC motif ligand 12 (CXCL12)) that are expressed on the stroma and tumor cells and can be associated with a poor prognosis in patients [173,174].

Cytotoxic T lymphocytes (CTLs) are another subpopulation of T lymphocytes that possess the ability to kill target cells. Regarding thyroid cancer, French and colleagues [175] found that a low concentration of CD8<sup>+</sup> T cells and a reduced ratio of CD8/Foxp3<sup>+</sup> T cells was correlated with a larger tumor diameter in PTC patients. In fact, a reduced number of CD8<sup>+</sup> T cells diminishes the lethality to cancer cells and accelerates their rapid growth and invasiveness. Natural killer (NK) cells destroy pathogenic cells, mainly by secreting perforin and granzyme, expressing Fas ligand (FasL), and destroying their targets through antibody-dependent cell-mediated cytotoxicity (ADCC) [176]. Studies have reported that CSCs secrete immunosuppressive factors, such as transforming growth factor- $\beta$  (TGF- $\beta$ ), indoleamine2,3-dioxygenase (IDO), arginase-1, and interleukin 6 (IL-6), which reduces the expression of NK cell surface-activated receptors and result in a decreased number and quality of NK cells [86,93,97,177].

MCs secrete cytokines, such as tumor necrosis factor  $\alpha$  (TNF- $\alpha$ ) and IL-8 to stimulate immune tolerance and enhance tumor progression [78,79,93,99]. The role of MCs has been widely studied in TC and its density has been positively correlated with cancer



aggressiveness [130]. Indeed, Visciano et al. [79] found that TC cells activate MCs to produce chemokines, such as Il-6 and TNF- $\alpha$ , which in turn induce the EMT and a stem-like phenotype in TC cells.

TAMs are the most abundant population of tumor-infiltrating immune cells in the TME and have strong plasticity, as they can switch between proinflammatory (M1) and anti-inflammatory (M2) phenotypes [178,179].

The frequency of TAM infiltration varies between TC subtypes, increasing with dedifferentiation and culminating in ATCs, where TAMs represent up to 50% of all immune cells [180]. In all TCs, TAM infiltration has been invariably correlated with poor prognosis, large tumor size, capsular invasion, extra-thyroid tumor extension, lymph node metastasis, and decreased survival [181–183].

Indeed, TAMs secrete a wide variety of cytokines and chemokines, such as CXCL-8, TGF- $\beta$ , and CCL-2, which influence CSC survival [61,71,79,86,184,185].

### 3.4. Exosomes in CSC Niches

Exosomes are extracellular vesicles with an endosomal origin that are produced by the different cell types present in the CSC niches [186,187]. Indeed, the intercellular communication mediated by exosomes plays a fundamental role in tumor development and aggressiveness [188].

In thyroid cancer, the CSCs produce exosomes containing different long non-coding RNAs (lncRNAs) that promote the EMT and the acquisition of a stem-like phenotype of the bulk cancer cells and induce a pro-metastatic phenotype [28,189–191]. Moreover, patients with metastatic PTC have significantly higher levels of circulating exosomal miRNAs and hypoxic PTC cells can secrete exosomes that modulate the expression of TGF- $\beta$  and collagen isoforms, enhancing the tumoral angiogenesis [192]. The exosomes secreted by CSCs also modulate the polarization of TAMs toward the M2 phenotype and suppress NK cell activity, promoting an immunosuppressive environment in CSC niches [193–196]. In turn, CAFs and TAMs also release exosomes that contribute to the regulation of the TME [187,197,198].

## 4. Genetic Alterations, TME, and CSCs

Many of the different genetic alterations present in TC cells not only confer a proliferative advantage to the cell themselves but also deeply influence the surrounding microenvironment and the survival of CSCs.

The most studied alteration in this regard is BRAFV600E. Mutated cells have an altered expression of factors that are crucial for ECM remodeling, such as thrombospondin 1, CD44, fibronectin, cathepsin B, TGF- $\beta$ 1, collagen 1, and LOX [117,131,132]. Indeed, the ECM of BRAFV600E TCs has a composition and stiffness that promote the EMT of TC cells and enhances the stem-like phenotype of CSCs. Moreover, the alterations induced by BRAF hyperactivation also induce a more acidic TME that also contributes to the induction of an undifferentiated cell phenotype [199].

Moreover, BRAFV600E also significantly induces HIF1 $\alpha$  in a hypoxia-unrelated way, and through TIMP-1 activation, synergizes with HIF1A itself to promote metastatic potential and a stem-like phenotype [200,201]. Similar alterations are also found in TC with PTEN loss, though fewer studies support these findings [117].

Alterations in p53 activity that are usually found in less differentiated TCs can deeply influence the CSCs phenotype and maintenance in different ways, from metabolic reprogramming to immune evasion. Even if p53 loss-of-function mutations are characteristic only of the less differentiated TCs, the proinflammatory TME induced by bulk cancer cells can suppress p53 function with various mechanisms. For instance, the activation of pathways such as NOTCH, WNT/b-catenin, and Hedgehog contribute to CSC stemness maintenance by suppressing p53 expression [202–206].

Indeed, p53 activity is critical for the maintenance of cell proliferation and differentiation, where the loss of p53 functionality promotes the dedifferentiation and maintenance of CSCs [207]. In addition, p53 suppression has also been reported in the thyrosphere

generated from wild-type p53 TCs [208], and the inhibition of p53 is also fundamental in the reprogramming process that allows for the generation of induced pluripotent stem-cells (iPS) cells [209–212].

Another mechanism by which p53 loss promotes stemness is the upregulation of Twist1 and Snail2 expression, which are two important regulators of the EMT process that promote the generation of CSCs through the dedifferentiation of cancer cells [213,214]. Moreover, p53 can also regulate CD44 expression by modulating its alternative splicings through the RNA-binding protein ZMAT3 [215].

Furthermore, a loss of p53 functions promotes the metabolic switch from cellular respiration to glycolysis known as the Warburg effect [216,217]. This is fundamental for the survival of CSCs in the altered tumor microenvironment, and especially in the hypoxic niches.

Lastly, epigenetic alterations also play a role in CSC maintenance, but this area has been scarcely investigated in TC. A significant number of genes with abnormally methylated promoters in TC are involved in the regulation of the MAPK pathways controlled by RAS, BRAF, and PI3K, and can act as regulators of the EMT [218–220]. In addition, in FTC, hypermethylation of the E-cadherin promoter has been reported and was hypothesized to be a further mechanism of the EMT [221,222]. A similar mechanism is also responsible for the suppression of thyroid differentiation markers, such as NIS and TTF1 [223,224].

### 5. Therapeutic Targeting of CSCs and TME Crosstalk

Because CSCs are the main cause of therapy resistance and disease relapse, in recent years, different strategies to target these cancer subpopulations have been developed. Indeed, CSC-targeting therapies rely mostly on three different strategies: the inhibition of CSC stem factors, the modulation of CSCs and TME crosstalk, and the promotion of CSC differentiation [225] (Figure 3 and Table 3).

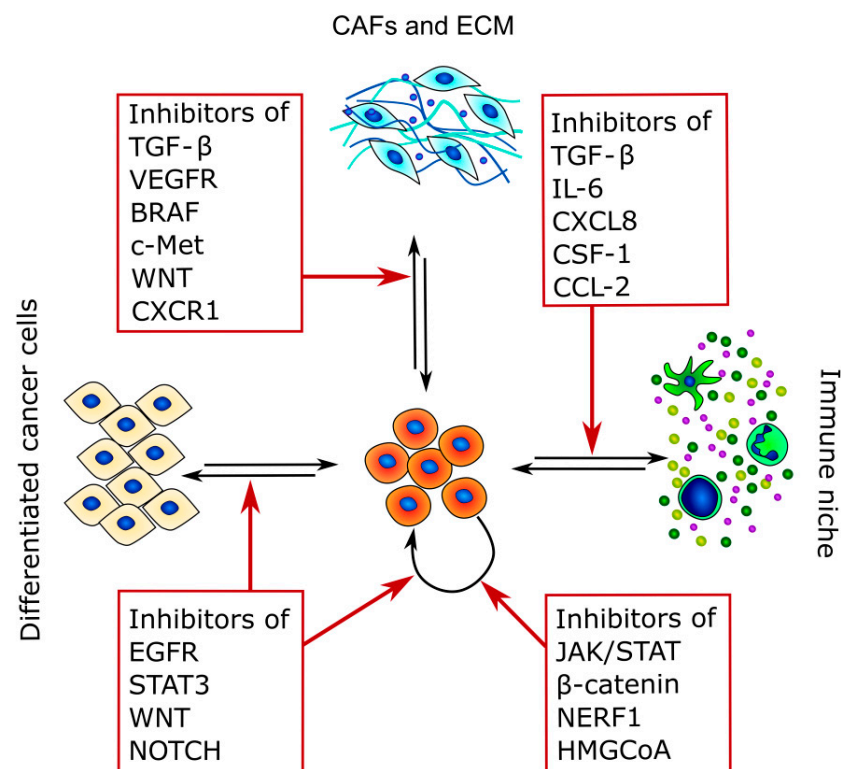


**Figure 3.** Therapeutic targets of CSCs and TME crosstalk. The figure summarizes the main pathways that can be targeted and highlights the main interactors of CSC crosstalk in which they are involved.

**Table 3.** Compounds that act against CSC-related pathways.

| Pathways     | Compound  | Cancer Type  | Clinical Trials  |
|--------------|---|--|--|
| CD44         | H90, P245, H4C4, RO5429083, SPL-108, AMC303                             | Ovarian, solid tumors  | NCT01358903, NCT03078400, NCT03009214  |
| CD133        | BsAb  | Glioblastoma   | NCT03085992  |
| Nanog        | BBi503  | Hepatocellular, advanced solid tumors  | NCT02483247, NCT01781455, NCT02279719  |
| EpCAM        | Catumaxomabr (emovab)   | Ovarian  | NCT00189345, NCT00106145, NCT01098344, NCT00645333, NCT01196416, NCT01232829, NCT02836600, NCT02518113, NCT03422679, NCT01363817, NCT02050178, NCT02092363, NCT02069145, NCT01973309, NCT02005315, NCT01606579, NCT01764477, NCT01398462, NCT02426723, NCT01951690, NCT01778803, NCT02004028, NCT01849744, NCT01594216, NCT00952289, NCT03450330, NCT01523171, NCT02178956, NCT02315534, NCT02352558, NCT02231723, NCT01190345, NCT00215644, NCT00522652, NCT01600573, NCT00194935, NCT02963090, NCT01579812, NCT01717482, NCT02179970, NCT02907099, NCT02765165, NCT00512252, NCT02452008, NCT04031872, NCT00844064, NCT01959490, NCT00431561, NCT00356460, NCT02947165 |
| Notch        | MK-0752, RO4929097, LY3039478, AL101, CB-103, BMS-906024                | Pancreatic, breast, melanoma, hematologic malignancies                           |  |
| Wnt          | Vantictumab, Ipafricept   | Pancreatic, ovarian, hepatocellular, breast                                      |  |
| B-catenin    | PRI-724, CWP232291  | Pancreatic, hematologic malignancies   |  |
| FAK          | Defactinib/Vs-6063, Vs-4718   | Lung, ovarian, non-hematologic   |  |
| JAK/STAT     | Ruxolitinib, AZD4205, SAR302503, BBI608                                 | Breast, glioblastoma, hematopoietic malignancies, pancreatic                     |  |
| EGFR         | Bevacizumab, Matuzumab  | Breast, gastric  |  |
| HIFs         | PX478, Topotecan  | Solid tumors, lymphoma, ovarian  |  |
| AMPK         | Metformin   | Ovarian, lung  |  |
| CXCR4        | Plerixafor, BL-8040, BKT140, BMS-936564, LY2510924, USL311, AMD3100     | Pancreatic, glioblastoma, hematologic malignancies                               |  |
| TGF- $\beta$ | Galunisertib, LY3200882, Trabectedin, Fresolimumab, Vactosertib, NIS793 | Prostate, colorectal, pancreatic, breast, melanoma, hepatocellular, glioblastoma |  |

The first approach is the use of different molecules that directly target the pathways necessary for CSC survival, alone or in combination with more classical anticancer drugs [226,227].

In this sense, tyrosine kinase inhibitors (TKIs) are the more studied compounds, as they can inhibit different pathways that are involved in either cell proliferation or stemness acquisition. TKIs against the EGFR pathway are the most studied, as many CSC characteristics, such as quiescence, glycolytic metabolism, and immunosuppressive activity, are modulated by EGFR and its downstream target STAT3 [228,229]. Indeed, STAT3 is required for the survival of CD133<sup>+</sup> TC cells, and inhibition of this transcription factor suppresses CSC tumorigenesis *in vitro* and *in vivo* [49].

Another pathway that has recently been explored for CSC targeted therapy is the Wnt/ $\beta$ -catenin one, together with its interactors NHERF1 and PTEN [230].

For example, Defactinib, which was developed first as a FADK1/2 inhibitor, was shown to directly target CSC survival through the modulation of  $\beta$ -catenin localization and activity [231]. Moreover, different inhibitors of Wnt and  $\beta$ -catenin are actually undergoing phase I and II clinical trials.

Besides TKIs, different compounds that were previously developed for other diseases had shown *in vitro* and *in vivo* efficacy against CSCs, principally by modulating their metabolism. For example, Lovastatin, which is an inhibitor of hydroxymethylglutaryl coenzyme A reductase, is able to target CSCs in mammary tumors due to its intrinsic mechanism of action [232,233].

Similarly, other statins and metabolically active drugs, such as metformin and menadione, efficiently target CSC survival in different cancer types [234–236].

As CSCs are a highly heterogeneous population that exist in a dynamic equilibrium between different differentiation states, they could easily escape one of the targeted therapies mentioned above, thus explaining the therapeutic failure of some TKIs. Moreover, conventional anticancer therapies are not only not effective against CSCs but can also induce CAFs to secrete different chemokines that indeed support CSC survival, thus finally resulting in relapses that are more aggressive than the original tumor [129]. Nevertheless, CAFs are a more stable population that is easily identifiable, and at the same time, the paracrine factors that they secrete are a fundamental support for CSCs. For these reasons, the disruption of the crosstalk between CSCs and CAFs by directly targeting the molecular signaling pathways involved may be successful.

For example, a gastric CSC population was significantly suppressed by TGF- $\beta$  inhibition [237,238]. Unfortunately, although TGF- $\beta$  secretion is dysregulated by the frequent TC BRAFV600E mutation, no clinical studies have been performed for TC in this sense.

Moreover, as previous studies revealed that c-Met silencing inhibits the metastatic potential of TC CSCs [21], this could be another potential target. Indeed, c-MET and  $\beta$ -catenin pathways are both regulated by CAF-secreted HGF and WNT [239,240], and their inhibitors are under investigation in phase I clinical trials [241,242].

The inhibition of IL-6 activity by specific antibodies in combination with chemotherapy successfully induced an almost complete regression in a PDX model of breast cancer by interrupting the inflammatory loop between the IL-6 and STAT-3 responsible for the EMT and stemness maintenance [243]. Besides IL-6, molecules that act against its downstream pathway are another opportunity for directly targeting CSCs and simultaneous inhibition of CSC–CAF crosstalk. Moreover, different molecules that disrupt the CSC–immune cells crosstalk are actually under investigation. For example, compounds targeting CXCR4 effectively induced remission in hematopoietic cancers.

## 6. Conclusions

Although TC is a manageable disease in the majority of the cases, the more aggressive and less differentiated types are still highly lethal diseases. The discovery of CSCs and the complex dynamics that exist in the tumor microenvironment and highly specialized niches may explain how TC subpopulations can survive different anticancer drugs, leading



to disease recurrence and therapeutic failure. Despite the CSC–TME interplay being well studied for other cancer types, this field is still evolving for TC, with some important studies that identified the TC CSCs but with scarce knowledge of the TME complexity. The understanding of the heterogeneous biology of TCs will prompt the development of more specific therapies, which can be directed not only against the cancer cell bulk but also aimed at disrupting the crosstalk between CSCs and the different components of the TME, and finally allowing for the complete eradication of the disease.

**Author Contributions:** E.S.G., V.G., and L.P. wrote and revised the manuscript. All authors have read and agreed to the published version of the manuscript.

**Funding:** Partially funded by Ricerca Corrente Funds of Istituto Auxologico Italiano (code: 05C825\_2018; PTC-Array).

**Institutional Review Board Statement:** Not applicable.

**Informed Consent Statement:** Not applicable.

**Data Availability Statement:** No new data were created or analyzed in this study. Data sharing is not applicable to this article.

**Conflicts of Interest:** The authors declare no conflict of interest.

## References

- Lin, R.-Y. Thyroid cancer stem cells. *Nat. Rev. Endocrinol.* **2011**, *7*, 609–616. [[CrossRef](#)]
- Veschi, V.; Verona, F.; Iacono, M.L.; D’Accardo, C.; Porcelli, G.; Turdo, A.; Gaggianesi, M.; Forte, S.; Giuffrida, D.; Memeo, L.; et al. Cancer Stem Cells in Thyroid Tumors: From the Origin to Metastasis. *Front. Endocrinol.* **2020**, *11*, 566. [[CrossRef](#)] [[PubMed](#)]
- Nagaiah, G.; Hossain, A.; Mooney, C.J.; Parmentier, J.; Remick, S.C. Anaplastic Thyroid Cancer: A Review of Epidemiology, Pathogenesis, and Treatment. *J. Oncol.* **2011**, *2011*, 542358. [[CrossRef](#)]
- Perri, F. Anaplastic thyroid carcinoma: A comprehensive review of current and future therapeutic options. *World J. Clin. Oncol.* **2011**, *2*, 150–157. [[CrossRef](#)]
- Kroll, T.G. PAX8-PPARgamma 1 Fusion in Oncogene Human Thyroid Carcinoma. *Science* **2000**, *289*, 1357–1360. [[CrossRef](#)] [[PubMed](#)]
- Hou, P.; Liu, D.; Shan, Y.; Hu, S.; Studeman, K.; Condouris, S.; Wang, Y.; Trink, A.; El-Naggar, A.K.; Tallini, G.; et al. Genetic Alterations and Their Relationship in the Phosphatidylinositol 3-Kinase/Akt Pathway in Thyroid Cancer. *Clin. Cancer Res.* **2007**, *13*, 1161–1170. [[CrossRef](#)] [[PubMed](#)]
- Chmielik, E.; Rusinek, D.; Oczko-Wojciechowska, M.; Jarzab, M.; Krajewska, J.; Czarniecka, A.; Jarzab, B. Heterogeneity of Thyroid Cancer. *Pathobiology* **2018**, *85*, 117–129. [[CrossRef](#)] [[PubMed](#)]
- Tanaka, K.; Sonoo, H.; Saito, W.; Ohta, Y.; Shimo, T.; Sohda, M.; Yamamoto, Y.; Kurebayashi, J. Analysis of Clinical Outcome of Patients with Poorly Differentiated Thyroid Carcinoma. *ISRN Endocrinol.* **2011**, *2011*, 308029. [[CrossRef](#)]
- Ibrahimovic, T.; Ghossein, R.; Shah, J.P.; Ganly, I. Poorly Differentiated Carcinoma of the Thyroid Gland: Current Status and Future Prospects. *Thyroid.* **2019**, *29*, 311–321. [[CrossRef](#)] [[PubMed](#)]
- Nishida, T.; Katayama, S.-I.; Tsujimoto, M.; Nakamura, J.-I.; Matsuda, H. Clinicopathological Significance of Poorly Differentiated Thyroid Carcinoma. *Am. J. Surg. Pathol.* **1999**, *23*, 205–211. [[CrossRef](#)]
- Aratake, M.Y.; Nomura, H.; Kotani, T.; Marutsuka, K.; Kobayashi, K.; Kuma, K.; Miyauchi, A.; Okayama, A.; Tamura, K. Coexistent Anaplastic and Differentiated Thyroid Carcinoma. *Am. J. Clin. Pathol.* **2006**, *125*, 399–406. [[CrossRef](#)] [[PubMed](#)]
- Dirkse, A.; Golebiewska, A.; Buder, T.; Nazarov, P.V.; Muller, A.; Poovathingal, S.; Brons, N.H.C.; Leite, S.; Sauvageot, N.; Sarkisjan, D.; et al. Stem cell-associated heterogeneity in Glioblastoma results from intrinsic tumor plasticity shaped by the microenvironment. *Nat. Commun.* **2019**, *10*, 1787. [[CrossRef](#)] [[PubMed](#)]
- Borovski, T.; Melo, F.D.S.E.; Vermeulen, L.; Medema, J.P. Cancer Stem Cell Niche: The Place to Be. *Cancer Res.* **2011**, *71*, 634–639. [[CrossRef](#)] [[PubMed](#)]
- Semenza, G.L. Regulation of the breast cancer stem cell phenotype by hypoxia-inducible factors. *Clin. Sci.* **2015**, *129*, 1037–1045. [[CrossRef](#)] [[PubMed](#)]
- Tirino, V.; Desiderio, V.; Paino, F.; De Rosa, A.; Papaccio, F.; La Noce, M.; Laino, L.; De Francesco, F.; Papaccio, G. Cancer stem cells in solid tumors: An overview and new approaches for their isolation and characterization. *FASEB J.* **2012**, *27*, 13–24. [[CrossRef](#)] [[PubMed](#)]
- Takaishi, S.; Okumura, T.; Tu, S.; Wang, S.S.W.; Shibata, W.; Vigneshwaran, R.; Gordon, S.A.K.; Shimada, Y.; Wang, T.C. Identification of Gastric Cancer Stem Cells Using the Cell Surface Marker CD44. *STEM CELLS* **2009**, *27*, 1006–1020. [[CrossRef](#)]
- O’Brien, C.A.; Pollett, A.; Gallinger, S.; Dick, J.E. A human colon cancer cell capable of initiating tumour growth in immunodeficient mice. *Nat. Cell Biol.* **2006**, *445*, 106–110. [[CrossRef](#)]
- Rosen, J.M.; Jordan, C.T. The Increasing Complexity of the Cancer Stem Cell Paradigm. *Science* **2009**, *324*, 1670–1673. [[CrossRef](#)]

19. Gupta, P.B.; Chaffer, C.L.; Weinberg, A.R. Cancer stem cells: Mirage or reality? *Nat. Med.* **2009**, *15*, 1010–1012. [[CrossRef](#)]
20. Derwahl, M.; Zheng, X.; Cui, D.; Xu, S.; Brabant, G. Doxorubicin fails to eradicate cancer stem cells derived from anaplastic thyroid carcinoma cells: Characterization of resistant cells. *Int. J. Oncol.* **2010**, *37*, 307–315. [[CrossRef](#)]
21. Todaro, M.; Iovino, F.; Eterno, V.; Cammareri, P.; Gambarà, G.; Espina, V.; Gulotta, G.; Dieli, F.; Giordano, S.; De Maria, R.; et al. Tumorigenic and Metastatic Activity of Human Thyroid Cancer Stem Cells. *Cancer Res.* **2010**, *70*, 8874–8885. [[CrossRef](#)]
22. Pietras, A.; Katz, A.M.; Ekström, E.J.; Wee, B.; Halliday, J.J.; Pitter, K.L.; Werbeck, J.L.; Amankulor, N.M.; Huse, J.T.; Holland, E.C. Osteopontin-CD44 Signaling in the Glioma Perivascular Niche Enhances Cancer Stem Cell Phenotypes and Promotes Aggressive Tumor Growth. *Cell Stem Cell* **2014**, *14*, 357–369. [[CrossRef](#)] [[PubMed](#)]
23. Chan, T.-S.; Shaked, Y.; Tsai, K.K. Targeting the Interplay Between Cancer Fibroblasts, Mesenchymal Stem Cells, and Cancer Stem Cells in Desmoplastic Cancers. *Front. Oncol.* **2019**, *9*, 688. [[CrossRef](#)] [[PubMed](#)]
24. Kondo, T.; Ezzat, S.; Asa, S.L. Pathogenetic mechanisms in thyroid follicular-cell neoplasia. *Nat. Rev. Cancer* **2006**, *6*, 292–306. [[CrossRef](#)] [[PubMed](#)]
25. Gianì, F.; Vella, V.; Tumino, D.; Malandrino, P.; Frasca, F. The Possible Role of Cancer Stem Cells in the Resistance to Kinase Inhibitors of Advanced Thyroid Cancer. *Cancers* **2020**, *12*, 2249. [[CrossRef](#)]
26. Takano, T.; Amino, N. Fetal Cell Carcinogenesis: A New Hypothesis for Better Understanding of Thyroid Carcinoma. *Thyroid* **2005**, *15*, 432–438. [[CrossRef](#)]
27. Hardin, H.; Montemayor-Garcia, C.; Lloyd, R.V. Thyroid cancer stem-like cells and epithelial-mesenchymal transition in thyroid cancers. *Hum. Pathol.* **2013**, *44*, 1707–1713. [[CrossRef](#)]
28. Hardin, H.; Helein, H.; Meyer, K.; Robertson, S.; Zhang, R.; Zhong, W.; Lloyd, R.V. Thyroid cancer stem-like cell exosomes: Regulation of EMT via transfer of lncRNAs. *Lab. Investig.* **2018**, *98*, 1133–1142. [[CrossRef](#)]
29. Dumont, J.E.; Lamy, F.; Roger, P.; Maenhaut, C. Physiological and pathological regulation of thyroid cell proliferation and differentiation by thyrotropin and other factors. *Physiol. Rev.* **1992**, *72*, 667–697. [[CrossRef](#)] [[PubMed](#)]
30. Cha, Y.J.; Koo, J.S. Next-generation sequencing in thyroid cancer. *J. Transl. Med.* **2016**, *14*, 322. [[CrossRef](#)] [[PubMed](#)]
31. Nikiforova, M.N.; Wald, A.I.; Roy, S.; Durso, M.B.; Nikiforov, Y.E. Targeted Next-Generation Sequencing Panel (ThyroSeq) for Detection of Mutations in Thyroid Cancer. *J. Clin. Endocrinol. Metab.* **2013**, *98*, E1852–E1860. [[CrossRef](#)] [[PubMed](#)]
32. Colombo, C.; Muzza, M.; Proverbio, M.C.; Tosi, D.; Soranna, D.; Pesenti, C.; Rossi, S.; Cirello, V.; De Leo, S.; Fusco, N.; et al. Impact of Mutation Density and Heterogeneity on Papillary Thyroid Cancer Clinical Features and Remission Probability. *Thyroid* **2019**, *29*, 237–251. [[CrossRef](#)] [[PubMed](#)]
33. Takano, T. Fetal cell carcinogenesis of the thyroid: Theory and practice. *Semin. Cancer Biol.* **2007**, *17*, 233–240. [[CrossRef](#)] [[PubMed](#)]
34. Bonnet, D.; Dick, J.E. Human acute myeloid leukemia is organized as a hierarchy that originates from a primitive hematopoietic cell. *Nat. Med.* **1997**, *3*, 730–737. [[CrossRef](#)]
35. Zhang, P.; Zuo, H.; Ozaki, T.; Nakagomi, N.; Kakudo, K. Cancer stem cell hypothesis in thyroid cancer. *Pathol. Int.* **2006**, *56*, 485–489. [[CrossRef](#)]
36. Zito, G.; Richiusa, P.; Bommarito, A.; Carissimi, E.; Russo, L.; Coppola, A.; Zerilli, M.; Rodolico, V.; Criscimanna, A.; Amato, M.; et al. In Vitro Identification and Characterization of CD133pos Cancer Stem-Like Cells in Anaplastic Thyroid Carcinoma Cell Lines. *PLoS ONE* **2008**, *3*, e3544. [[CrossRef](#)]
37. Nguyen, L.V.; Vanner, R.; Dirks, P.B.; Eaves, C.J. Cancer stem cells: An evolving concept. *Nat. Rev. Cancer* **2012**, *12*, 133–143. [[CrossRef](#)] [[PubMed](#)]
38. Cirello, V.; Vaira, V.; Grassi, E.S.; Vezzoli, V.; Ricca, D.; Colombo, C.; Bosari, S.; Vicentini, L.; Persani, L.; Ferrero, S.; et al. Multicellular spheroids from normal and neoplastic thyroid tissues as a suitable model to test the effects of multikinase inhibitors. *Oncotarget* **2017**, *8*, 9752–9766. [[CrossRef](#)] [[PubMed](#)]
39. Gao, Y.-J.; Li, B.; Wu, X.-Y.; Cui, J.; Han, J.-K. Thyroid tumor-initiating cells: Increasing evidence and opportunities for anticancer therapy (Review). *Oncol. Rep.* **2014**, *31*, 1035–1042. [[CrossRef](#)] [[PubMed](#)]
40. Weiswald, L.-B.; Bellet, D.; Dangles-Marie, V. Spherical Cancer Models in Tumor Biology. *Neoplasia* **2015**, *17*, 1–15. [[CrossRef](#)]
41. Zane, M.; Scavo, E.; Catalano, V.J.; Bonanno, M.; Todaro, M.; De Maria, R.; Stassi, G. Normal vs cancer thyroid stem cells: The road to transformation. *Oncogene* **2016**, *35*, 805–815. [[CrossRef](#)] [[PubMed](#)]
42. Clarke, M.F.; Dick, J.E.; Dirks, P.B.; Eaves, C.J.; Jamieson, C.H.; Jones, D.L.; Visvader, J.; Weissman, I.L.; Wahl, G.M. Cancer Stem Cells—Perspectives on Current Status and Future Directions: AACR Workshop on Cancer Stem Cells. *Cancer Res.* **2006**, *66*, 9339–9344. [[CrossRef](#)] [[PubMed](#)]
43. Cheung, A.M.S.; Wan, T.S.K.; Leung, J.C.K.; Chan, L.Y.Y.; Huang, H.; Kwong, Y.L.; Liang, R.; Leung, A.Y.H. Aldehyde dehydrogenase activity in leukemic blasts defines a subgroup of acute myeloid leukemia with adverse prognosis and superior NOD/SCID engrafting potential. *Leukemia* **2007**, *21*, 1423–1430. [[CrossRef](#)] [[PubMed](#)]
44. Ginstier, C.; Hur, M.H.; Charafe-Jauffret, E.; Monville, F.; Dutcher, J.; Brown, M.; Jacquemier, J.; Viens, P.; Kleer, C.G.; Liu, S.; et al. ALDH1 Is a Marker of Normal and Malignant Human Mammary Stem Cells and a Predictor of Poor Clinical Outcome. *Cell Stem Cell* **2007**, *1*, 555–567. [[CrossRef](#)]
45. Marcato, P.; Dean, C.A.; Giacomantonio, C.A.; Lee, P.W. Aldehyde dehydrogenase: Its role as a cancer stem cell marker comes down to the specific isoform. *Cell Cycle* **2011**, *10*, 1378–1384. [[CrossRef](#)]

46. Tanei, T.; Morimoto, K.; Shimazu, K.; Kim, S.J.; Tanji, Y.; Taguchi, T.; Tamaki, Y.; Noguchi, S. Association of Breast Cancer Stem Cells Identified by Aldehyde Dehydrogenase 1 Expression with Resistance to Sequential Paclitaxel and Epirubicin-Based Chemotherapy for Breast Cancers. *Clin. Cancer Res.* **2009**, *15*, 4234–4241. [[CrossRef](#)]
47. Shimamura, M.; Nagayama, Y.; Matsuse, M.; Yamashita, S.; Mitsutake, N. Analysis of multiple markers for cancer stem-like cells in human thyroid carcinoma cell lines. *Endocr. J.* **2014**, *61*, 481–490. [[CrossRef](#)]
48. Malaguarnera, R.; Frasca, F.; Garozzo, A.; Giani, F.; Pandini, G.; Vella, V.; Vigneri, R.; Belfiore, A. Insulin Receptor Isoforms and Insulin-Like Growth Factor Receptor in Human Follicular Cell Precursors from Papillary Thyroid Cancer and Normal Thyroid. *J. Clin. Endocrinol. Metab.* **2011**, *96*, 766–774. [[CrossRef](#)] [[PubMed](#)]
49. Tseng, L.-M.; Huang, P.-I.; Chen, Y.-R.; Chou, Y.-C.; Chen, Y.-W.; Chang, Y.-L.; Hsu, H.-S.; Lan, Y.-T.; Chen, K.-H.; Chi, C.-W.; et al. Targeting Signal Transducer and Activator of Transcription 3 Pathway by Cucurbitacin I Diminishes Self-Renewing and Radiochemoresistant Abilities in Thyroid Cancer-Derived CD133+ Cells. *J. Pharmacol. Exp. Ther.* **2012**, *341*, 410–423. [[CrossRef](#)] [[PubMed](#)]
50. Ahn, S.-H.; Henderson, Y.C.; Williams, M.D.; Lai, S.Y.; Clayman, G.L. Detection of Thyroid Cancer Stem Cells in Papillary Thyroid Carcinoma. *J. Clin. Endocrinol. Metab.* **2014**, *99*, 536–544. [[CrossRef](#)]
51. Sugihara, E.; Saya, H. Complexity of cancer stem cells. *Int. J. Cancer* **2012**, *132*, 1249–1259. [[CrossRef](#)] [[PubMed](#)]
52. Lan, L.; Cui, D.; Nowka, K.; Derwahl, M. Stem Cells Derived from Goiters in Adults Form Spheres in Response to Intense Growth Stimulation and Require Thyrotropin for Differentiation into Thyrocytes. *J. Clin. Endocrinol. Metab.* **2007**, *92*, 3681–3688. [[CrossRef](#)] [[PubMed](#)]
53. Hadnagy, A.; Gaboury, L.; Beaulieu, R.; Balicki, D. SP analysis may be used to identify cancer stem cell populations. *Exp. Cell Res.* **2006**, *312*, 3701–3710. [[CrossRef](#)] [[PubMed](#)]
54. Mitsutake, N.; Iwao, A.; Nagai, K.; Namba, H.; Ohtsuru, A.; Saenko, V.; Yamashita, S. Characterization of Side Population in Thyroid Cancer Cell Lines: Cancer Stem-Like Cells Are Enriched Partly but Not Exclusively. *Endocrinol.* **2007**, *148*, 1797–1803. [[CrossRef](#)] [[PubMed](#)]
55. Lan, L.; Luo, Y.; Cui, D.; Shi, B.-Y.; Deng, W.; Huo, L.-L.; Chen, H.-L.; Zhang, G.-Y.; Deng, L.-L. Epithelial-mesenchymal transition triggers cancer stem cell generation in human thyroid cancer cells. *Int. J. Oncol.* **2013**, *43*, 113–120. [[CrossRef](#)] [[PubMed](#)]
56. Liu, J.; Brown, E.R. Immunohistochemical detection of epithelialmesenchymal transition associated with stemness phenotype in anaplastic thyroid carcinoma. *Int. J. Clin. Exp. Pathol.* **2010**, *3*, 755–762.
57. Heiden, K.B.; Williamson, A.J.; Doscas, M.E.; Ye, J.; Wang, Y.; Liu, D.; Xing, M.; Prinz, R.A.; Xu, X. The Sonic Hedgehog Signaling Pathway Maintains the Cancer Stem Cell Self-Renewal of Anaplastic Thyroid Cancer by Inducing Snail Expression. *J. Clin. Endocrinol. Metab.* **2014**, *99*, E2178–E2187. [[CrossRef](#)]
58. Ma, R.; Minsky, N.; Morshed, S.A.; Davies, T.F. Stemness in Human Thyroid Cancers and Derived Cell Lines: The Role of Asymmetrically Dividing Cancer Stem Cells Resistant to Chemotherapy. *J. Clin. Endocrinol. Metab.* **2014**, *99*, E400–E409. [[CrossRef](#)]
59. Fulawka, L.; Donizy, P.; Halon, A. Cancer stem cells—the current status of an old concept: Literature review and clinical approaches. *Biol. Res.* **2014**, *47*, 66. [[CrossRef](#)]
60. Ferrari, S.M.; Elia, G.; Piaggi, S.; Baldini, E.; Ulisse, S.; Miccoli, M.; Materazzi, G.; Antonelli, A.; Fallahi, P. CCL2 is Modulated by Cytokines and PPAR- $\gamma$  in Anaplastic Thyroid Cancer. *Anti-Cancer Agents Med. Chem.* **2018**, *18*, 458–466. [[CrossRef](#)]
61. Tsuyada, A.; Chow, A.; Wu, J.; Somlo, G.; Chu, P.; Loera, S.; Luu, T.; Li, A.X.; Wu, X.; Ye, W.; et al. CCL2 Mediates Cross-talk between Cancer Cells and Stromal Fibroblasts That Regulates Breast Cancer Stem Cells. *Cancer Res.* **2012**, *72*, 2768–2779. [[CrossRef](#)] [[PubMed](#)]
62. Huang, F.-J.; Zhou, X.-Y.; Ye, L.; Fei, X.-C.; Wang, S.; Wang, W.; Ning, G. Follicular thyroid carcinoma but not adenoma recruits tumor-associated macrophages by releasing CCL15. *BMC Cancer* **2016**, *16*, 98. [[CrossRef](#)] [[PubMed](#)]
63. Aust, G.; Steinert, M.; Boltze, C.; Kiessling, S.; Simchen, C. GRO- $\alpha$  in normal and pathological thyroid tissues and its regulation in thyroid-derived cells. *J. Endocrinol.* **2001**, *170*, 513–520. [[CrossRef](#)] [[PubMed](#)]
64. Melillo, R.M.; Guarino, V.; Avilla, E.; Galdiero, M.R.; Liotti, F.; Prevete, N.; Rossi, F.W.; Basolo, F.; Ugolini, C.; De Paulis, A.; et al. Mast cells have a protumorigenic role in human thyroid cancer. *Oncogene* **2010**, *29*, 6203–6215. [[CrossRef](#)] [[PubMed](#)]
65. Biffi, G.; Oni, T.E.; Spielman, B.; Hao, Y.; Elyada, E.; Park, Y.; Preall, J.; Tuveson, D.A. IL1-Induced JAK/STAT Signaling Is Antagonized by TGF $\beta$  to Shape CAF Heterogeneity in Pancreatic Ductal Adenocarcinoma. *Cancer Discov.* **2019**, *9*, 282–301. [[CrossRef](#)]
66. Chung, S.Y.; Park, E.S.; Park, S.Y.; Song, J.-Y.; Ryu, H.S. CXC motif ligand 12 as a novel diagnostic marker for papillary thyroid carcinoma. *Head Neck* **2014**, *36*, 1005–1012. [[CrossRef](#)]
67. Liu, Z.; Sun, D.-X.; Teng, X.-Y.; Xu, W.-X.; Meng, X.-P.; Wang, B.-S. Expression of Stromal Cell-Derived Factor 1 and CXCR7 in Papillary Thyroid Carcinoma. *Endocr. Pathol.* **2012**, *23*, 247–253. [[CrossRef](#)]
68. Wagner, P.L.; Moo, T.-A.; Arora, N.; Liu, Y.-F.; Zarnegar, R.; Scognamiglio, T.; Fahey, T.J. The Chemokine Receptors CXCR4 and CCR7 are Associated with Tumor Size and Pathologic Indicators of Tumor Aggressiveness in Papillary Thyroid Carcinoma. *Ann. Surg. Oncol.* **2008**, *15*, 2833–2841. [[CrossRef](#)]
69. Jung, Y.Y.; Park, I.A.; Kim, A.M.; Min, H.S.; Won, J.K.; Ryu, H.S. Application of Chemokine CXC Motif Ligand 12 as a Novel Diagnostic Marker in Preoperative Fine-Needle Aspiration Biopsy for Papillary Thyroid Carcinoma. *Acta Cytol.* **2013**, *57*, 447–454. [[CrossRef](#)]

70. Todaro, M.; Gaggianesi, M.; Catalano, V.; Benfante, A.; Iovino, F.; Biffoni, M.; Apuzzo, T.; Sperduti, I.; Volpe, S.; Cocorullo, G.; et al. CD44v6 Is a Marker of Constitutive and Reprogrammed Cancer Stem Cells Driving Colon Cancer Metastasis. *Cell Stem Cell* **2014**, *14*, 342–356. [[CrossRef](#)]
71. Rotondi, M.; Coperchini, F.; Latrofa, F.; Chiovato, L. Role of Chemokines in Thyroid Cancer Microenvironment: Is CXCL8 the Main Player? *Front. Endocrinol.* **2018**, *9*, 314. [[CrossRef](#)] [[PubMed](#)]
72. Martins, M.B.; Marcello, M.A.; Batista, F.D.A.; Peres, K.C.; Meneghetti, M.; Ward, M.A.L.; Etchebehere, E.C.S.D.C.; Da Assumpção, L.V.M.; Ward, L.S. Serum interleukin measurement may help identify thyroid cancer patients with active disease. *Clin. Biochem.* **2018**, *52*, 1–7. [[CrossRef](#)]
73. Sanmamed, M.F.; Carranza-Rua, O.; Alfaro, C.; Oñate, C.; Martín-Algarra, S.; Perez, G.; Landazuri, S.F.; Gonzalez, Á.; Gross, S.; Rodriguez, I.; et al. Serum Interleukin-8 Reflects Tumor Burden and Treatment Response across Malignancies of Multiple Tissue Origins. *Clin. Cancer Res.* **2014**, *20*, 5697–5707. [[CrossRef](#)]
74. Zachariae, C.O.C.; Thestrup-Pedersen, K.; Matsushima, K. Expression and Secretion of Leukocyte Chemotactic Cytokines by Normal Human Melanocytes and Melanoma Cells. *J. Investig. Dermatol.* **1991**, *97*, 593–599. [[CrossRef](#)]
75. Ivarsson, K.; Runesson, E.; Sundfeldt, K.; Haeger, M.; Hedin, L.; Janson, P.O.; Brännström, M. The Chemotactic Cytokine Interleukin-8—A Cyst Fluid Marker for Malignant Epithelial Ovarian Cancer? *Gynecol. Oncol.* **1998**, *71*, 420–423. [[CrossRef](#)]
76. Orditura, M.; De Vita, F.; Catalano, G.; Infusino, S.; Lieto, E.; Martinelli, E.; Morgillo, F.; Castellano, P.; Pignatelli, C.; Galizia, G. Elevated Serum Levels of Interleukin-8 in Advanced Non-Small Cell Lung Cancer Patients: Relationship with Prognosis. *J. Interf. Cytokine Res.* **2002**, *22*, 1129–1135. [[CrossRef](#)] [[PubMed](#)]
77. Brew, R.; Erikson, J.S.; West, D.C.; Kinsella, A.R.; Slavin, J.; Christmas, E.S. Interleukin-8 as an autocrine growth factor for human colon carcinoma cells in vitro. *Cytokine* **2000**, *12*, 78–85. [[CrossRef](#)] [[PubMed](#)]
78. Kobawala, T.P.; Patel, G.H.; Gajjar, D.R.; Patel, K.N.; Thakor, P.B.; Parekh, U.B.; Patel, K.M.; Shukla, S.N.; Shah, P.M. Clinical Utility of Serum Interleukin-8 and Interferon-Alpha in Thyroid Diseases. *J. Thyroid. Res.* **2011**, *2011*, 1–10. [[CrossRef](#)] [[PubMed](#)]
79. Visciano, C.; Liotti, F.; Prevete, N.; Cali', G.; Franco, R.; Collina, F.; De Paulis, A.; Marone, G.; Santoro, M.; Melillo, R.M. Mast cells induce epithelial-to-mesenchymal transition and stem cell features in human thyroid cancer cells through an IL-8–Akt–Slug pathway. *Oncogene* **2015**, *34*, 5175–5186. [[CrossRef](#)]
80. Mineo, R.; Costantino, A.; Frasca, F.; Sciacca, L.; Russo, S.; Vigneri, R.; Belfiore, A. Activation of the Hepatocyte Growth Factor (HGF)- Met System in Papillary Thyroid Cancer: Biological Effects of HGF in Thyroid Cancer Cells Depend on Met Expression Levels. *Endocrinology* **2004**, *145*, 4355–4365. [[CrossRef](#)]
81. Vella, V.; Nicolosi, M.L.; Cantafio, P.; Massimino, M.; Lappano, R.; Vigneri, P.; Ciuni, R.; Gangemi, P.; Morrione, A.; Malaguarnera, R.; et al. DDR1 regulates thyroid cancer cell differentiation via IGF-2/IR-A autocrine signaling loop. *Endocrine-Related Cancer* **2019**, *26*, 197–214. [[CrossRef](#)] [[PubMed](#)]
82. Chen, W.-J.; Ho, C.-C.; Chang, Y.-L.; Chen, H.-Y.; Lin, C.-A.; Ling, T.-Y.; Yu, S.-L.; Yuan, S.-S.; Chen, Y.-J.L.; Lin, C.-Y.; et al. Cancer-associated fibroblasts regulate the plasticity of lung cancer stemness via paracrine signalling. *Nat. Commun.* **2014**, *5*, 3472. [[CrossRef](#)] [[PubMed](#)]
83. Iliopoulos, D.; Hirsch, H.A.; Struhl, K. An Epigenetic Switch Involving NF- $\kappa$ B, Lin28, Let-7 MicroRNA, and IL6 Links Inflammation to Cell Transformation. *Cell* **2009**, *139*, 693–706. [[CrossRef](#)] [[PubMed](#)]
84. Sullivan, N.; Sasser, A.K.; Axel, E.A.; Vesuna, F.; Raman, V.; Ramirez, N.C.; Oberyzyzn, T.M.; Hall, B.M. Interleukin-6 induces an epithelial–mesenchymal transition phenotype in human breast cancer cells. *Oncogene* **2009**, *28*, 2940–2947. [[CrossRef](#)]
85. Mani, S.A.; Guo, W.; Liao, M.J.; Eaton, E.N.; Ayyanan, A.; Zhou, A.Y.; Brooks, M.; Reinhard, F.; Zhang, C.C.; Shipitsin, M.; et al. The Epithelial–Mesenchymal Transition Generates Cells with Properties of Stem Cells. *Cell* **2008**, *133*, 704–715. [[CrossRef](#)]
86. Zheng, R.; Chen, G.; Li, X.; Wei, X.; Liu, C.; Derwahl, M. Effect of IL-6 on proliferation of human thyroid anaplastic cancer stem cells. *Int. J. Clin. Exp. Pathol.* **2019**, *12*, 3992–4001. [[PubMed](#)]
87. Korkaya, H.; Kim, G.-I.; Davis, A.; Malik, F.; Henry, N.L.; Ithimakin, S.; Quraishi, A.A.; Tawakkol, N.; D'Angelo, R.; Paulson, A.K.; et al. Activation of an IL6 Inflammatory Loop Mediates Trastuzumab Resistance in HER2+ Breast Cancer by Expanding the Cancer Stem Cell Population. *Mol. Cell* **2012**, *47*, 570–584. [[CrossRef](#)]
88. Iliopoulos, D.; Hirsch, H.A.; Wang, G.; Struhl, K. Inducible formation of breast cancer stem cells and their dynamic equilibrium with non-stem cancer cells via IL6 secretion. *Proc. Natl. Acad. Sci. USA* **2011**, *108*, 1397–1402. [[CrossRef](#)]
89. Ginestier, C.; Liu, S.; Diebel, M.E.; Korkaya, H.; Luo, M.; Brown, M.; Wicinski, J.; Cabaud, O.; Charafe-Jauffret, E.; Birnbaum, D.; et al. CXCR1 blockade selectively targets human breast cancer stem cells in vitro and in xenografts. *J. Clin. Investig.* **2010**, *120*, 485–497. [[CrossRef](#)]
90. Kim, M.P.; Fleming, J.B.; Wang, H.; Abbruzzese, J.L.; Choi, W.; Kopetz, S.; McConkey, D.J.; Evans, D.B.; Gallick, G.E. ALDH Activity Selectively Defines an Enhanced Tumor-Initiating Cell Population Relative to CD133 Expression in Human Pancreatic Adenocarcinoma. *PLoS ONE* **2011**, *6*, e20636. [[CrossRef](#)]
91. Chen, L.; Fan, J.; Chen, H.; Meng, Z.; Chen, Z.; Wang, P.; Liu, L. The IL-8/CXCR1 axis is associated with cancer stem cell-like properties and correlates with clinical prognosis in human pancreatic cancer cases. *Sci. Rep.* **2014**, *4*, 5911. [[CrossRef](#)] [[PubMed](#)]
92. Armstrong, T.; Packham, G.; Murphy, L.B.; Bateman, A.C.; Conti, J.A.; Fine, D.R.; Johnson, C.D.; Benyon, R.C.; Iredale, J.P. Type I Collagen Promotes the Malignant Phenotype of Pancreatic Ductal Adenocarcinoma. *Clin. Cancer Res.* **2004**, *10*, 7427–7437. [[CrossRef](#)] [[PubMed](#)]



93. Yin, H.; Tang, Y.; Guo, Y.; Wen, S. Immune Microenvironment of Thyroid Cancer. *J. Cancer* **2020**, *11*, 4884–4896. [[CrossRef](#)] [[PubMed](#)]
94. Lenos, K.J.; Miedema, D.M.; Lodestijn, S.C.; Nijman, L.E.; Bosch, T.V.D.; Ros, X.R.; Lourenço, F.C.; Lecca, M.C.; Van Der Heijden, M.; Van Neerven, S.M.; et al. Stem cell functionality is microenvironmentally defined during tumour expansion and therapy response in colon cancer. *Nat. Cell Biol.* **2018**, *20*, 1193–1202. [[CrossRef](#)]
95. Ferreira, L.B.; Tavares, C.; Pestana, A.; Pereira, C.L.; Eloy, C.; Pinto, M.T.; Castro, P.; Batista, R.; Rios, E.; Sobrinho-Simões, M.; et al. Osteopontin-a splice variant is overexpressed in papillary thyroid carcinoma and modulates invasive behavior. *Oncotarget* **2016**, *7*, 52003–52016. [[CrossRef](#)] [[PubMed](#)]
96. Guarino, V.; Faviana, P.; Salvatore, G.; Castellone, M.D.; Cirafici, A.M.; De Falco, V.; Celetti, A.; Giannini, R.; Basolo, F.; Melillo, R.M.; et al. Osteopontin Is Overexpressed in Human Papillary Thyroid Carcinomas and Enhances Thyroid Carcinoma Cell Invasiveness. *J. Clin. Endocrinol. Metab.* **2005**, *90*, 5270–5278. [[CrossRef](#)] [[PubMed](#)]
97. Sun, W.; Xu, Y.; Zhao, C.; Hao, F.; Chen, N.; Guan, J.; Zhang, K. Targeting TGF- $\beta$ 1 suppresses survival of and invasion by anaplastic thyroid carcinoma cells. *Am. J. Transl. Res.* **2017**, *9*, 1418–1425.
98. Coperchini, F.; Pignatti, P.; Leporati, P.; Carbone, A.; Croce, L.; Magri, F.; Chiovato, L.; Rotondi, M. Normal human thyroid cells, BCPAP, and TPC-1 thyroid tumor cell lines display different profile in both basal and TNF- $\alpha$ -induced CXCL8 secretion. *Endocrine* **2015**, *54*, 123–128. [[CrossRef](#)]
99. Coperchini, F.; Pignatti, P.; Carbone, A.; Bongianino, R.; Di Buduo, C.A.; Leporati, P.; Croce, L.; Magri, F.; Balduini, A.; Chiovato, L.; et al. TNF- $\alpha$  increases the membrane expression of the chemokine receptor CCR6 in thyroid tumor cells, but not in normal thyrocytes: Potential role in the metastatic spread of thyroid cancer. *Tumor Biol.* **2015**, *37*, 5569–5575. [[CrossRef](#)]
100. Tarabichi, M.; Antoniou, A.; Le Pennec, S.; Gacquer, D.; Aubain, N.D.S.; Craciun, L.; Cielen, T.; Laios, I.; Larsimont, D.; Andry, G.; et al. Distinctive Desmoplastic 3D Morphology Associated With BRAFV600E in Papillary Thyroid Cancers. *J. Clin. Endocrinol. Metab.* **2018**, *103*, 1102–1111. [[CrossRef](#)]
101. Koperek, O.; Asari, R.; Niederle, B.; Kaserer, K. Desmoplastic stromal reaction in papillary thyroid microcarcinoma. *Histopathology* **2011**, *58*, 919–924. [[CrossRef](#)]
102. Liotta, L.A.; Kohn, E.C. The microenvironment of the tumour–host interface. *Nat. Cell Biol.* **2001**, *411*, 375–379. [[CrossRef](#)] [[PubMed](#)]
103. Orimo, A.; Gupta, P.B.; SgROI, D.C.; Arenzana-Seisdedos, F.; Delaunay, T.; Naeem, R.; Carey, V.J.; Richardson, A.L.; Weinberg, R.A. Stromal Fibroblasts Present in Invasive Human Breast Carcinomas Promote Tumor Growth and Angiogenesis through Elevated SDF-1/CXCL12 Secretion. *Cell* **2005**, *121*, 335–348. [[CrossRef](#)] [[PubMed](#)]
104. Karnoub, A.E.; Dash, A.B.; Vo, A.P.; Sullivan, A.; Brooks, M.W.; Bell, G.W.; Richardson, A.L.; Polyak, K.; Tubo, R.; Weinberg, R.A. Mesenchymal stem cells within tumour stroma promote breast cancer metastasis. *Nat. Cell Biol.* **2007**, *449*, 557–563. [[CrossRef](#)] [[PubMed](#)]
105. Minamoto, T.; Ool, A.; Okada, Y.; Mai, M.; Nagai, Y.; Nakanishi, I. Desmoplastic reaction of gastric carcinoma: A light- and electron-microscopic immunohistochemical analysis using collagen type-specific antibodies. *Hum. Pathol.* **1988**, *19*, 815–821. [[CrossRef](#)]
106. Isella, C.; Terrasi, A.; Bellomo, S.E.; Petti, C.; Galatola, G.; Muratore, A.; Mellano, A.; Senetta, R.; Cassenti, A.; Sonetto, C.; et al. Stromal contribution to the colorectal cancer transcriptome. *Nat. Genet.* **2015**, *47*, 312–319. [[CrossRef](#)] [[PubMed](#)]
107. Kalluri, R. The biology and function of fibroblasts in cancer. *Nat. Rev. Cancer* **2016**, *16*, 582–598. [[CrossRef](#)] [[PubMed](#)]
108. Erez, N.; Truitt, M.; Olson, P.; Hanahan, D. Cancer-Associated Fibroblasts Are Activated in Incipient Neoplasia to Orchestrate Tumor-Promoting Inflammation in an NF- $\kappa$ B-Dependent Manner. *Cancer Cell* **2010**, *17*, 135–147. [[CrossRef](#)] [[PubMed](#)]
109. Hanahan, D.; Weinberg, R.A. The Hallmarks of Cancer. *Cell* **2000**, *100*, 57–70. [[CrossRef](#)]
110. McAllister, S.S.; Weinberg, R.A. Tumor-Host Interactions: A Far-Reaching Relationship. *J. Clin. Oncol.* **2010**, *28*, 4022–4028. [[CrossRef](#)]
111. Yamaguchi, H.; Yoshida, N.; Takanashi, M.; Ito, Y.; Fukami, K.; Yanagihara, K.; Yashiro, M.; Sakai, R. Stromal Fibroblasts Mediate Extracellular Matrix Remodeling and Invasion of Scirrhus Gastric Carcinoma Cells. *PLoS ONE* **2014**, *9*, e85485. [[CrossRef](#)]
112. Karagiannis, G.S.; Poutahidis, T.; Erdman, S.E.; Kirsch, R.; Riddell, R.H.; Diamandis, E.P. Cancer-Associated Fibroblasts Drive the Progression of Metastasis through both Paracrine and Mechanical Pressure on Cancer Tissue. *Mol. Cancer Res.* **2012**, *10*, 1403–1418. [[CrossRef](#)]
113. Loeffler, M.; Krüger, J.A.; Niethammer, A.G.; Reisfeld, R.A. Targeting tumor-associated fibroblasts improves cancer chemotherapy by increasing intratumoral drug uptake. *J. Clin. Investig.* **2006**, *116*, 1955–1962. [[CrossRef](#)] [[PubMed](#)]
114. Zou, X.; Feng, B.; Dong, T.; Yan, G.; Tan, B.; Shen, H.; Huang, A.; Zhang, X.; Zhang, M.; Yang, P.; et al. Up-regulation of type I collagen during tumorigenesis of colorectal cancer revealed by quantitative proteomic analysis. *J. Proteom.* **2013**, *94*, 473–485. [[CrossRef](#)] [[PubMed](#)]
115. Kauppila, S.; Stenbäck, F.; Risteli, J.; Jukkola, A.; Risteli, L. Aberrant type I and type III collagen gene expression in human breast cancer in vivo. *J. Pathol.* **1998**, *186*, 262–268. [[CrossRef](#)]
116. Ramaswamy, S.; Ross, K.N.; Lander, E.S.; Golub, T.R. A molecular signature of metastasis in primary solid tumors. *Nat. Genet.* **2003**, *33*, 49–54. [[CrossRef](#)] [[PubMed](#)]

117. Jolly, L.A.; Novitskiy, S.; Owens, P.; Massoll, N.; Cheng, N.; Fang, W.; Moses, H.L.; Franco, A.T. Fibroblast-Mediated Collagen Remodeling Within the Tumor Microenvironment Facilitates Progression of Thyroid Cancers Driven by BrafV600E and Pten Loss. *Cancer Res.* **2016**, *76*, 1804–1813. [[CrossRef](#)] [[PubMed](#)]
118. Spill, F.; Reynolds, D.S.; Kamm, R.D.; Zaman, M.H. Impact of the physical microenvironment on tumor progression and metastasis. *Curr. Opin. Biotechnol.* **2016**, *40*, 41–48. [[CrossRef](#)]
119. Johansson, E.; Grassi, E.S.; Pantazopoulou, V.; Tong, B.; Lindgren, D.; Berg, T.J.; Pietras, E.J.; Axelson, H.; Pietras, A. CD44 Interacts with HIF-2 $\alpha$  to Modulate the Hypoxic Phenotype of Perinecrotic and Perivascular Glioma Cells. *Cell Rep.* **2017**, *20*, 1641–1653. [[CrossRef](#)]
120. Hynes, R.O. The extracellular matrix: Not just pretty fibrils. *Science* **2009**, *326*, 1216–1219. [[CrossRef](#)]
121. Bigoni-Ordóñez, G.D.; Czarnowski, D.; Parsons, T.; Madlambayan, G.J.; Villa-Diaz, L.G. Integrin  $\alpha 6$  (CD49f), The Microenvironment and Cancer Stem Cells. *Curr. Stem Cell Res. Ther.* **2019**, *14*, 428–436. [[CrossRef](#)]
122. Bierie, B.; Pierce, S.E.; Kroeger, C.; Stover, D.G.; Pattabiraman, D.R.; Thiru, P.; Donaher, J.L.; Reinhardt, F.; Chaffer, C.L.; Keckesova, Z.; et al. Integrin- $\beta 4$  identifies cancer stem cell-enriched populations of partially mesenchymal carcinoma cells. *Proc. Natl. Acad. Sci. USA* **2017**, *114*, E2337–E2346. [[CrossRef](#)] [[PubMed](#)]
123. Moon, J.H.; Rho, Y.S.; Lee, S.H.; Koo, B.S.; Lee, H.J.; Do, S.I.; Cho, J.H.; Eun, Y.G.; Park, M.W.; Shin, H.A.; et al. Role of integrin  $\beta 1$  as a biomarker of stemness in head and neck squamous cell carcinoma. *Oral Oncol.* **2019**, *96*, 34–41. [[CrossRef](#)] [[PubMed](#)]
124. Korkaya, H.; Liu, S.; Wicha, M.S. Breast cancer stem cells, cytokine networks, and the tumor microenvironment. *J. Clin. Investig.* **2011**, *121*, 3804–3809. [[CrossRef](#)] [[PubMed](#)]
125. Lonardo, E.; Hermann, P.C.; Mueller, M.-T.; Huber, S.; Balic, A.; Miranda-Lorenzo, I.; Zagorac, S.; Alcalá, S.; Rodriguez-Arabaolaza, I.; Ramirez, J.C.; et al. Nodal/Activin Signaling Drives Self-Renewal and Tumorigenicity of Pancreatic Cancer Stem Cells and Provides a Target for Combined Drug Therapy. *Cell Stem Cell* **2011**, *9*, 433–446. [[CrossRef](#)] [[PubMed](#)]
126. Shi, Y.; Gao, W.; Lytle, N.K.; Huang, P.; Yuan, X.; Dann, A.M.; Ridinger-Saison, M.; DelGiorno, K.E.; Antal, C.E.; Liang, G.; et al. Targeting LIF-mediated paracrine interaction for pancreatic cancer therapy and monitoring. *Nat. Cell Biol.* **2019**, *569*, 131–135. [[CrossRef](#)]
127. Lotti, F.; Jarrar, A.M.; Pai, R.K.; Hitomi, M.; Lathia, J.; Mace, A.; Gantt, G.A.; Sukhdeo, K.; DeVecchio, J.; Vasanji, A.; et al. Chemotherapy activates cancer-associated fibroblasts to maintain colorectal cancer-initiating cells by IL-17A. *J. Exp. Med.* **2013**, *210*, 2851–2872. [[CrossRef](#)]
128. Cazet, A.S.; Hui, M.N.; Elsworth, B.L.; Wu, S.Z.; Roden, D.; Chan, C.-L.; Skhinas, J.N.; Collot, R.; Yang, J.; Harvey, K.; et al. Targeting stromal remodeling and cancer stem cell plasticity overcomes chemoresistance in triple negative breast cancer. *Nat. Commun.* **2018**, *9*, 3992. [[CrossRef](#)]
129. Chan, T.-S.; Hsu, C.-C.; Pai, V.C.; Liao, W.-Y.; Huang, S.-S.; Tan, K.-I.; Yen, C.-J.; Hsu, S.-C.; Chen, W.-Y.; Shan, Y.-S.; et al. Metronomic chemotherapy prevents therapy-induced stromal activation and induction of tumor-initiating cells. *J. Exp. Med.* **2016**, *213*, 2967–2988. [[CrossRef](#)]
130. Ferrari, S.M.; Fallahi, P.; Galdiero, M.R.; Ruffilli, I.; Elia, G.; Ragusa, F.; Paparo, S.R.; Patrizio, A.; Mazzi, V.; Varricchi, G.; et al. Immune and Inflammatory Cells in Thyroid Cancer Microenvironment. *Int. J. Mol. Sci.* **2019**, *20*, 4413. [[CrossRef](#)]
131. Nucera, C.; Porrello, A.; Antonello, Z.A.; Mekel, M.; Nehs, M.A.; Giordano, T.J.; Gerald, D.; Benjamin, L.E.; Priolo, C.; Puxeddu, E.; et al. B-RafV600E and thrombospondin-1 promote thyroid cancer progression. *Proc. Natl. Acad. Sci. USA* **2010**, *107*, 10649–10654. [[CrossRef](#)] [[PubMed](#)]
132. Nucera, C.; Lawler, J.; Parangi, S. BRAFV600E and Microenvironment in Thyroid Cancer: A Functional Link to Drive Cancer Progression. *Cancer Res.* **2011**, *71*, 2417–2422. [[CrossRef](#)] [[PubMed](#)]
133. Fozzatti, L.; Alaminio, V.A.; Park, S.; Giusiano, L.; Volpini, X.; Zhao, L.; Stempin, C.C.; Donadio, A.C.; Cheng, S.-Y.; Pellizas, C.G. Interplay of fibroblasts with anaplastic tumor cells promotes follicular thyroid cancer progression. *Sci. Rep.* **2019**, *9*, 8028. [[CrossRef](#)] [[PubMed](#)]
134. Schito, L.; Semenza, G.L. Hypoxia-Inducible Factors: Master Regulators of Cancer Progression. *Trends Cancer* **2016**, *2*, 758–770. [[CrossRef](#)]
135. Semenza, G.L. Hypoxia-Inducible Factors in Physiology and Medicine. *Cell* **2012**, *148*, 399–408. [[CrossRef](#)]
136. Horsman, M.R.; Overgaard, J. The impact of hypoxia and its modification of the outcome of radiotherapy. *J. Radiat. Res.* **2016**, *57*, i90–i98. [[CrossRef](#)]
137. O'Reilly, D.; Johnson, P.; Buchanan, P.J. Hypoxia induced cancer stem cell enrichment promotes resistance to androgen deprivation therapy in prostate cancer. *Steroids* **2019**, *152*, 108497. [[CrossRef](#)]
138. Sun, X.; Lv, X.; Yan, Y.; Zhao, Y.; Ma, R.; He, M.; Wei, M. Hypoxia-mediated cancer stem cell resistance and targeted therapy. *Biomed. Pharmacother.* **2020**, *130*, 110623. [[CrossRef](#)]
139. D'Ignazio, L.; Batie, M.; Rocha, S. Hypoxia and Inflammation in Cancer, Focus on HIF and NF- $\kappa$ B. *Biomedicines* **2017**, *5*, 21. [[CrossRef](#)]
140. VanDyke, K.; Zeissig, M.; Hewett, D.R.; Martin, S.K.; Mrozik, K.M.; Cheong, C.M.; Diamond, P.; To, L.B.; Gronthos, S.; Peet, D.J.; et al. HIF-2 $\alpha$  Promotes Dissemination of Plasma Cells in Multiple Myeloma by Regulating CXCL12/CXCR4 and CCR1. *Cancer Res.* **2017**, *77*, 5452–5463. [[CrossRef](#)]
141. Ma, X.; Zhang, H.; Xue, X.; Shah, Y.M. Hypoxia-inducible factor 2 $\alpha$  (HIF-2 $\alpha$ ) promotes colon cancer growth by potentiating Yes-associated protein 1 (YAP1) activity. *J. Biol. Chem.* **2017**, *292*, 17046–17056. [[CrossRef](#)]

142. Garziera, M.; Scarabel, L.; Toffoli, G. Hypoxic Modulation of HLA-G Expression through the Metabolic Sensor HIF-1 in Human Cancer Cells. *J. Immunol. Res.* **2017**, *2017*, 4587520. [[CrossRef](#)]
143. Mohlin, S.; Wigerup, C.; Jögi, A.; Pählman, S. Hypoxia, pseudohypoxia and cellular differentiation. *Exp. Cell Res.* **2017**, *356*, 192–196. [[CrossRef](#)]
144. Shi, Q.Y.; Zhang, S.J.; Liu, L.; Chen, Q.S.; Yu, L.N.; Yan, M. Sevoflurane promotes the expansion of glioma stem cells through activation of hypoxia-inducible factors in vitro. *Br. J. Anaesth.* **2015**, *114*, 825–830. [[CrossRef](#)]
145. Grassi, E.S.; Pantazopoulou, V.; Pietras, A. Hypoxia-induced release, nuclear translocation, and signaling activity of a DLK1 intracellular fragment in glioma. *Oncogene* **2020**, *39*, 4028–4044. [[CrossRef](#)] [[PubMed](#)]
146. Badowska-Kozakiewicz, A.M.; Sobol, M.; Patera, J. Expression of multidrug resistance protein P-glycoprotein in correlation with markers of hypoxia (HIF-1 $\alpha$ , EPO, EPO-R) in invasive breast cancer with metastasis to lymph nodes. *Arch. Med. Sci.* **2017**, *6*, 1303–1314. [[CrossRef](#)]
147. Rodríguez, M.E.; Catrinacio, C.; Ropolo, A.; Rivarola, V.A.; Vaccaro, M.I. A novel HIF-1 $\alpha$ /VMP1-autophagic pathway induces resistance to photodynamic therapy in colon cancer cells. *Photochem. Photobiol. Sci.* **2017**, *16*, 1631–1642. [[CrossRef](#)] [[PubMed](#)]
148. Zhang, Q.; Lou, Y.; Zhang, J.; Fu, Q.; Wei, T.; Sun, X.; Chen, Q.; Yang, J.; Bai, X.; Liang, T. Hypoxia-inducible factor-2 $\alpha$  promotes tumor progression and has crosstalk with Wnt/ $\beta$ -catenin signaling in pancreatic cancer. *Mol. Cancer* **2017**, *16*, 119. [[CrossRef](#)] [[PubMed](#)]
149. Jun, J.C.; Rathore, A.; Younas, H.; Gilkes, D.; Polotsky, V.Y. Hypoxia-Inducible Factors and Cancer. *Curr. Sleep Med. Rep.* **2017**, *3*, 1–10. [[CrossRef](#)] [[PubMed](#)]
150. Sun, J.C.; He, F.; Yi, W.; Wan, M.H.; Li, R.; Wei, X.; Wu, R.; Niu, D.L. High expression of HIF-2 $\alpha$  and its anti-radiotherapy effect in lung cancer stem cells. *Genet. Mol. Res.* **2015**, *14*, 18110–18120. [[CrossRef](#)]
151. Santoyo-Ramos, P.; Likhatcheva, M.; García-Zepeda, E.A.; Castañeda-Patlán, M.C.; Robles-Flores, M. Hypoxia-Inducible Factors Modulate the Stemness and Malignancy of Colon Cancer Cells by Playing Opposite Roles in Canonical Wnt Signaling. *PLoS ONE* **2014**, *9*, e112580. [[CrossRef](#)]
152. Yan, Y.; Liu, F.; Han, L.; Zhao, L.; Chen, J.; Olopade, I.O.; He, M.; Wei, M. HIF-2 $\alpha$  promotes conversion to a stem cell phenotype and induces chemoresistance in breast cancer cells by activating Wnt and Notch pathways. *J. Exp. Clin. Cancer Res.* **2018**, *37*, 256. [[CrossRef](#)] [[PubMed](#)]
153. Taccaliti, A.; Silvetti, F.; Palmonella, G.; Boscaro, M. Anaplastic Thyroid Carcinoma. *Front. Endocrinol.* **2012**, *3*, 84. [[CrossRef](#)]
154. Bárdos, J.I.; Ashcroft, M. Negative and positive regulation of HIF-1: A complex network. *Biochim. Biophys. Acta* **2005**, *1755*, 107–120. [[CrossRef](#)] [[PubMed](#)]
155. Burrows, N.; Resch, J.; Cowen, R.L.; Von Wasielewski, R.; Hoang-Vu, C.; West, C.M.; Williams, K.J.; Brabant, G. Expression of hypoxia-inducible factor 1 $\alpha$  in thyroid carcinomas. *Endocrine-Related Cancer* **2010**, *17*, 61–72. [[CrossRef](#)] [[PubMed](#)]
156. Garcia, A.J. HIFing the Brakes: Therapeutic Opportunities for Treatment of Human Malignancies. *Sci. Signal.* **2006**, *2006*, pe25. [[CrossRef](#)]
157. Paes, J.E.; Ringel, M.D. Dysregulation of the Phosphatidylinositol 3-Kinase Pathway in Thyroid Neoplasia. *Endocrinol. Metab. Clin. N. Am.* **2008**, *37*, 375–387. [[CrossRef](#)]
158. Kalthori, V.; Kemppainen, K.; Asghar, M.Y.; Bergelin, N.; Jaakkola, P.; Törnquist, K. Sphingosine-1-Phosphate as a Regulator of Hypoxia-Induced Factor-1 $\alpha$  in Thyroid Follicular Carcinoma Cells. *PLoS ONE* **2013**, *8*, e66189. [[CrossRef](#)]
159. Burrows, N.; Babur, M.; Resch, J.; Ridsdale, S.; Mejin, M.; Rowling, E.J.; Brabant, G.; Williams, K.J. GDC-0941 Inhibits Metastatic Characteristics of Thyroid Carcinomas by Targeting both the Phosphoinositide-3 Kinase (PI3K) and Hypoxia-Inducible Factor-1 $\alpha$  (HIF-1 $\alpha$ ) Pathways. *J. Clin. Endocrinol. Metab.* **2011**, *96*, E1934–E1943. [[CrossRef](#)]
160. Yasuda, M.; Ogane, N.; Hayashi, H.; Kameda, Y.; Miyagi, Y.; Iida, T.; Mori, Y.; Tsukinoki, K.; Minematsu, T.; Osamura, Y. Glucose transporter-1 expression in the thyroid gland: Clinicopathological significance for papillary carcinoma. *Oncol. Rep.* **2005**, *14*, 1499–1504. [[CrossRef](#)]
161. Tuttle, R.M.; Fleisher, M.; Francis, G.L.; Robbins, R.J. Serum Vascular Endothelial Growth Factor Levels Are Elevated in Metastatic Differentiated Thyroid Cancer but Not Increased by Short-Term TSH Stimulation. *J. Clin. Endocrinol. Metab.* **2002**, *87*, 1737–1742. [[CrossRef](#)]
162. Schönberger, J.; Rüschoff, J.; Grimm, D.; Marienhagen, J.; Rümmele, P.; Meyringer, R.; Kossmehl, P.; Hofstaedter, F.; Eilles, C. Glucose Transporter 1 Gene Expression is Related to Thyroid Neoplasms with an Unfavorable Prognosis: An Immunohistochemical Study. *Thyroid* **2002**, *12*, 747–754. [[CrossRef](#)]
163. Kim, Y.W.; Do, I.G.; Park, Y.-K. Expression of the GLUT1 glucose transporter, p63 and p53 in thyroid carcinomas. *Pathol. Res. Pr.* **2006**, *202*, 759–765. [[CrossRef](#)]
164. Poulaki, V.; Mitsiades, C.S.; McMullan, C.; Sykoutri, D.; Fanourakis, G.; Kotoula, V.; Tseleni-Balafouta, S.; Koutras, D.A.; Mitsiades, N. Regulation of Vascular Endothelial Growth Factor Expression by Insulin-Like Growth Factor I in Thyroid Carcinomas. *J. Clin. Endocrinol. Metab.* **2003**, *88*, 5392–5398. [[CrossRef](#)]
165. Chiche, J.; Ilc, K.; Laferrrière, J.; Trottier, E.; Dayan, F.; Mazure, N.M.; Brahimi-Horn, M.C.; Pouysségur, J. Hypoxia-Inducible Carbonic Anhydrase IX and XII Promote Tumor Cell Growth by Counteracting Acidosis through the Regulation of the Intracellular pH. *Cancer Res.* **2009**, *69*, 358–368. [[CrossRef](#)]
166. Dunn, G.P.; Bruce, A.T.; Ikeda, H.; Old, L.J.; Schreiber, R.D. Cancer immunoeediting: From immunosurveillance to tumor escape. *Nat. Immunol.* **2002**, *3*, 991–998. [[CrossRef](#)]



167. Wang, Z.; Liu, W.; Wang, C.; Li, Y.; Ai, Z. Acetylcholine promotes the self-renewal and immune escape of CD133+ thyroid cancer cells through activation of CD133-Akt pathway. *Cancer Lett.* **2020**, *471*, 116–124. [\[CrossRef\]](#)
168. Ospina-Muñoz, N.; Vernot, J.-P. Partial acquisition of stemness properties in tumorspheres obtained from interleukin-8-treated MCF-7 cells. *Tumor Biol.* **2020**, *42*. [\[CrossRef\]](#)
169. Pallasch, F.B.; Schumacher, U. Angiotensin Inhibition, TGF- $\beta$  and EMT in Cancer. *Cancers* **2020**, *12*, 2785. [\[CrossRef\]](#)
170. Angell, T.E.; Lechner, M.G.; Jang, J.K.; Lopresti, J.S.; Epstein, A.L. MHC Class I Loss Is a Frequent Mechanism of Immune Escape in Papillary Thyroid Cancer That Is Reversed by Interferon and Selumetinib Treatment In Vitro. *Clin. Cancer Res.* **2014**, *20*, 6034–6044. [\[CrossRef\]](#)
171. Cunha, L.L.; Marcello, M.A.; Morari, E.C.; Nonogaki, S.; Conte, F.F.; Gerhard, R.; Soares, F.A.; Vassallo, J.; Ward, L.S. Differentiated thyroid carcinomas may elude the immune system by B7H1 upregulation. *Endocrine-Related Cancer* **2012**, *20*, 103–110. [\[CrossRef\]](#)
172. Wei, J.; Wu, A.; Kong, L.-Y.; Wang, Y.; Fuller, G.; Fokt, I.; Melillo, G.; Priebe, W.; Heimberger, A.B. Hypoxia Potentiates Glioma-Mediated Immunosuppression. *PLoS ONE* **2011**, *6*, e16195. [\[CrossRef\]](#) [\[PubMed\]](#)
173. Betts, G.; Jones, E.; Junaid, S.; El-Shanawany, T.; Scurr, M.; Mizen, P.; Kumar, M.; Jones, S.; Rees, B.; Williams, G.; et al. Suppression of tumour-specific CD4+T cells by regulatory T cells is associated with progression of human colorectal cancer. *Gut* **2011**, *61*, 1163–1171. [\[CrossRef\]](#) [\[PubMed\]](#)
174. Curiel, T.J.; Coukos, G.; Zou, L.; Alvarez, X.; Cheng, P.; Mottram, P.; Evdemon-Hogan, M.; Conejo-Garcia, J.R.; Zhang, L.; Burow, M.; et al. Specific recruitment of regulatory T cells in ovarian carcinoma fosters immune privilege and predicts reduced survival. *Nat. Med.* **2004**, *10*, 942–949. [\[CrossRef\]](#) [\[PubMed\]](#)
175. French, J.D.; Weber, Z.J.; Fretwell, D.L.; Said, S.; Klopper, J.P.; Haugen, B.R. Tumor-Associated Lymphocytes and Increased FoxP3+ Regulatory T Cell Frequency Correlate with More Aggressive Papillary Thyroid Cancer. *J. Clin. Endocrinol. Metab.* **2010**, *95*, 2325–2333. [\[CrossRef\]](#) [\[PubMed\]](#)
176. Trapani, J.A.; Smyth, M.J. Functional significance of the perforin/granzyme cell death pathway. *Nat. Rev. Immunol.* **2002**, *2*, 735–747. [\[CrossRef\]](#)
177. Vahidian, F.; Duijff, P.H.; Safarzadeh, E.; Derakhshani, A.; Baghbanzadeh, A.; Baradaran, B. Interactions between cancer stem cells, immune system and some environmental components: Friends or foes? *Immunol. Lett.* **2019**, *208*, 19–29. [\[CrossRef\]](#)
178. Piccolo, V.; Curina, A.; Genua, M.; Ghisletti, S.; Simonatto, S.G.M.; Sabò, A.; Amati, A.S.B.; Ostuni, M.G.R.; Natoli, V.P.A.C.B.A.G. Opposing macrophage polarization programs show extensive epigenomic and transcriptional cross-talk. *Nat. Immunol.* **2017**, *18*, 530–540. [\[CrossRef\]](#)
179. Kim, M.J.; Sun, H.J.; Song, Y.S.; Yoo, S.-K.; Kim, A.Y.; Seo, J.-S.; Park, Y.J.; Cho, S.W. CXCL16 positively correlated with M2-macrophage infiltration, enhanced angiogenesis, and poor prognosis in thyroid cancer. *Sci. Rep.* **2019**, *9*, 13288. [\[CrossRef\]](#)
180. Jung, K.Y.; Cho, S.W.; Kim, A.Y.; Kim, D.; Oh, B.-C.; Park, D.J.; Park, Y.J. Cancers with Higher Density of Tumor-Associated Macrophages Were Associated with Poor Survival Rates. *J. Pathol. Transl. Med.* **2015**, *49*, 318–324. [\[CrossRef\]](#)
181. Ryder, M.; Ghossein, R.A.; Ricarte-Filho, J.C.M.; Knauf, J.A.; Fagin, J.A. Increased density of tumor-associated macrophages is associated with decreased survival in advanced thyroid cancer. *Endocrine-Related Cancer* **2008**, *15*, 1069–1074. [\[CrossRef\]](#)
182. Kim, S.; Cho, S.W.; Min, H.S.; Kim, K.M.; Yeom, G.J.; Kim, E.Y.; Lee, K.E.; Yun, Y.G.; Park, D.J.; Park, Y.J. The Expression of Tumor-Associated Macrophages in Papillary Thyroid Carcinoma. *Endocrinol. Metab.* **2013**, *28*, 192–198. [\[CrossRef\]](#)
183. Fang, W.; Ye, L.; Shen, L.; Cai, J.; Huang, F.; Wei, Q.; Fei, X.; Chen, X.; Guan, H.; Wang, W.; et al. Tumor-associated macrophages promote the metastatic potential of thyroid papillary cancer by releasing CXCL8. *Carcinog.* **2014**, *35*, 1780–1787. [\[CrossRef\]](#)
184. Hardin, H.; Guo, Z.; Shan, W.; Montemayor-Garcia, C.; Asioli, S.; Yu, X.-M.; Harrison, A.D.; Chen, H.; Lloyd, R.V. The Roles of the Epithelial-Mesenchymal Transition Marker PRRX1 and miR-146b-5p in Papillary Thyroid Carcinoma Progression. *Am. J. Pathol.* **2014**, *184*, 2342–2354. [\[CrossRef\]](#)
185. Ruffini, P.A. The CXCL8-CXCR1/2 Axis as a Therapeutic Target in Breast Cancer Stem-Like Cells. *Front. Oncol.* **2019**, *9*, 40. [\[CrossRef\]](#)
186. Doyle, L.M.; Wang, M.Z. Overview of Extracellular Vesicles, Their Origin, Composition, Purpose, and Methods for Exosome Isolation and Analysis. *Cells* **2019**, *8*, 727. [\[CrossRef\]](#)
187. Wortzel, I.; Dror, S.; Kenific, C.M.; Lyden, D. Exosome-Mediated Metastasis: Communication from a Distance. *Dev. Cell* **2019**, *49*, 347–360. [\[CrossRef\]](#)
188. Tai, Y.-L.; Chu, P.-Y.; Lee, B.-H.; Chen, K.-C.; Yang, C.-Y.; Kuo, W.-H.; Shen, T.-L. Basics and applications of tumor-derived extracellular vesicles. *J. Biomed. Sci.* **2019**, *26*, 35. [\[CrossRef\]](#)
189. Dai, W.; Jin, X.; Han, L.; Huang, H.; Ji, Z.; Xu, X.; Tang, M.; Jiang, B.; Chen, W. Exosomal lncRNA DOCK9-AS2 derived from cancer stem cell-like cells activated Wnt/ $\beta$ -catenin pathway to aggravate stemness, proliferation, migration, and invasion in papillary thyroid carcinoma. *Cell Death Dis.* **2020**, *11*, 743. [\[CrossRef\]](#)
190. Luo, D.; Zhan, S.; Xia, W.; Huang, L.; Ge, W.; Wang, T. Proteomics study of serum exosomes from papillary thyroid cancer patients. *Endocrine-Related Cancer* **2018**, *25*, 879–891. [\[CrossRef\]](#)
191. Boufraquech, M.; Zhang, L.; Jain, M.; Patel, D.; Ellis, R.; Xiong, Y.; He, M.; Nilubol, N.; Merino, M.J.; Kebebew, E. miR-145 suppresses thyroid cancer growth and metastasis and targets AKT3. *Endocrine-Related Cancer* **2014**, *21*, 517–531. [\[CrossRef\]](#)
192. Wu, F.; Li, F.; Lin, X.; Xu, F.; Cui, R.-R.; Zhong, J.-Y.; Zhu, T.; Shan, S.-K.; Liao, X.-B.; Yuan, L.-Q.; et al. Exosomes increased angiogenesis in papillary thyroid cancer microenvironment. *Endocrine-Related Cancer* **2019**, *26*, 525–538. [\[CrossRef\]](#) [\[PubMed\]](#)



193. Baig, M.S.; Roy, A.; Rajpoot, S.; Liu, D.; Savai, R.; Banerjee, S.; Kawada, M.; Faisal, S.M.; Saluja, R.; Saqib, U.; et al. Tumor-derived exosomes in the regulation of macrophage polarization. *Inflamm. Res.* **2020**, *69*, 435–451. [[CrossRef](#)]
194. Huyan, T.; Du, Y.; Huang, Q.; Huang, Q.; Li, Q. Uptake Characterization of Tumor Cell-derived Exosomes by Natural Killer Cells. *Iran. J. Public Health* **2018**, *47*, 803–813.
195. Hedlund, M.; Nagaeva, O.; Kargl, D.; Baranov, V.; Mincheva-Nilsson, L. Thermal- and Oxidative Stress Causes Enhanced Release of NKG2D Ligand-Bearing Immunosuppressive Exosomes in Leukemia/Lymphoma T and B Cells. *PLoS ONE* **2011**, *6*, e16899. [[CrossRef](#)]
196. Bavisotto, C.C.; Cipolla, C.; Graceffa, G.; Barone, R.; Bucchieri, F.; Bulone, D.; Cabibi, D.; Campanella, C.; Gammazza, A.M.; Pitruzzella, A.; et al. Immunomorphological Pattern of Molecular Chaperones in Normal and Pathological Thyroid Tissues and Circulating Exosomes: Potential Use in Clinics. *Int. J. Mol. Sci.* **2019**, *20*, 4496. [[CrossRef](#)]
197. Farias, V.D.A.; O'Valle, F.; Serrano-Saenz, S.; Anderson, P.; Andrés, E.; López-Peñalver, J.; Tovar, I.; Nieto, A.; Santos, A.; Martín, F.; et al. Exosomes derived from mesenchymal stem cells enhance radiotherapy-induced cell death in tumor and metastatic tumor foci. *Mol. Cancer* **2018**, *17*, 122. [[CrossRef](#)]
198. Kalluri, R.; LeBleu, V.S. The biology, function, and biomedical applications of exosomes. *Science* **2020**, *367*, eaau6977. [[CrossRef](#)]
199. Andreucci, E.; Peppicelli, S.; Ruzzolini, J.; Bianchini, F.; Biagioni, A.; Papucci, L.; Magnelli, L.; Mazzanti, B.; Stecca, B.; Calorini, L. The acidic tumor microenvironment drives a stem-like phenotype in melanoma cells. *J. Mol. Med.* **2020**, *98*, 1431–1446. [[CrossRef](#)]
200. Bommarito, A.; Richiusa, P.; Carissimi, E.; Pizzolanti, G.; Rodolico, V.; Zito, G.; Criscimanna, A.; Di Blasi, F.; Pitrone, M.; Zerilli, M.; et al. BRAFV600E mutation, TIMP-1 upregulation, and NF- $\kappa$ B activation: Closing the loop on the papillary thyroid cancer trilogy. *Endocrine-Related Cancer* **2011**, *18*, 669–685. [[CrossRef](#)]
201. Ilie, M.I.; Lassalle, S.; Long-Mira, E.; Hofman, V.; Zangari, J.; Bénaim, G.; Bozec, A.; Guevara, N.; Haudebourg, J.; Birtwisle-Peyrottes, I.; et al. In papillary thyroid carcinoma, TIMP-1 expression correlates with BRAF V600E mutation status and together with hypoxia-related proteins predicts aggressive behavior. *Virchows Archiv für Pathologische Anatomie und Physiologie und für Klinische Medizin* **2013**, *463*, 437–444. [[CrossRef](#)]
202. Reya, T.; Morrison, S.J.; Clarke, M.F.; Weissman, I.L. Stem cells, cancer, and cancer stem cells [Internet]. *Nature* **2001**, 105–111. [[CrossRef](#)]
203. Takebe, N.; Miele, L.; Harris, P.J.; Jeong, W.; Bando, H.; Kahn, M.G.; Yang, S.X.; Ivy, S.P. Targeting Notch, Hedgehog, and Wnt pathways in cancer stem cells: Clinical update. *Nat. Rev. Clin. Oncol.* **2015**, *12*, 445–464. [[CrossRef](#)]
204. Abe, Y.; Oda-Sato, E.; Tobiume, K.; Kawachi, K.; Taya, Y.; Okamoto, K.; Oren, M.; Tanaka, N. Hedgehog signaling overrides p53-mediated tumor suppression by activating Mdm2. *Proc. Natl. Acad. Sci. USA* **2008**, *105*, 4838–4843. [[CrossRef](#)]
205. Beverly, L.J.; Felsher, D.W.; Capobianco, A.J. Suppression of p53 by Notch in Lymphomagenesis: Implications for Initiation and Regression. *Cancer Res.* **2005**, *65*, 7159–7168. [[CrossRef](#)]
206. Riascos-Bernal, D.F.; Chinnasamy, P.; Cao, L.; Dunaway, C.M.; Valenta, T.; Basler, K.; Sibinga, N.E.S.  $\beta$ -Catenin C-terminal signals suppress p53 and are essential for artery formation. *Nat. Commun.* **2016**, *7*, 12389. [[CrossRef](#)]
207. Armesilla-Diaz, A.; Elvira, G.; Silva, A. p53 regulates the proliferation, differentiation and spontaneous transformation of mesenchymal stem cells. *Exp. Cell Res.* **2009**, *315*, 3598–3610. [[CrossRef](#)]
208. Cirello, V.; Gaudenzi, G.; Grassi, E.S.; Colombo, C.; Vicentini, L.; Ferrero, S.; Persani, L.; Vitale, G.; Fugazzola, L. Tumor and normal thyroid spheroids: From tissues to zebrafish. *Minerva Endocrinol.* **2017**, *43*, 1–10.
209. Hong, H.; Takahashi, K.; Ichisaka, T.; Aoi, T.; Kanagawa, O.; Nakagawa, M.; Okita, K.; Yamanaka, S. Suppression of induced pluripotent stem cell generation by the p53–p21 pathway. *Nat. Cell Biol.* **2009**, *460*, 1132–1135. [[CrossRef](#)]
210. Li, H.; Collado, M.; Villasante, A.; Strati, K.; Ortega, S.; Cañamero, M.; Blasco, M.A.; Serrano, M. The Ink4/Arf locus is a barrier for iPS cell reprogramming. *Nat. Cell Biol.* **2009**, *460*, 1136–1139. [[CrossRef](#)]
211. Marión, R.M.; Strati, K.; Li, H.; Murga, M.; Blanco, R.; Ortega, S.; Fernandez-Capetillo, O.; Serrano, M.; Blasco, M.A. A p53-mediated DNA damage response limits reprogramming to ensure iPS cell genomic integrity. *Nat. Cell Biol.* **2009**, *460*, 1149–1153. [[CrossRef](#)]
212. Utikal, J.; Polo, J.M.; Stadtfeld, M.; Maherali, N.; Kulalert, W.; Walsh, R.M.; Khalil, A.; Rheinwald, J.G.; Hochedlinger, K. Immortalization eliminates a roadblock during cellular reprogramming into iPS cells. *Nat. Cell Biol.* **2009**, *460*, 1145–1148. [[CrossRef](#)]
213. Wang, S.-P.; Wang, W.-L.; Chang, Y.-L.; Wu, C.-T.; Chao, Y.-C.; Kao, S.-H.; Yuan, A.; Lin, C.-W.; Yang, S.-C.; Chan, W.-K.; et al. p53 controls cancer cell invasion by inducing the MDM2-mediated degradation of Slug. *Nat. Cell Biol.* **2009**, *11*, 694–704. [[CrossRef](#)]
214. Lamouille, S.; Xu, J.; Derynck, R. Molecular mechanisms of epithelial–mesenchymal transition. *Nat. Rev. Mol. Cell Biol.* **2014**, *15*, 178–196. [[CrossRef](#)]
215. Muys, B.R.; Anastasakis, D.G.; Claypool, D.; Pongor, L.; Li, X.L.; Grammatikakis, I.; Liu, M.; Wang, X.; Prasanth, K.V.; Aladjem, M.I.; et al. The p53-induced RNA-binding protein ZMAT3 is a splicing regulator that inhibits the splicing of oncogenic CD44 variants in colorectal carcinoma. *Genes Dev.* **2021**, *35*, 102–116. [[CrossRef](#)]
216. Vousden, K.H.; Ryan, K.M. p53 and metabolism. *Nat. Rev. Cancer* **2009**, *9*, 691–700. [[CrossRef](#)]
217. Koppenol, W.H.; Bounds, P.L.; Dang, C.V. Otto Warburg's contributions to current concepts of cancer metabolism. *Nat. Rev. Cancer* **2011**, *11*, 325–337. [[CrossRef](#)]

218. Rodríguez-Rodero, S.; Fernández, A.F.; Fernandez-Morera, J.L.; Castro-Santos, P.; Bayon, G.F.; Ferrero, C.; Urdinguio, R.G.; Gonzalez-Marquez, R.; Suarez, C.; Fernández-Vega, I.; et al. DNA Methylation Signatures Identify Biologically Distinct Thyroid Cancer Subtypes. *J. Clin. Endocrinol. Metab.* **2013**, *98*, 2811–2821. [[CrossRef](#)]
219. Mancikova, V.; Buj, R.; Castelblanco, E.; Inglada-Pérez, L.; Diez, A.; De Cubas, A.A.; Curras-Freixes, M.; Maravall, F.X.; Mauricio, D.; Matias-Guiu, X.; et al. DNA methylation profiling of well-differentiated thyroid cancer uncovers markers of recurrence free survival. *Int. J. Cancer* **2013**, *135*, 598–610. [[CrossRef](#)]
220. Ellis, R.J.; Wang, Y.; Stevenson, H.S.; Boufraqueh, M.; Patel, D.; Nilubol, N.; Davis, S.; Edelman, D.C.; Merino, M.J.; He, M.; et al. Genome-Wide Methylation Patterns in Papillary Thyroid Cancer Are Distinct Based on Histological Subtype and Tumor Genotype. *J. Clin. Endocrinol. Metab.* **2014**, *99*, E329–E337. [[CrossRef](#)]
221. Rocha, A.S.; Soares, A.P.; Fonseca, E.; Cameselleiteijeiro, J.; Oliveira, M.C.; Sobrinhosimoes, M. E-cadherin loss rather than  $\beta$ -catenin alterations is a common feature of poorly differentiated thyroid carcinomas. *Histopathology* **2003**, *42*, 580–587. [[CrossRef](#)]
222. Soares, P.; Berx, G.; Van Roy, F.; Sobrinho-Simões, M. E-cadherin gene alterations are rare events in thyroid tumors. *Int. J. Cancer* **1997**, *70*, 32–38. [[CrossRef](#)]
223. Vu-Phan, D.; Koenig, R.J. Genetics and epigenetics of sporadic thyroid cancer. *Mol. Cell. Endocrinol.* **2014**, *386*, 55–66. [[CrossRef](#)] [[PubMed](#)]
224. De Moraes, R.M.; Sobrinho, A.B.; Silva, C.M.D.S.; De Oliveira, J.R.; Da Silva, I.C.R.; Nóbrega, O.D.T. The Role of the NIS (SLC5A5) Gene in Papillary Thyroid Cancer: A Systematic Review. *Int. J. Endocrinol.* **2018**, *2018*, 1–11. [[CrossRef](#)] [[PubMed](#)]
225. Wang, T.; Narayanaswamy, R.; Ren, H.; Torchilin, V.P. Combination therapy targeting both cancer stem-like cells and bulk tumor cells for improved efficacy of breast cancer treatment. *Cancer Biol. Ther.* **2016**, *17*, 698–707. [[CrossRef](#)] [[PubMed](#)]
226. Rausch, V.; Liu, L.; Kallifatidis, G.; Baumann, B.; Mattern, J.; Gladkikh, J.; Wirth, T.; Schemmer, P.; Büchler, M.W.; Zöller, M.; et al. Synergistic Activity of Sorafenib and Sulforaphane Abolishes Pancreatic Cancer Stem Cell Characteristics. *Cancer Res.* **2010**, *70*, 5004–5013. [[CrossRef](#)]
227. Kim, J.-H.; Chae, M.; Kim, W.K.; Kim, Y.-J.; Kang, H.S.; Kim, H.S.; Yoon, S. Salinomycin sensitizes cancer cells to the effects of doxorubicin and etoposide treatment by increasing DNA damage and reducing p21 protein. *Br. J. Pharmacol.* **2011**, *162*, 773–784. [[CrossRef](#)]
228. Talukdar, S.; Emdad, L.; Das, S.K.; Fisher, P.B. EGFR: An essential receptor tyrosine kinase-regulator of cancer stem cells. In *Advances in Cancer Research*; Elsevier BV: Amsterdam, The Netherlands, 2020; pp. 161–188.
229. Kharkar, P.S. Computational Approaches for the Design of (Mutant-)Selective Tyrosine Kinase Inhibitors: State-of-the-Art and Future Prospects. *Curr. Top. Med. Chem.* **2020**, *20*, 1564–1575. [[CrossRef](#)]
230. Coluccia, A.; La Regina, G.; Naccarato, V.; Nalli, M.; Orlando, V.; Biagioni, S.; De Angelis, M.L.; Baiocchi, M.; Gautier, C.; Gianni, S.; et al. Drug Design and Synthesis of First in Class PDZ1 Targeting NHERF1 Inhibitors as Anticancer Agents. *ACS Med. Chem. Lett.* **2019**, *10*, 499–503. [[CrossRef](#)]
231. Kolev, V.N.; Tam, W.F.; Wright, Q.G.; McDermott, S.P.; Vidal, C.M.; Shapiro, I.M.; Xu, Q.; Wicha, M.S.; Pachter, J.A.; Weaver, D.T. Inhibition of FAK kinase activity preferentially targets cancer stem cells. *Oncotarget* **2017**, *8*, 51733–51747. [[CrossRef](#)]
232. Vásquez-Bochm, L.X.; Velázquez-Paniagua, M.; Castro-Vázquez, S.S.; Guerrero-Rodríguez, S.L.; Mondragon-Peralta, A.; De La Fuente-Granada, M.; Pérez-Tapia, S.M.; González-Arenas, A.; Velasco-Velázquez, M.A. Transcriptome-based identification of lovastatin as a breast cancer stem cell-targeting drug. *Pharmacol. Rep.* **2019**, *71*, 535–544. [[CrossRef](#)] [[PubMed](#)]
233. Mok, E.H.K.; Lee, T.K.W. The Pivotal Role of the Dysregulation of Cholesterol Homeostasis in Cancer: Implications for Therapeutic Targets. *Cancers* **2020**, *12*, 1410. [[CrossRef](#)] [[PubMed](#)]
234. Bigelsen, S. Evidence-based complementary treatment of pancreatic cancer: A review of adjunct therapies including paricalcitol, hydroxychloroquine, intravenous vitamin C, statins, metformin, curcumin, and aspirin. *Cancer Manag. Res.* **2018**, *10*, 2003–2018. [[CrossRef](#)] [[PubMed](#)]
235. Ehmsen, S.; Pedersen, M.H.; Wang, G.; Terp, M.G.; Arslanagic, A.; Hood, B.L.; Conrads, T.P.; Leth-Larsen, R.; Ditzel, H.J. Increased Cholesterol Biosynthesis Is a Key Characteristic of Breast Cancer Stem Cells Influencing Patient Outcome. *Cell Rep.* **2019**, *27*, 3927–3938.e6. [[CrossRef](#)] [[PubMed](#)]
236. Jagust, P.; De Luxán-Delgado, B.; Parejo-Alonso, B.; Sancho, P. Metabolism-Based Therapeutic Strategies Targeting Cancer Stem Cells. *Front. Pharmacol.* **2019**, *10*, 203. [[CrossRef](#)]
237. Hasegawa, T.; Yashiro, M.; Nishii, T.; Matsuoka, J.; Fuyuhiko, Y.; Morisaki, T.; Fukuoka, T.; Shimizu, K.; Shimizu, T.; Miwa, A.; et al. Cancer-associated fibroblasts might sustain the stemness of scirrhous gastric cancer cells via transforming growth factor- $\beta$  signaling. *Int. J. Cancer* **2013**, *134*, 1785–1795. [[CrossRef](#)] [[PubMed](#)]
238. Sherman, M.H.; Yu, R.T.; Engle, D.D.; Ding, N.; Atkins, A.R.; Tiriach, H.; Collisson, E.A.; Connor, F.; Van Dyke, T.; Kozlov, S.; et al. Vitamin D Receptor-Mediated Stromal Reprogramming Suppresses Pancreatitis and Enhances Pancreatic Cancer Therapy. *Cell* **2014**, *159*, 80–93. [[CrossRef](#)]
239. Hu, Y.-B.; Yan, C.; Mu, L.; Mi, Y.; Zhao, H.; Hu, H.; Li, X.-L.; Tao, D.-D.; Wu, Y.-Q.; Gong, J.-P.; et al. Exosomal Wnt-induced dedifferentiation of colorectal cancer cells contributes to chemotherapy resistance. *Oncogene* **2019**, *38*, 1951–1965. [[CrossRef](#)]
240. Fu, L.; Zhang, C.; Zhang, L.-Y.; Dong, S.-S.; Lu, L.-H.; Chen, J.; Dai, Y.; Li, Y.; Kong, K.L.; Kwong, D.L.; et al. Wnt2 secreted by tumour fibroblasts promotes tumour progression in oesophageal cancer by activation of the Wnt/ $\beta$ -catenin signalling pathway. *Gut* **2011**, *60*, 1635–1643. [[CrossRef](#)]

241. Kahlert, U.D.; Suwala, A.K.; Koch, K.; Natsumeda, M.; Orr, B.A.; Hayashi, M.; Maciaczyk, J.; Eberhart, C.G. Pharmacologic Wnt Inhibition Reduces Proliferation, Survival, and Clonogenicity of Glioblastoma Cells. *J. Neuropathol. Exp. Neurol.* **2015**, *74*, 889–900. [[CrossRef](#)]
242. Cheng, Y.; Phoon, Y.P.; Jin, X.; Chong, S.Y.S.; Ip, J.C.Y.; Wong, B.W.Y.; Lung, M.L. Wnt-C59 arrests stemness and suppresses growth of nasopharyngeal carcinoma in mice by inhibiting the Wnt pathway in the tumor microenvironment. *Oncotarget* **2015**, *6*, 14428–14439. [[CrossRef](#)] [[PubMed](#)]
243. Su, S.; Chen, J.; Yao, H.; Liu, J.; Yu, S.; Lao, L.; Wang, M.; Luo, M.; Xing, Y.; Chen, F.; et al. CD10+GPR77+ Cancer-Associated Fibroblasts Promote Cancer Formation and Chemoresistance by Sustaining Cancer Stemness. *Cell* **2018**, *172*, 841–856.e16. [[CrossRef](#)] [[PubMed](#)]